UV NEWS

The official newsletter of the Thematic Network for Ultraviolet Measurements

Issue 12 / March 2017

Aalto University

EMRP
European Metrology Research Programme
Programme of EURAMET

The EMRP is jointly funded by the EMRP participating countries within EURAMET and the European Union

Contents

ISSN 1456-2537

Aalto University, Espoo 2017

UVNews is the official newsletter of the Thematic Network for Ultraviolet Measurements. The Network was originally funded by the Standards, Measurements and Testing programme of the Commission of the European Communities, as project number SMT4-CT97-7510. During 2014 – 2017, the Network receives financing from the Euramet through project EMRP ENV59 “Traceability for atmospheric total column ozone.” *UVNews* is published at irregular intervals. It is aimed to exchange knowledge between the participants of the Network and to disseminate information on the forthcoming and past activities of the Network. The newsletter also contains scientific and technical articles on UV measurements and a news-section about activities in the field of UV measurements. The newsletter welcomes all announcements and articles that might be of importance for the readers. The editor of the Newsletter may be reached by:

Aalto University
Metrology Research Institute
Petri Kärhä
P. O. Box 13000
FI-00076 Aalto, Finland

http://metrology.hut.fi/uvnet/

E-mail: petri.karha@aalto.fi

In case of all material to publish, submission by E-mail is preferred.

Photographs: Cover: Devices in the Izaña campaign (Picture by L. Egli). Page 3: Participants of the Izaña campaign (Photo by AEMet - Agencia Estatal de Meteorología).

Editorial

Petri Kärhä

Aalto University, Espoo, Finland

EMRP project ENV59 ATMOZ "Traceability for atmospheric total column ozone" has been running for three years since 2014 and is approaching its end. Our latest issue of *UVNews* reported on the outcome of the project in its first half, and now this *UVNews* 12 reports some of the final outcomes.

The project has developed various techniques for atmospheric ozone measurements. Lot of effort has been put e.g. on studying characteristics of Dobson and Brewer spectrophotometers. Methods for uncertainty evaluation have been developed, which is the topic of three articles in this paper. A Fourier Transform Spectroradiometer has been tested for measuring hyper-spectral solar UV spectra Methodology for determining the solar extraterrestrial irradiance spectrum from the surface has been developed. Also new devices have been built, such as a wavelength ruler and a tunable and portable radiation source for field instrument characterization

The techniques developed have and will be demonstrated in various activities during the second half of the project. Various presentations on the project activities were given with the Brewer Ozone Spectrophotometer/Metrology Open Workshop in Ponta Delgada, Azores, on May 17 to 20, 2016. Presentations given in this workshop can be found in the web pages of the ATMOZ project: http://projects.pmodwrc.ch/atmoz/index.php/publications

A Total Ozone Measurements Intercomparison was arranged at Izaña, Tenerife, on September 12 – 30, 2016. Various articles in this *UVNews* address issues of this campaign.

The final meeting of the ATMOZ project will be arranged in May – June 2017 in El Arenozillo, Spain, also combined with an intercomparison campaign: http://www.eubrewnet.org/cost1207/2016/12/07/arenosillo-2017-campaign/.

EMRP project ENV59 ATMOZ has financed the Thematic Network for Ultraviolet Measurement to publish the two latest issues of *UVNews*. The schedule of next issues is unknown, but they will come. To receive information on the Network, please register to the *UVNet* mailing list (http://metrology.tkk.fi/uvnet/lists.htm) if you do not receive our E-mails already. The same page can be used to unsubscribe from the mailing list. This mailing list will be available free of charge for UV related announcements also after the funding period. Please consider this opportunity to reach your colleagues!

Finally, I would like to wish you all a nice spring and summer, and hope to see you in the coming UV activities!

EMRP ENV59 Traceability for atmospheric total column ozone

Preliminary uncertainty calculations of total column ozone retrievals from spectral direct irradiance measurements

Luca Egli[1], Petri Kärhä[2], Anna Vaskuri[2], and Julian Gröbner[1]

1. Physikalisch-Meteorologisches Observatorium Davos, World Radiation Center, Davos, Switzerland
2. Metrology Research Institute, Aalto University, P.O. Box 15500, FI-00076 Aalto, Finland

Introduction

One particular aim of the EMRP–ENV59 project ATMOZ – "Traceability for atmospheric total column ozone" is to evaluate the overall uncertainty of total column ozone (TOC) from different instruments measuring direct solar irradiance. These instruments include Dobson and Brewer instruments, which are established in worldwide operational networks (e.g. [5, 7]), but also array spectroradiometers.

The Brewer and Dobson Instruments are using four specific wavelengths in the UV band for the retrieval of ozone with the double ratio technique [8], while array spectroradiometers are able to take into account the full spectrum in the wavelength band between 300 – 340 nm for the retrieval of total column ozone. It is expected that this larger amount of spectral information in the atmospheric ozone absorption band could lead to better estimation of TOC with lower uncertainties. One aim of the project is to characterize and calibrate array spectroradiometers, in order to assess the individual sources of uncertainties of the measurements. The second objective within the project is to calculate a comprehensive uncertainty budged of TOC retrieval with array spectroradiometers. Contrary to uncertainty determination of physical measurements only, the retrieval of TOC also includes the uncertainty of the model and the quantities related to the model. Therefore, the overall uncertainty budget should consider the spectral measurements, the model, and their interactions altogether.

This article describes field measurements of the ATMOZ field campaign in Izaña, Tenerife, Spain from two instruments measuring direct spectra and the corresponding model of retrieving ozone. Second, the overall uncertainty is estimated by varying all input parameters with Monte Carlo ensemble runs. The impact of uncertainties either from measurements or the model will result in preliminary calculation of the expected overall uncertainty of TOC, when using spectral measurements in the UV band, and will demonstrate the first approach in determining a comprehensive uncertainty budget. The approach should be reviewed with other approaches towards a final software tool for the next ATMOZ TOC field campaign in Huelva, Spain.

Data And Method

Measured spectra

The first ATMOZ field campaign took place between 12 – 25 September 2016 at the Izaña Atmospheric Observatory, Canary Island Spain at 2373 m.a.s.l, organized by the Spanish Meteorological Agency (AEMET) and the World Radiation Center (PMOD/WRC); see: http://rbcce.aemet.es/2015/11/24/atmoz-intercomparison-campaign-at-izana-tenerife-september-2016/ . The objective of the campaign was to measure direct solar irradiance under clear sky conditions and to compare the TOC measurements of the different participating instruments, such as the Brewer spectroradiometers. For this study, two instruments were selected to test the method of calculating the overall uncertainty budget of the TOC retrieval.

1. The **QASUME** portable world reference for global UV radiation [1] operated by PMOD/WRC within the World Calibration Center – Ultraviolet Section (WCC-UV). The instrument is a Bentham DM150 double monochromator scanning spectroradiometer, measuring the entire spectrum between 290 nm to 500 nm within around 12 minutes. The full width at half maximum resolution of the slit function of QASUME is 0.8 nm.

Figure 1. The QASUME (large tube) and Avodor direct irradiance entrance optics mounted on a solar tracker on the measurement platform at the atmospheric observatory in Izaña.

The double monochromator is connected by quartz fiber to a global entrance optics equipped with a tube to ensure an acceptance angle of around 2.5° (see Fig. 1). To measure direct solar irradiance, the optics with the tube are mounted to a solar tracker, following the sun from sunrise to sunset. The system was operated outdoors, and therefore the instrument was located in a weatherproof and temperature stabilized box. The temperature was monitored

continuously and the variation was within 0.5°C during the measurement campaign. Furthermore, in order to monitor the overall stability of the reference spectroradiometer's spectral response, a portable irradiance calibrator and 3 different 250 W portable standard halogen lamps were used. The mean responsivity varied by less than 0.5 %, demonstrating that the entire unit was stable during the intercomparison and an expanded uncertainty of 3% of the direct solar spectra in the wavelength range 300 nm to 305 nm and 2% between 305 nm and 500 nm can be assumed. Furthermore, according to Hülsen et al. [3], a wavelength uncertainty of max. 0.01 nm is estimated and used later in this study.

2. Contrary to the high-end instrument QASUME, a commercially available array spectroradiometer was assembled by PMOD/WRC for the participation at the campaign. The objective of this system – called "**Avodor**" was to test the ability of a commercially available array spectroradiometer for TOC retrieval without sophisticated technical improvements to the instrument. This system consists of an *Avantes* AvaSpec-ULS2048LTEC spectroradiometer with a back-thinned CCD array detector, which was kept at a cooled Temperature of 5°C, and exhibiting a spectral bandwidth of 0.5 nm. All optical parts of the system were placed in a weatherproof outdoor box which was stabilized to a temperature of 24°C. The spectroradiometer was equipped with commercial direct entrance optics (J1004-SMA-SHUT) from Schreder GmbH, which also contained a shutter in front of the fiber to measure the dark signal. As an additional feature to suppress straylight from the visible and the infrared parts of the solar spectrum, two filters were placed as "in-fiber" filter before the radiation is transmitted to the entrance slit of the instrument. The filters only allow the transmission of radiation between 295 and 345 nm, while the other wavelengths are blocked. The two filters ensured a blocking of the IR part of the spectrum to better than 10^{-6} (according to the specification of the filters). The instrument was calibrated with a 1000 W standard lamp from PTB in the laboratory at Izaña. The response of the Avantes array spectroradiometer showed a spectral noise of about 5 %, while the uncertainty of wavelength could be determined to be about 0.01 nm.

Due to the high computational time required for estimating the overall uncertainty of TOC with the method described below, only one day (September 17, 2016) was selected.

Because of the scanning operation of QASUME, fewer spectra were available for Qasume than for Avodor. For QASUME, in total 38 spectra were available during 8:15 to 17:45 UTC. During this time span, the air-mass was less than 3.5. Avodor was able to measure the entire spectrum quasisimultaneously and therefore, every 30 s a full spectrum was available for the analysis and the retrieval of the uncertainty. During 17 September 2016 and between 8:25 and 17:37 UTC, 1163 spectra were measured with Avodor.

Ozone retrieval

The retrieval of TOC from high resolution continuous spectra used in this study was described in Huber et al. [2]. The algorithm is basically a linear least square fit model to the measured direct solar spectra. Based on the Beer-Lambert law,

$$I_\lambda = I_\lambda^0 e^{-\tau_\lambda m} \quad (1)$$

Where I_λ is the measured irradiance at wavelength λ, I_λ^0 represents the irradiance at the top of the atmosphere, m the airmass and τ_λ the optical depth at wavelength λ. The model is using an extraterrestrial spectrum, and it calculates the attenuation of the direct irradiance through the atmosphere due to ozone absorption, aerosol absorption and scattering, and Rayleigh scattering.

In Eq. 1, I_λ^0 is the extraterrestrial spectrum generated during the previous EMRP-ENV03 project "Solar UV" (see: http://www.pmodwrc.ch/annual_report/annualreport2012.pdf, page 35) and $\tau_\lambda m$ is the atmospheric absorption term.

The atmospheric absorption term $\tau_\lambda m$ can be written as

$$\tau_\lambda m = \tau_\lambda^{\mathrm{R}} m_{\mathrm{R}} + \tau_\lambda^{\mathrm{O_3}} m_{\mathrm{O_3}} + \tau_\lambda^{\mathrm{aod}} m_{\mathrm{aod}}, \quad (2)$$

where $m_{\mathrm{R}}, m_{\mathrm{O_3}}, m_{\mathrm{aod}}$ are different air-masses for the respective absorption terms, calculated by a "Matlab" algorithm based on the geographical parameters, such as the location of the station and the time of measurements. The absorption terms $\tau_\lambda^{\mathrm{R}}$ were parametrized according to Nicolet [5]. The wavelength dependence of the aerosol optical depth (*aod*) for the term $\tau_\lambda^{\mathrm{aod}}$ was defined as

$$aod = \beta * \lambda^{-\alpha}, \quad (1)$$

where the wavelength λ is indicated in micrometers and α and β are the Ångström coefficients. In analogy to the simulation tool described in *UVNews* **11** (see: http://metrology.tkk.fi/uvnet/reports.htm) the absorption term for the ozone layer $\tau_\lambda^{\mathrm{O_3}}$ was based on two different absorption cross-sections:

1. Bass and Paur (BP), which is the cross-section for the brewer retrieval [6]. A set with quadratic coefficient is used for the temperature interpolation (http://igaco-o3.fmi.fi/ACSO/files/cross_sections/Bass-Paur/bp.par)
2. Bremen [6] cross-section, a newly measured cross-section from the University of Bremen, (http://igaco-o3.fmi.fi/ACSO/files/cross_sections/Serdyuchenko/SerdyuchenkoGorshelev5digits.dat). The cross-sections for different temperatures (193 – 293 K) was interpolated by a linear fit to the temperature used for the retrieval.

Ensemble run calculations

In order to calculate the overall uncertainty of the TOC retrieval using the linear least square fit of the atmospheric model, the spectra and the different input parameters were varied within the uncertainty of these parameters.

For the measured input spectra, the wavelength uncertainty and the calibration uncertainty (as described in the data section) were randomly applied for each QASUME and Avodor spectrum.

Random variation means that a Gaussian distribution with the standard deviation (standard uncertainty, *k*=1) of the known uncertainty was generated and then randomly applied to each input spectrum. The standard deviation applied for QASUME and Avodor are:

QASUME:

- Uncertainty of direct solar spectrum: 1% for the full spectrum (standard uncertainty)

- Uncertainty of wavelength: 0.01 nm (standard uncertainty)

Avodor:

- Uncertainty of direct solar spectrum: 5% (standard uncertainty)
- Uncertainty of wavelength: 0.01 nm (standard uncertainty)

Please note that in case of the uncertainty of the direct solar spectrum the randomly selected value from the Gaussian distribution was applied at each wavelength for every single run. For the wavelength uncertainty, one randomly selected value (again from the Gaussian distribution) was applied for the entire spectrum, indicating a shift over the full spectrum.

As for the measured spectrum, the input parameters for the atmospheric model were also randomly varied within the expected uncertainties for both instruments.

This means for the individual parameters:

- Stratospheric temperature was varied between 223 and 232 K from a uniform distribution.
- Extraterrestrial Spectrum from a Gaussian distribution with standard deviation of 3% (standard uncertainty, $k = 1$)
- ozone absorption cross section from a Gaussian distribution with 2.5% (standard uncertainty, $k = 1$).

One further crucial issue when retrieving ozone from a full spectrum is the selection of the wavelength range. The wavelength range for the retrieval of TOC was first chosen to be from 300 to 340 nm, where the major impact of the ozone absorption is expected. However, when analyzing the TOC retrieval for different setting of wavelength ranges, it was found that the retrieved TOC also varied depending on the selected wavelength ranges. Figure 2 shows the changes in the TOC values, differing of about 4 DU for the Bass and Paur and the Bremen cross-sections, when the lower cut-on wavelength is varied between 300 nm and 310 nm. Since the correct wavelength range cannot be determined so far, the selection of the wavelength range can also be considered as a source of uncertainty in the retrieval of TOC. Respecting this finding, the aforementioned ensemble runs were also calculated for different wavelength ranges, further called as cut-on wavelength, between 300 nm and 310 nm. The upper wavelength was always set at 340 nm.

Figure 2 also clearly shows that the TOC estimates depend on the selected cross section used for the retrieval. The Bremen cross section produces ~1 DU higher TOC values than the Bass-Paur cross section. Assuming that both cross-sections are the best datasets available so far and the observed differences are not effects of the standard uncertainty of the two cross-sections, the selection of cross section is also a systematic source of uncertainty. Therefore, the ensemble calculations were performed with both cross-sections.

In summary: The measured spectra were randomly varied in terms of their measurement uncertainties, and the TOC values were retrieved with two different cross-sections, for different wavelength ranges, and randomly varied input parameters for the atmospheric model. The linear square fit procedure, fitting TOC and the Ångström coefficients, was repeated 50 times for each spectrum and selected wavelength range.

The overall uncertainty is finally indicated as the standard deviation of all ensemble runs.

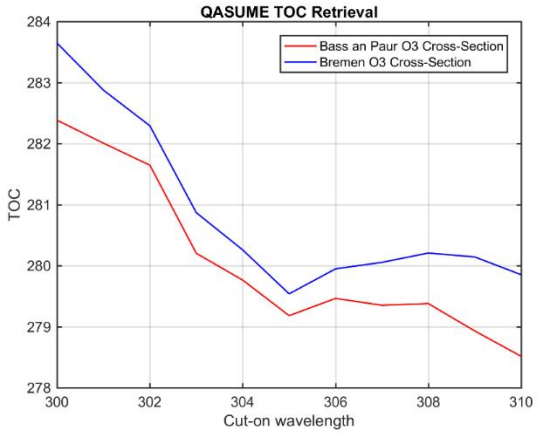

Figure 2. Dependence of TOC on the selected wavelength range. The wavelength range for the retrieval was chosen to be from the cut-on wavelength between 300 nm and 310 nm. The upper wavelength was set to 340 nm.

Results and Discussion

QASUME

For 17 September 2017, 38 spectra of the QASUME measurements with air-mass smaller than 3.5 were used for the retrieval and the uncertainty estimation methods described above.

Figure 3a) shows the mean value of the 50 TOC retrievals with the Bass and Paur cross section, when averaging the TOC values at cut-on wavelengths between 300 nm and 310 nm, and averaging over all varied input parameters (blue line). The blue line of Figure 3b) shows the standard deviation over all 50 ensemble-runs and all cut-on wavelengths between 300 nm and 310 nm. Remarkably, the TOC are comparable to the TOC obtained by the Brewer 185 spectrometer (green circles). They differ from the QASUME measurements by maximum of about 2 DU. However, when considering the entire wavelength range from 300 nm to 340 nm (red line), the TOC is remarkably higher than the Brewer TOC. On the other hand, the uncertainty of this larger wavelength-band is only about 1.5 DU (Figure 3 b), which is about 1 DU lower than when calculating the average between cut-on wavelength from 300 to 310 nm. When using the short wavelength band between 310 to 340 nm, the TOC values are lower than the Brewer TOC, with an uncertainty of around 3 DU at local noon.

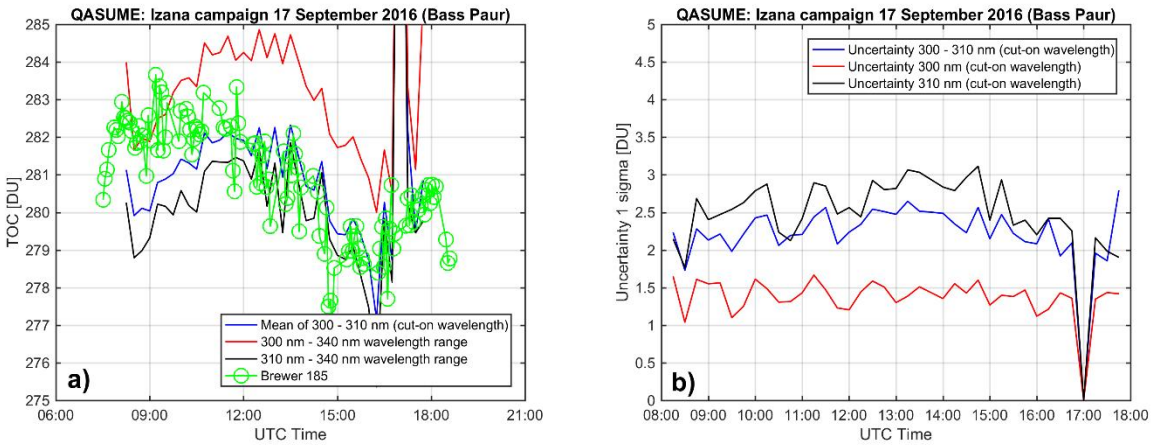

Figure 3 a) TOC retrieval and b) the corresponding uncertainties, obtained with QASUME using the Bass and Paur cross section. Brewer 185 results have been included for comparison.

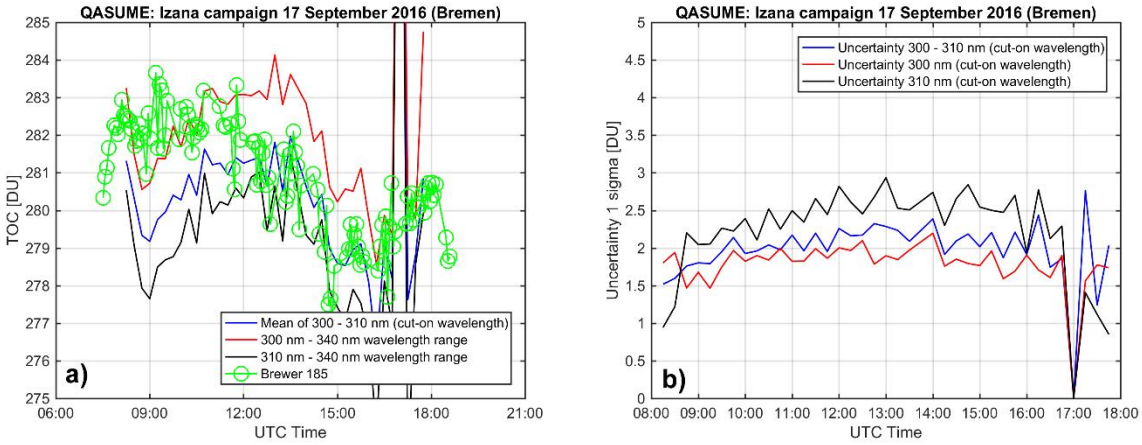

Figure 4 a) TOC retrieval and b) the corresponding uncertainties obtained with QASUME using the Bremen cross-section. Brewer 185 results have been included for comparison.

Figure 4. shows the same calculations as presented in Figure 3, but contrary to the first analysis, the Bremen cross-section was applied for the retrieval. Similarly to the previous results, the average of all considered cut-on wavelength ranges is closer to the TOC of the Brewer 185 than using a cut-on wavelength at 300 nm or 310 nm. Again, cut-on wavelength at 300 or 310 nm result in higher or lower TOC than the Brewer. Differently to the Bass and Paur cross-section, the larger wavelength range between 300 and 340 nm shows a considerably large uncertainty of about 2 DU, similar to calculating the average over all possible wavelength ranges.

As mentioned before, it shall not be determined here, which cross-section is the best for the TOC retrieval. Therefore, the overall uncertainty budget should also include the variation originating from the use of the different cross-section.

Figure 5 depicts the mean value of TOC over all wavelength ranges between 300 and 310 nm to 340 nm and, all variations of the input parameters either for the measured spectra, or from the input parameters from the retrieval model. TOC values obtained with different cut-on wavelengths (ranging between 300nm and 310 nm) and with the two different cross sections have been averaged to draw the blue line in Figure 5. The dashed lines in Figure 5 indicate the standard uncertainty (+/-1 sigma, $k = 1$) of the respective retrieval. The uncertainties are ranging from 2 DU in the morning and evening at low solar zenith angles to 2.5 DU at the local noon. This corresponds to relative standard uncertainties of 0.7 to 0.9 %.

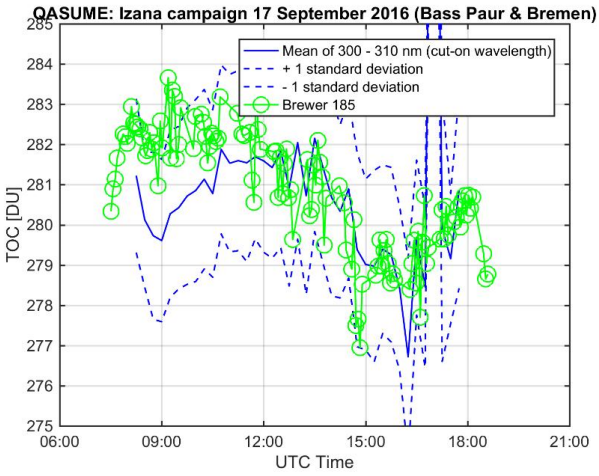

Figure 5. TOC retrieval for QASUME and both cross-sections in monte-carlo ensemble runs. The dashed lines indicate +/- 1 standard deviation of the mean value which is the overall uncertainty of TOC retrieval with QASUME.

AVODOR

The same analysis as for the QASUME measurements was carried out for AVODOR spectra. The results are presented in Figs. 6 to .8. For air-masses smaller than 3.5 (between 8:25 and 17:35 UTC), 166 spectra were used for the analysis. Originally every 30 s, a spectrum was measured by AVODOR. In order to reduce the calculation time, every tenth spectrum was taken for the monte-carlo ensemble run. Therefore every 5 minutes, a TOC was retrieved from the AVODOR measurements. Remarkably, the variation of TOC between two subsequent retrievals may vary by more than 8 DU. This measurement to measurement variation is even larger when using the cut-on wavelength at 300 nm with an overestimation of about 8 DU as compared to the Brewer (Figs. 6 and 7 a). However, at this large wavelength range, the uncertainty is about 3 DU (Figure 6 b). When averaging over all used cut-on wavelength ranges (300 nm to 310 nm) the TOC is about 4 DU lower than the estimates from Brewer 185 and the uncertainty ranges from 4 DU in the morning to 12 DU at noon. When considering a smaller wavelength range between 310 nm and 340 nm, TOC decreases down to 10 DU as compared to the Brewer 185 with an uncertainty between 4 DU and 12 DU.

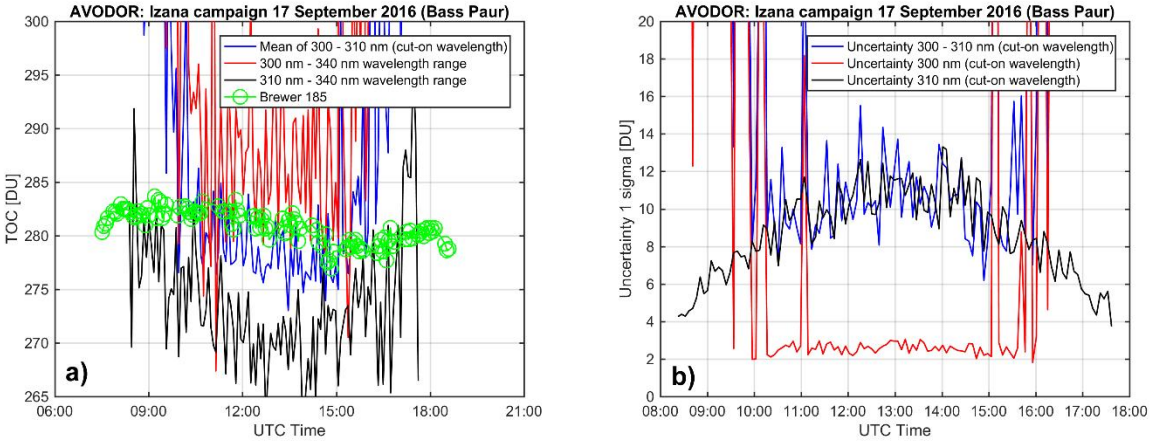

Figure 5. a) TOC retrieval and the b) corresponding uncertainties obtained with Avodor and using the Bass and Paur cross-section. Brewer 185 results have been included for comparison.

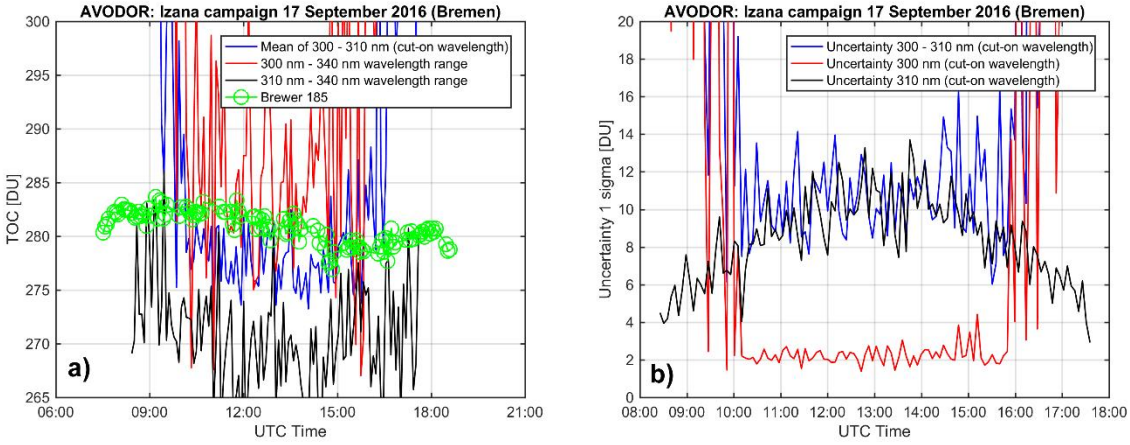

Figure 7. a) TOC retrieval and b) the corresponding uncertainties obtained with Avodor and using the Bremen cross-section. Brewer 185 results have been included for comparison.

The same analysis as above was done for retrievals using the Bremen cross-section. Figure 7 shows the corresponding results. Due to the large variations, the effect of using different cross-sections is negligible for Avodor. Again, the averaged TOC retrievals between 300 and 310 nm are closest to the Brewer 185 and again exhibiting uncertainties of up to 12 DU.

Finally, the overall uncertainty of retrieving TOC with Avodor is shown in Figure 8, taking into account all sources of uncertainty either form the model or from the measurements and both ozone cross-sections. The standard uncertainty (1 sigma, $k = 1$) is shown as dashed lines and is around 4%.

Conclusions

This study presents first results of estimating the overall uncertainty budget of retrieving TOC from a full spectrum. The results show that the TOC retrieval based on QASUME measurements are within 1% considering all known sources of uncertainty either from the retrieval model or from the measurements. The QASUME system is a well characterized and calibrated portable reference double monochromator with high sensitivity due to a photomultiplier detector. These measurements also allow to obtain low uncertainty of TOC retrieval.

In contrast, the Avodor system is based on a commercially available monochromator equipped with an array detector, with limited sensitivity and therefore high noise at short wavelength. The uncertainty of TOC obtained with this

roughly characterized system is up to 12 DU or around 4%. Furthermore, the large variation between one measurement to the subsequent measurement hints that the system shows an instability which is not understood yet.

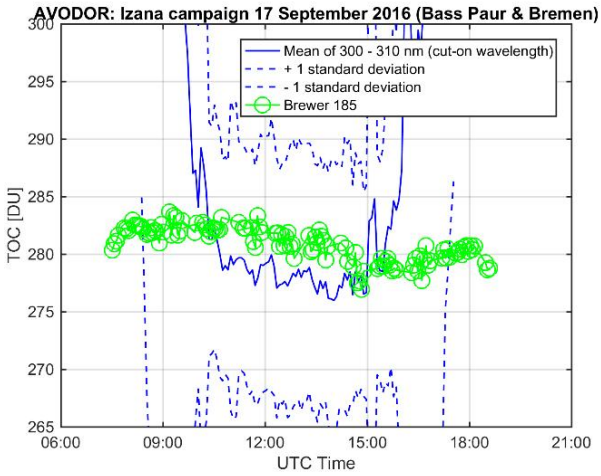

Figure 8. TOC retrieval for Avodor measurements and both cross-sections in monte-carlo ensemble runs. The blue line is a running mean over 30 min from measurements every 5 min. The dashed lines indicate the variation from the mean value and is considered as the overall uncertainty of TOC retrieval with QASUME.

These first considerations of TOC uncertainty show that an overall uncertainty of around 1% may be achieved from a full spectrum in the UV band, with adequate equipment. However, the differences of TOC retrieval when using a wavelength range between 300 to 340 nm or between 310 and 340 nm is not fully understood. Further investigations are needed to determine the best wavelength range or to further optimize the retrieval method for each system individually in order to minimize the overall uncertainty budget.

Acknowledgments This study was performed within the EMRP ENV59 Project - ATMOZ "Traceability for atmospheric total column ozone". The EMRP is jointly funded by the EMRP participating countries within EURAMET and the European Union. Authors also thank Omar El Gawhary from VSL for fruitful discussions regarding overall uncertainty budget of TOC retrieval.

References

[1] Gröbner, J., J. Schreder, S. Kazadzis, A. F. Bais, M. Blumthaler, P. Görts, R. Tax, T. Koskela, G. Seckmeyer, A. R. Webb, and D. Rembges, Traveling reference spectroradiometer for routine quality assurance of spectral solar ultraviolet irradiance measurements, Applied Optics, 44, 25, 5321-5331, 2005.

[2] Huber, M., Blumthaler, M., Ambach, W., and Staehelin, J.: Total atmospheric ozone determined from spectral measurements of direct solar UV irradiance. Geophys. Res. Lett. 22, 53–56 ,1995.

[3] Hülsen, G., J. Gröbner, S. Nevas, P. Sperfeld, L. Egli, G. Porrovecchio, and M. Smid, Traceability of solar UV measurements using the QASUME reference spectroradiometer, Applied Optics, 55, 26, 7265-7275, 2016.

[4] Kerr, J. B.: New methodology for deriving total ozone and other atmospheric variables from Brewer spectrophotometer direct Sun spectra, J. Geophys. Res., 107(D23), 4731, doi:10.1029/2001JD001227, 2002.

[5] Nicolet, M.: On the molecular scattering in the terrestrial atmosphere: An empirical formula for its calculation in the homosphere, Planetary and Space Science, 32,11, 1467-1468, 1984.

[6] Redondas, A., Evans, R., Stuebi, R., Köhler, U. and Weber, M.: Evaluation of the use of five laboratory-determined ozone absorption cross sections in Brewer and Dobson retrieval algorithms, Atmos.Chem. Phys., 14, 1635–1648, doi:10.5194/acp-14-1635-2014, 2014.

[7] Vanier, J., and I. Wardle: The effects of spectral resolution on total ozone measurements, Q. J. R. Meteorol. Soc., 95, 395–399, 1969.

[8] World Meteorological Organization (WMO): Comparison of total ozone measurements of Dobson and Brewer spectrophotometers and recommended transfer function, Global Ozone Res. Monit. Proj. Rep. 149, Geneva, Switzerland, 2003.

Monte Carlo -Based Method for Determining Total Ozone Column Uncertainty, Part I: Methodology

Petri Kärhä[1, a)], Anna Vaskuri[1], Julian Gröbner[2], Luca Egli[2], and Erkki Ikonen[1,3]

1. Metrology Research Institute, Aalto University, Espoo, Finland
2. Physikalisch-Meteorologisches Observatorium Davos, World Radiation Center, Davos, Switzerland
3. VTT Technical Research Centre of Finland Ltd., Espoo, Finland

Abstract

We present a Monte Carlo based model to study effects that possible correlations in spectral irradiance data may have on the derived total ozone column values. Correlations may produce systematic errors in the spectral irradiance which behave differently from uncorrelated data. The effects are demonstrated by analyzing the data of one day's measurements.

introduction

Monte Carlo (MC) analysis is a convenient method to derive uncertainties of quantities in cases where analytical calculation is complicated. In MC analysis, input quantities are varied within their uncertainties and the resulting deviations in the derived quantities give their uncertainties.

With spectrally derived quantities, where the quantity is calculated from a measured spectrum using e.g. integration or recursive analysis, MC analysis can be carried out by varying the measured spectral irradiance values. However, this approach may be problematic because of correlations in the data. The uncertainties of the spectral data may hide systematic wavelength dependent errors e.g. due to interpolation of data, wavelength shifts, geometrical factors, or systematic errors in the standard lamps. Guide to the Expression of Uncertainty in Measurement [1] presents ways to take correlation in data into account. However, if the correlations are unknown, these methods cannot be used.

With unknown correlations, assumptions need to be made. The most typical assumption is that the data are not correlated. This may lead into underestimated uncertainties, because spectrally varying systematic errors often produce larger deviations than wavelength independent noise-like variations.

Kärhä *et al.* have recently proposed a method to study measurement errors that unknown correlations may introduce in derived quantities and applied this to study uncertainties of the correlated color temperature [2]. Spectral error functions with varying order of complexity are formed and used to find maximum errors that the uncertainties permit. In this paper, based on a paper published in IRS 2016 [3], we test the method [2] to study uncertainties of the total atmospheric ozone determined from spectral measurements of direct solar UV irradiance [4].

Materials and Methods

Deriving ozone from measured spectrum

Huber *et al.* have presented a method for deriving total ozone column values (*TOC*) from high resolution spectral measurements of direct solar UV irradiance [3]. In our analysis, we consider measurements in the spectral range λ = [295, 340] nm with wavelength interval $\Delta\lambda$ = 0.5 nm. *TOC* is determined by fitting model calculations to the measured spectra.

Spectral irradiance $E(\lambda)$ measured at Earth level can be calculated from the extraterrestrial irradiance $E_{Ext}(\lambda)$ by

$$E(\lambda) = E_{Ext}(\lambda) \cdot e^{-\tau(\lambda)\cdot m}, \quad (1)$$

where m is the relative air mass and $\tau(\lambda)$ is the optical depth of the atmosphere. $\tau(\lambda)$ consists of factors such as the ozone absorption cross section $\alpha_{O_3}(\lambda)$, the total ozone column TOC, the Rayleigh scattering optical depth $d_{Rayleigh}(\lambda)$ and the aerosol optical depth $d_{aod}(\lambda)$.

In the analysis, TOC and the aerosol optical depth are varied to minimize the differences between the measured and the modeled irradiance values using least squares fitting. Convolution is accounted for by convoluting the extraterrestrial data with the instrument's slit function.

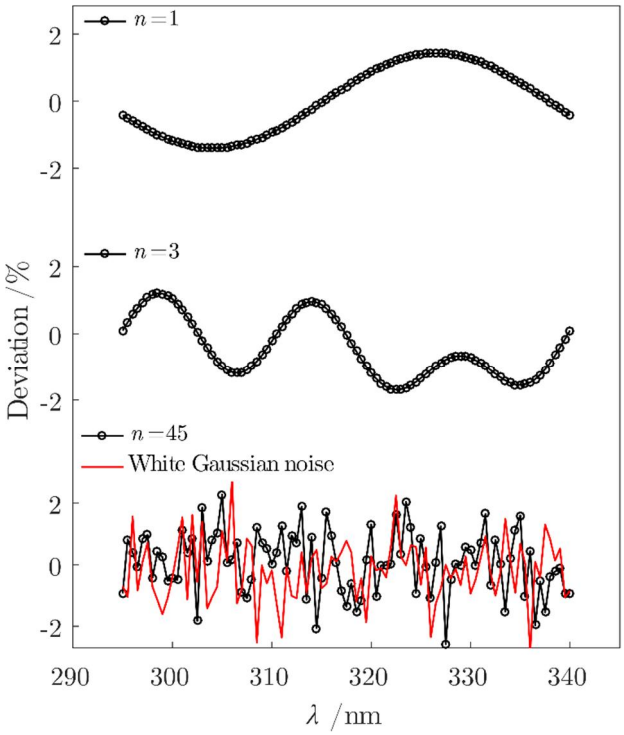

Figure 1. Examples of error functions produced using Eq. (3). White Gaussian noise has been added to the lowest figure to demonstrate that at the Nyquist criterion, correlation is lost, and the function resembles noise.

Model for studying effects of possible correlations

The model is based on orthogonal base functions formed as a series of Sines,

$$E(\lambda) = \begin{cases} f_i(\lambda) = \sqrt{2}\sin\left[i\left(2\pi\frac{\lambda-\lambda_1}{\lambda_2-\lambda_1}\right)+\phi_i\right], \\ f_0(\lambda) = 1 \end{cases} \quad (2)$$

which all have variances $s^2 = 1$. Wavelength limits l_1= 295 nm and l_2 = 340 nm may be varied e.g. in the case of noisy data. Phase terms ϕ_i vary the locations of sign changes within the wavelength range. The phase shift of each base function is uniformly distributed.

An error function is formed by combining the N + 1 first terms with varying weights,

$$\delta(\lambda) = \sum_{i=0}^{N} \gamma_i f_i(\lambda). \quad (3)$$

The weights γ_i are chosen randomly from the surface of an N + 1 dimensional sphere to keep variance at 1. Figure 1 shows three examples of error functions with three different values of N. The spectral irradiance data are disturbed as

$$E_e(\lambda) = [1 + \delta(\lambda)\, u_c(\lambda)]E(\lambda), \quad (4)$$

and the resulting $E_e(\lambda)$ are used to calculate *TOC*. The results are repeated to calculate standard deviations, and the order of complexity N is varied to see how different waveforms affect the uncertainties.

Results and discussion

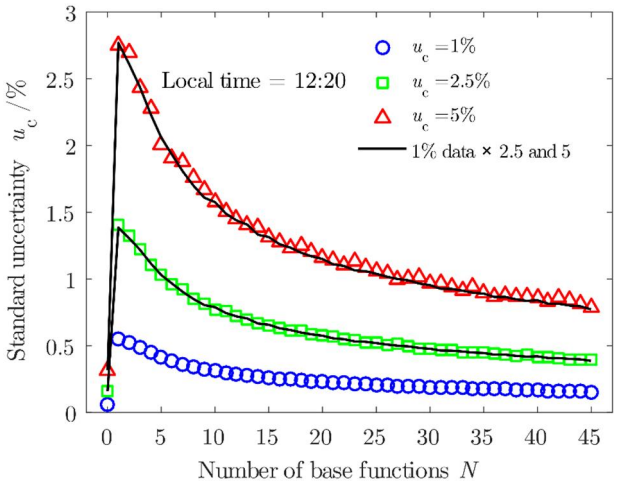

Figure 2. Uncertainties of TOC at noon as a function of the order of complexity N at three different levels of uncertainty in spectral irradiance indicated with symbols in the figure legend. The black solid lines obtained by multiplying the 1% uncertainties indicate scalability of the model.

The method was applied on spectra measured in Mauna Loa, USA on Nov 30, 2001 at 6:14 – 18:54. The analyzed *TOC* was ~264 DU. Figure 2 presents uncertainties at noon (12:20) analyzed for three uncertainty levels in spectral irradiance, u_c (k = 1) = 1%, 2.5%, and 5%. The maximum uncertainty is found at N = 1 indicating that a simple slope-like error would produce the highest uncertainty. The first term, N = 0, indicates that fully correlated data, where all wavelengths have the same error, produces very small errors in *TOC*. The last data point at N = 45, which is the Nyquist limit for the analysis, gives an uncertainty in the case assuming no correlations. The black solid lines demonstrate that the analysis method is scalable. Values obtained with u_c = 1% can thus be used as sensitivities and scaled with the actual uncertainty. For a typical expanded uncertainty value U (k = 2) = 5%, we can see that the resulting uncertainty in *TOC* is U_{TOC} = 0.3% assuming full correlation, U_{TOC} = 0.8% assuming no correlation, and U_{TOC} = 2.75% assuming the worst possible correlation. These values give practical limits for the uncertainty. Assuming that the correlation is equally distributed among the three cases would yield U_{TOC} = 1.3% (3.4 DU) by simple averaging.

Figure 3 presents the uncertainties of *TOC* analyzed throughout the day assuming u_c (k = 1) = 2.5% for the spectral irradiance. Sensitivity of the *TOC* uncertainty on uncertainty in irradiance is highest at Noon and lowest in the evening and morning. On the other hand, uncertainties of spectral irradiance are also higher in the evening and morning due to lower signal levels, which the model does not yet take into account.

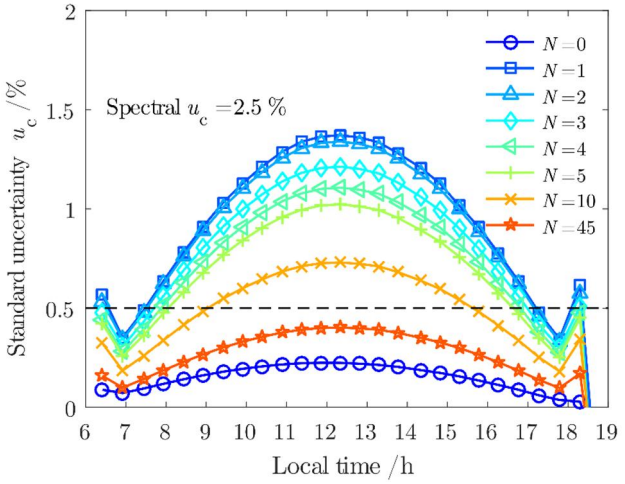

Figure 3. Uncertainties of TOC during the day at various order of complexity levels N indicated in the figure legend.

Conclusions

We have demonstrated that the uncertainty of *TOC* derived from direct solar UV spectral irradiance measurements may be seriously affected by possible spectrally varying systematic wavelength dependent errors that unknown correlations may well produce within the uncertainties. We have also presented a model that can be used to study the limits of these errors. The presented model only takes into account uncertainty of the spectral irradiance. In practice, also factors such as the extraterrestrial irradiance $E_{Ext}(\lambda)$, the air mass m, the ozone absorption cross section $\alpha_{O_3}(\lambda)$, and the aerosol optical depth $d_{aod}(\lambda)$ have uncertainties that should be accounted for. Some of these factors are located in the exponent of Eq. 1 and thus require separate analysis. In the second part of this article [5], we demonstrate how the methodology can be used in a component-by-component analysis of uncertainty.

Acknowledgments: This work has been supported by the European Metrology Research Programme (EMRP) within the joint research project ENV59 "Traceability for atmospheric total column ozone" (ATMOZ). The EMRP is jointly funded by the EMRP participating countries within EURAMET and the European Union. Tomi Pulli is acknowledged for fruitful discussions on the mathematics.

References

1. JCGM 101:2008, *Evaluation of measurement data — Guide to the expression of uncertainty in measurement* (Joint Committee for Guides in Metrology JCGM, 2008), 120 p.
2. P. Kärhä, A. Vaskuri, H. Mäntynen, N. Mikkonen, and E. Ikonen, "Method for estimating effects of unknown correlations in spectral irradiance data on uncertainties of spectrally integrated colorimetric quantities," (submitted).
3. P. Kärhä, A. Vaskuri, J. Gröbner, L. Egli, and E. Ikonen, "Monte Carlo analysis of uncertainty of total atmospheric ozone derived from measured spectra," *AIP Conference Proceedings* **1810**, 110005 (2017). http://doi.org/10.1063/1.4975567
4. M. Huber, M. Blumthaler, W. Ambach, and J. Staehelin, "Total atmospheric ozone determined from spectral measurements of direct solar UV irradiance," *Geophys. Res. Lett.* **22**, 53–56 (1995).
5. A. Vaskuri, P. Kärhä, L. Egli, J. Gröbner, and E. Ikonen, "Monte Carlo -Based Method for Determining Total Ozone Column Uncertainty, Part II: Izaña campaign," *UVNews* **12**, 13–14 (2017).

Monte Carlo -Based Method for Determining Total Ozone Column Uncertainty, Part II: Izaña Campaign

Anna Vaskuri[1], Petri Kärhä[1,2], Luca Egli[3], Julian Gröbner[3], and Erkki Ikonen[1,2]

[1]Metrology Research Institute, Aalto University, Espoo, Finland
[2]MIKES Metrology, VTT Technical Research Centre of Finland Ltd, Espoo, Finland
[3]Physikalisch-Meteorologisches Observatorium Davos, World Radiation Center, Davos, Switzerland

Abstract

We demonstrate a Monte Carlo -based model to calculate uncertainties of total ozone column *TOC* derived from ground-based spectral irradiance measurements. The model takes into account effects that correlations in the spectral irradiance data may have on the results. The model is tested with spectral data measured with three spectroradiometers at Izaña, Tenerife on September 17, 2016. The *TOC* values derived have expanded uncertainties of 2.99–3.03%, 3.1–3.6%, and 3.3–3.9%, the uncertainty being the highest at noon.

INTRODUCTION

Total Ozone Column *TOC* can be determined from spectral measurements of direct solar UV irradiance [1]. One often overlooked problem with these measurements is that the spectral data may hide systematic wavelength dependent errors due to correlations. Omitting possible correlations may lead into underestimated uncertainties for derived quantities, since spectrally varying systematic errors typically produce larger deviations, than traditionally expected uncorrelated noise-like variations. In part I of this article [2], we presented a Monte Carlo (MC) -based model to estimate uncertainties of the derived *TOC* values, and to study effects that possible correlations may have. In this article, we show how this methodology can be used in a component-by-component analysis of the uncertainty of *TOC* by analysing measurement results acquired within the Izaña campaign in 2016.

Table 1. Example of an uncertainty budget. Parameter $\tau(\lambda)$ describes total optical depth in the square brackets in Eq. (1).

Source of uncertainty	Standard uncertainty $E(\lambda)$ %	Standard uncertainty $\tau(\lambda)\cdot m$ %	Correlation Full	Correlation Unfavourable Fraction	Correlation Random	*TOC* DU
Measurement						
Standard lamp	1.0		1/3	1/3	1/3	0.48
Interpolation	0.2		0	1	0	0.49
Distance in calibration	0.2		1	0	0	0.03
Ageing of lamp	0.5		0	1	0	1.23
Drift of spectroradiometer	0.2		0	1	0	0.49
Linearity	0.3		0	1	0	0.74
Alignment	0.2		1	0	0	0.03
Other	0.2		1/3	1/3	1/3	0.09
Uncertainties related to $E(\lambda)$						
Extraterrestrial spectrum	2.3		1/6	2/3	1/6	2.69
Slit convolution	0.0					0.00
Wavelength shift due to air	0.0					0.00
Uncertainties related to $\tau(\lambda)\cdot m$						
Air mass (O_3 layer altitude of 7.9%)		0.025		(a)		0.07
Reference O_3 cross-section		1.0	1/3	1/3	1/3	1.36
Temperature of O_3 cross-section at -45 ± 15 °C		6.0		(b)		2.88
Aerosol optical depth (std. mean of the fit)		0.1	0	0	1	0.00
Rayleigh scattering optical depth		0.1	1/3	1/3	1/3	0.05

(a) Air mass varies as a function of ozone layer height.
(b) O_3 cross-section varies as a function of temperature.

ATMOSPHERIC MODEL

The relationship between the measured spectral irradiance $E(\lambda)$ and the extraterrestrial solar spectrum $E_{\text{ext}}(\lambda)$ can be defined as [1]

$$E(\lambda) = E_{\text{ext}}(\lambda) \times e^{-\left[a_{O_3}(\lambda)\times TOC + d_R(\lambda) + d_{\text{AOD}}(\lambda)\right]\times m}, \quad (1)$$

where $\alpha_{O3}(\lambda)$ is the ozone absorption cross section, $d_R(\lambda)$ is the Rayleigh scattering optical depth, and m is the relative air mass. The aerosol optical depth is approximated as

$$d_{\text{AOD}}(\lambda) = b\lambda^{-a}, \quad (2)$$

where $\alpha = 1.4$ is the Ångström coefficient, and β is a scaling factor. The model spectrum is fitted with parameters *TOC* and β to the measured ground-based spectrum using least squares fitting method.

UNCERTAINTY ESTIMATION

Uncertainties are modelled with a MC model described in more detail in [2, 3]. Possible systematic deviations contained within uncertainties are reproduced using cumulative Fourier series with sinusoidal base functions f_i, where index i depicts the order of complexity of the deviation [2]. Function f_0 depicts full correlation and $f_0 + f_1 + \ldots + f_N$ (N determined by the Nyquist criterion) depicts random spectral deviation. In Ref [3], we found that simple slope type errors produce largest errors in *TOC*. Thus, function $f_0 + f_1$ is a good selection to resemble effects of unfavourable correlations within wavelength range 300 – 340 nm.

The uncertainties included in the model are listed in the first column of Table 1. The second and third columns separate, whether the component affects the measurement directly through $E(\lambda)$ or via the exponent $t(\lambda)\cdot m$, as these need separate analysis. The next columns "Full," "Unfavourable," and "Random" define estimated fractions on assortment of correlations. "Full" indicates that error is wavelength independent, such as with geometrical factors. "Random" indicates no correlation (noise). "Unfavourable" indicates a spectrally varying error, such as a slope that produces a large error in *TOC*. The last column states the standard uncertainty produced by each uncertainty component to the *TOC*, with the assumed fractions of correlations, calculated with a spectrum measured at local noon with QASUME [4]. The expanded uncertainty of *TOC* for this spectral measurement can be calculated as a square sum of the individual components to be 9.0 DU (3.2%).

Uncertainties related to "Measurement" are typical to solar irradiance [5]. Division of the standard lamp uncertainty to equal fractions is based on typical correlations noted in intercomparisons [6]. In the measurement, the largest contribution to uncertainty comes from the ageing of the lamp. When the lamp ages, its temperature drops, which changes the shape of the spectrum. Thus, worst case correlation is assumed. This is perhaps a little bit overestimated and could be reduced by using real correlation data.

For $E_{ext}(l)$, we use data by Vanhoosier *et al.* [7]. The largest source of uncertainty reported for the measurement was a broken device, so we estimate that 2/3 of the uncertainty may be severely correlated. The uncertainties arising from the slit function and the 0.1 nm wavelength shift are expected to be negligible.

The ozone layer is placed at the altitude of 22 ± 3 km, and the Rayleigh scattering at the altitude of 5 km [8]. Vertical profiles are not implemented in the model. For calculating $d_R(\lambda)$, we use a model by Bodhaine *et al.* [9] with 0.1% uncertainty. The correlations for the $\alpha_{O3}(\lambda)$ cross section [10] are unknown, so we assume equal fractions of correlation to it, similar to spectral irradiance. This forms one major component in the uncertainty. The atmospheric temperature is assumed to uniformly vary –45 ± 15 °C leading to the spectral correlations of $\alpha_{O3}(\lambda)$. Such a temperature dependence of $\alpha_{O3}(\lambda)$ was interpolated by a second degree polynomial at each wavelength. As can be seen, this is the most dominating source of uncertainty.

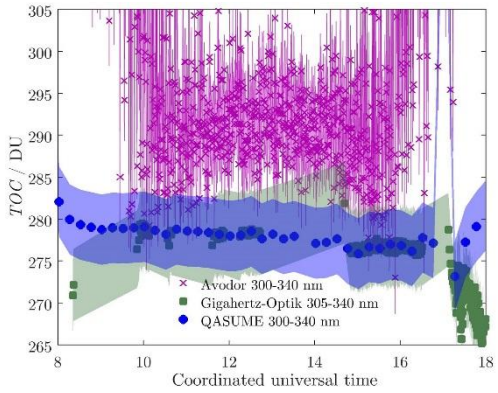

Figure 1. Absolute total ozone columns with k = 1 uncertainties derived from three different data sets.

RESULTS AND DISCUSSION

The calculated *TOC* values with their uncertainties, obtained using the spectral irradiance data by three different spectroradiometers at Izaña campaign, Tenerife September 17, 2016 are presented in Fig. 1. The spectroradiometers used were a double-monochromator QASUME spectroradiometer, and an Avodor array spectroradiometer, both operated by PMOD/WRC, and a Gigahertz-Optik GmbH BTS2048-UV-S series array spectroradiometer operated by PTB [11].

The combined measurement uncertainties in spectral irradiance were 0.5% for QASUME [4], and roughly estimated to be 1.0% for Gigahertz and 2.5% for Avodor. These values are equally distributed between "Full," "Unfavourable," and "Random" correlations, and they replace all the uncertainties related to "Measurement" in Table 1. Since the uncertainties related to extraterrestrial spectrum, total optical depth, and relative air mass remain unchanged despite the ground-based measurement, we have calculated each uncertainty component of Table 1 separately and then calculated the combined expanded uncertainty to reduce the computational time of the algorithm.

The expanded uncertainties of the data sets in Fig. 1 are U_{QASUME} = 8.4 – 8.5 DU, $U_{Gigahertz}$ = 8.6 – 10.1 DU, and U_{Avodor} = 9.2 – 11.0 DU (2.99 – 3.03%, 3.1 – 3.6%, and 3.3 – 3.9%) being the highest at noon when m = 1. If we treat QASUME results as reference, and compare Gigahertz-Optik and Avodor results with the QASUME results between 10:00 – 16:00, the absolute difference is on the average 3 DU for the Gigahertz-Optik instrument and 16 DU for the Avodor. When the time interval is extended to cover 9:00 – 17:00, the difference is still 3 DU for Gigahertz-Optik, but 36 DU for Avodor, respectively. The 3-DU deviations of the Gigahertz-Optik device fit well within the estimated uncertainty of ~9 DU. However, the results by Avodor exceed the approximated uncertainties of ~10 DU by a factor of up to 3.6. One possible reason for that is poor straylight properties severely distorting the spectral shape. Correlations cannot explain such large deviations. Assuming worst possible correlations for the 2.5% measurement uncertainty, would only increase the corresponding uncertainty in *TOC* to 6.3 DU.

We have also carried out a more comprehensive uncertainty estimation of the Izaña data by using atmospheric layer structure with randomly varying vertical layer profiles, assuming no unknown correlations [12]. Our method gives a factor of ~2 larger uncertainties for QASUME and a factor of ~0.5 smaller uncertainties for Avodor than the method in Ref. [12]. The latter might be because our model does not include a component for noise that is quite pronounced with the Avodor instrument. The standard deviation of the residual errors between the measured and modeled irradiances ranges from 50% in the morning and evening to 10% in the noon for the AVODOR instrument, whereas with Gigahertz-Optik and QUASUME devices the noise at noon is of the order of 2%.

ACKNOWLEDGMENTS. This work has been supported by the European Metrology Research Programme (EMRP) within the joint research project ENV59 "Traceability for atmospheric total column ozone" (ATMOZ). The EMRP is jointly funded by the EMRP participating countries within EURAMET and the European Union. Authors are grateful for the incentive grant by the Emil Aaltonen Foundation, Finland. Peter Sperfeld from PTB is acknowledged for measuring and providing the Gigahertz-Optik data set.

REFERENCES

1. M. Huber, M. Blumthaler, W. Ambach, and J. Staehelin, "Total atmospheric ozone determined from spectral measurements of direct UV irradiance," *Geophys. Res. Lett.* **22**, 53–56, 1995.
2. P. Kärhä, A. Vaskuri, J. Gröbner, L. Egli, and E. Ikonen, "Monte Carlo -Based Method for Determining Total Ozone Column Uncertainty, Part I: Methodology, " *UVNews* **12**, 10–12 (2017).
3. P. Kärhä, A. Vaskuri, J. Gröbner, L. Egli, and E. Ikonen, "Monte Carlo analysis of uncertainty of total atmospheric ozone derived from measured spectra," *AIP Conference Proceedings* **1810**, 110005 (2017).
4. G. Hülsen, J. Gröbner, S. Nevas, P. Sperfeld, L. Egli, G. Porrovecchio, and M. Smid, "Traceability of solar UV measurements using the QASUME reference spectroradiometer," *Appl. Opt.* **55**, 7265–7275 (2016).
5. G. Bernhard and G. Seckmeyer, "Uncertainty of measurements of spectral solar UV irradiance," *J. Geophys. Res.* **104**, 14321–14345 (1999).
6. P. Kärhä, A. Vaskuri, T. Pulli, and E. Ikonen, "Key comparison CCPR-K1.a as an interlaboratory comparison of correlated colour temperature," NEWRAD 2017, Tokyo, Japan (submitted).

7. M. E. Vanhoosier, J.-D. F. Bartoe, G. E. Brueckner, and D. K. Prinz, "Absolute Solar Spectral Irradiance 120 nm - 400 nm (Results from the Solar Ultraviolet Spectral Irradiance Monitor-SUSIM-Experiment on Board Spacelab 2)," *Astro. Lett. and Communications* **29**, 163–168 (1988).
8. J. Gröbner and J. B. Kerr, "Ground-based determination of the spectral ultraviolet extraterrestrial solar irradiance: Providing a link between space-based and ground-based solar UV measurements," *J. Geophys. Res.* **106**, 7211–7217 (2001).
9. B. A. Bodhaine, N. B. Wood, E. G. Dutton, and J. R. Slusser, "On Rayleigh Optical Depth Calculations," *J. Atmos. Oceanic Tech.* **16**, 1854–1861 (1999).
10. W. Chehade, B. Gür, P. Spietz, V. Gorshelev, A. Serdyuchenko, J. P. Burrows, and M. Weber, "Temperature dependent ozone absorption cross section spectra measured with the GOME-2 FM3 spectrometer and first application in satellite retrievals," *Atmos. Meas. Tech.* **6**, 1623–1632 (2013).
11. R. Zuber, P. Sperfeld *et al.*, "A high dynamic stray light corrected array spectroradiometer for complex measurements in the UV spectral range," NEWRAD 2017, Tokyo, Japan (submitted).
12. L. Egli, P. Kärhä, A. Vaskuri, and J. Gröbner, "Preliminary uncertainty calculations of total column ozone retrievals from spectral direct irradiance measurements," *UVNews* **12**, 4–9 (2017).

Total ozone retrieval from the Phaethon DOAS system at the Izaña campaign in September 2016

Fani Gkertsi[1], Alkiviadis Bais[1], Natalia Kouremeti[1,2], and Theano Drosoglou[1]

1. Aristotle University of Thessaloniki, Laboratory of Atmospheric Physics, Thessaloniki, Greece
2. Physikalisch-Meteorologisches Observatorium Davos, World Radiation Center, Davos, Switzerland

Introduction

In the framework of the ATMOZ project, a campaign was organized in September 2016 at the Izaña Atmospheric Observatory in Tenerife, Spain. One of the objectives of the campaign was to acquire data of solar spectral irradiance for several days, suitable for Langley evaluations that are used for deriving total ozone measurements by different systems. The Phaethon system of the Laboratory of Atmospheric Physics, AUTH, Greece [*Kouremeti et al.*, 2013] also took part in this campaign, in order to participate in the intercomparison with other standard TOC systems, such as Brewer and Dobson spectrophotometers.

This study presents briefly the methodology followed for the retrieval of TOC from direct solar radiance spectra measured by the Phaethon system, which is based on the Differential Optical Absorption Spectroscopy (DOAS) technique [*Platt and Stutz*, 2008], but focusses mainly on the determination of the Slant Column Density of the reference spectrum (SCD_{REF}) which is an essential part of the retrieval method. For this purpose, data acquired by Phaethon for 14 days have been analyzed with different variants of the Langley extrapolation methods following the suggestions of [*Kiedron and Michalsky*, 2016]. Finally the TOC data of Phaethon are compared with data of a Brewer spectrophotometer.

Instrumentation and data

Phaethon is a DOAS/maxDOAS system based on a cooled, miniature CCD spectrograph (AvaSpec-ULS2048LTEC) operating in the UV-visible region (300-450nm) [*Kouremeti et al.*, 2013]. It is used for the retrieval of total and tropospheric columns of atmospheric trace gases (e.g., O_3, NO_2 and HCHO) from spectrally resolved measurements of, respectively, direct solar irradiance and sky radiance at different elevation angles [*Drosoglou et al.*, 2016]. Particularly for the total ozone column, the direct irradiance spectral measurements of Phaethon are analyzed using the QDOAS software [*Danckaert et al.*, 2013] to derive differential slant column densities relative to a selected reference spectrum. With the appropriate methodology and calibration, the differential slant column densities are used to retrieve the TOC [*Gkertsi et al.*, 2016].

In the framework of the ATMOZ campaign, direct-sun spectral radiance measurements were acquired by Phaethon in 14-27 September 2016 at the Izaña Atmospheric Observatory in Tenerife, Spain (Figure 1). The input optics of the system were installed at the tower of the observatory and the spectrometer in an acclimatized room one floor below. Measurements were performed continuously from sunrise to sunset in sets lasting for about 3 min. Every second set, the data were taken with a short-pass filter that cuts off the signal at wavelengths longer than about 360 nm, leading to enhanced signal in the ozone sensitive range (315 – 337 nm) which is used in the TOC retrieval. Clouds are usually rare at the altitude of the Observatory (2380 m) therefore only on a few occasions measurements were contaminated by clouds. During the 14 days of the campaign ~1450 sets of 3-min spectral measurements were collected. About 250 data sets were rejected either by the DOAS retrieval algorithm or by a filter that was used to screen data with retrieval errors larger than 3 DU.

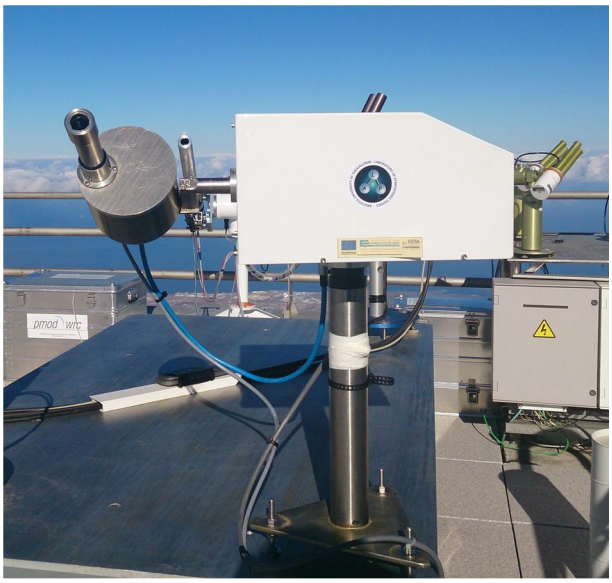

Figure 1. The tracker with entrance optics of Phaethon on the terrace where instruments participated in the ATMOZ campaign were installed.

The TOC derived from Phaethon has been compared with data of a collocated Brewer spectrophotometer (#183) which is one of the reference triad Brewers that are maintained by AEMET in Izaña [*Redondas et al.*, 2016]. The Brewer measured TOC every about 4 minutes.

Retrieval of TOC by Phaethon

Methodology

The methodology for the retrieval of TOC from Phaethon direct-sun radiance spectra is described in detail in [*Gkertsi et al.*, 2016]. Briefly, it is based on the estimation of the differential slant column density (*dSCD*) that is derived from the DOAS analysis of each spectrum with respect to a selected reference spectrum,

$$dSCD_i = SCD_i - SCD_{REF} = TOC_i \times AMF_i - SCD_{REF}, \quad (1)$$

where SCD_i is the slant column density of ozone for the i^{th} radiance spectrum, SCD_{REF} is the slant column density of ozone for the reference spectrum, and AMF_i the airmass factor, which for direct spectra is approximated by the secant of the solar zenith angle (SZA) at the mean altitude

of the ozone layer at midlatitude locations (~22 km), and for SZAs smaller than about 75°.

The SCD_{REF} can be derived by Langley extrapolation during periods with fairly constant *TOC*, when (1) is linear. The data collected during the campaign provide a unique opportunity to estimate the SCD_{REF} for the reference spectrum that is used in the DOAS analysis and was recorded on day 258 at 13.01 UT. It is noted that this dataset can be used to determine the SCD_{REF} for any reference spectrum, even if it has been recorded at a different time in another location, as long as it is recorded by the same system.

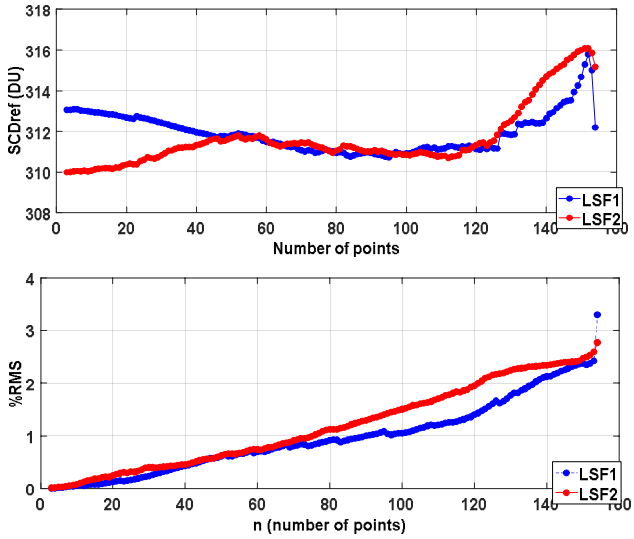

Figure 2. SCD_{REF} as a function of the number of points entering the Langley regression of dSCD vs AMF after removing sequentially one outlier at a time, for the two methods LSF1 and LSF2 (upper panel). The corresponding percentage of the RMS of residuals (lower panel).

Methods to determine SCD_{REF}

Usually, when applying the Langley extrapolation of a dataset, outliers are removed by the operator based on rather subjective criteria. This procedure has several advantages, but also disadvantages, as the result of the same dataset may be different when the method is applied by different operators. In order to determine the SCD_{REF} of the spectrum that has been used as reference in the DOAS analysis of the campaign data of Phaethon, the Langley extrapolation was first applied using this subjective (eye and mind) procedure. This method yields a mean value of SCD_{REF} = 314.6 DU, or 315.5 DU when excluded the days 258 and 260 for which the Langley regression resulted in much different values, likely due to changing TOC during these days.

However, based on the work of [*Kiedron and Michalsky*, 2016], we explored additionally three different methods of Langley extrapolation on the campaign data. The first two methods are based on least-squares fitting (LSF) of the *dSCD* with respect to *AMF* with sequential removal of outliers.

In the first method (LSF1), the linear regression is $y = ax + b$, where $y = dSCD$ and $x = AMF$. A least-squares fit is applied to the dataset and the residuals are calculated. The data pair corresponding to the absolutely largest residual is removed and the root mean square (RMS) of the remaining residuals is calculated as percentage of the average of *dSCD*s,

$$RMS\% = \frac{RMS}{\overline{dSCD}} \cdot 100 \cdot \qquad (2)$$

The process is repeated with the new dataset until the RMS% becomes smaller than 1%. The constant term of the linear regression at that point gives the $-SCD_{REF}$, while the slope of the regression corresponds to the mean *VCD or TOC*.

The second method (LSF2) is a variant of the first with the linear regression being $y/x = a + b/x$. In this case y/x = $dSCD/AMF$ and 1/x = $1/AMF$. This transformation gives less weight to the data at large SZAs which are sparser than data recorded closer to local noon. In this case the term $-SCD_{REF}$ is given by the slope of the regression. As with the previous method, the residuals from the regression $y = ax + b$ are calculated and the data pairs with the largest residuals are removed sequentially until RMS%≤1%.

Figure 2 illustrates the effect of the removal of outliers on day 270 of 2016. The derived SCD_{REF} as a function of data pairs entering the regression is shown together with the corresponding RMS%. Evidently, the derived SCD_{REF} is more variable when all points are used, but soon its variation becomes smoother when the first outliers are removed. The 1% of RMS% is achieved roughly when 90 points are left in the data set for the LSF1 method, but for less than 75 points for the LSF2 method. However, it appears from the upper panel of Figure 2 that already at about 120 points the SCD_{REF} is stabilized to a value close to 311 DU and remains close to this value for at least down to 60 points. Therefore the criterion of RMS%≤1% seems to work fine for this case. Obviously when the remaining data points are too few the derived SCD_{REF} starts to deviate as the regression is based on a small range of AMF variation.

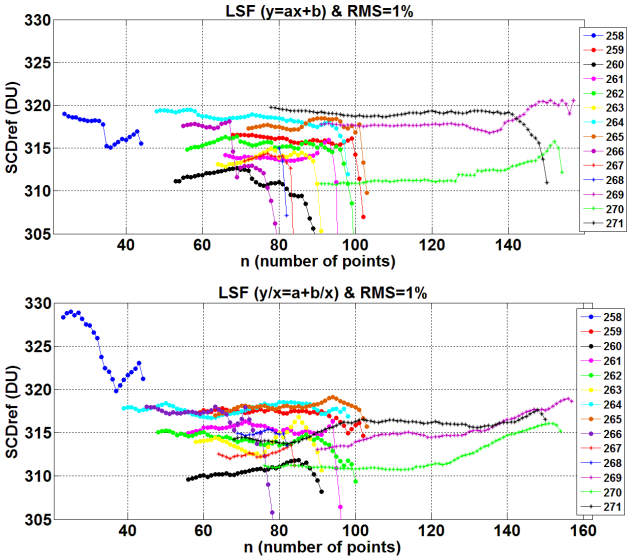

Figure 3. Variation of SCD_{REF} as a function of the number of data points in the regression up to the point where RMS = 1% for all days of the campaign using the LSF1 (upper panel) and the LSF2 (lower panel) methods.

In Figure 3 the results from all days are summarized. This figure is similar to the upper panel of Figure 2, with the

exception that the derivation of the SCD_{REF} for each day is stopped when the RMS% = 1% is achieved. For the LSF1 method (upper panel) the derived SCD_{REF} for all days are within ~9 DU, while for the LSF2 (lower panel) the range of variation is much larger particularly for day 258. When this day is excluded the differences range within ~8 DU. The final estimates of the SCD_{REF} from all three methods are shown in Figure 4 as a function of day of year. Obviously one could distinguish 2-3 groups of days with very similar results. However, as there is no objective reason to choose a specific group of days, for the calculation of TOC we used the average SCD_{REF} from all days. These estimates are practically the same for both methods: 315.7 DU for LSF1 and 315.6 DU for LSF2, and very close to the values determined by the eye and mind method (314.6 DU). These differences are well within the uncertainties of the TOC retrieval method. Finally, even when the RMS% criterion for the removal of outliers is set to 1.5%, the mean SCD_{REF} is practically the same, 315.6 DU for both methods (see Figure 4).

Ideally, the same value of SCD_{REF} should be derived from the Langley extrapolation applied on data from different days, as long as the spectral characteristics of the instrument remain the same and the TOC during each day remains constant. However, this has not been the case for all days of the campaign due mainly to changing TOC.

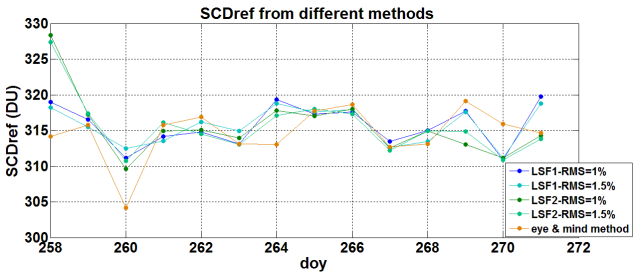

Figure 4. The SCD_{REF} resulted from the three Langley methods as a function of the day of year 2016, using for the removal of outliers the RMS% criteria of 1% and 1.5 %.

Finally, [*Kiedron and Michalsky*, 2016] have discussed one more method for determining the SCD_{REF}, the so-called non-parametric fit (NPF), introduced by [*Theil*, 1950]. A set of n points $P(x_i, y_i)$ produces an $n \times n$ matrix of all possible slopes $a_{i,j}$, where $a_{i,j}=(y_i - y_j)/(x_i - x_j)$, and the slope of the regression is determined as the median of all slopes. From the slope α, the intercept (in our case the SCD_{REF}) is obtained also as the median of $(y_i - \alpha x_i)$. The outliers are removed sequentially until RMS% reaches 1% (1.5%) or until 29% of the outliers are removed. It appears that SCD_{REF} is overestimated for RMS%=1% (327.1 DU) and underestimated for RMS%=1.5% (312 DU). Therefore this method although applied on the campaign data, it has not been taken into account for the TOC retrieval.

Once the SCD_{REF} is determined from the Langley regressions, the TOC for each 3-min set of direct radiance spectra is calculated as:

$$TOC_i = \frac{DSCD_i + SCD_{REF}}{AMF_i}. \qquad (3)$$

Comparison with TOC derived from the AEMET Brewer

Measurements of the Brewer spectrophotometer (#183) are used for the evaluation of the TOC derived from Phaethon. The retrieval of TOC by Brewer spectrophotometers is historically based on the cross-sections by Bass and Paur (BP) [*Paur and Bass*, 1984]. To avoid discrepancies in the comparison caused by the used cross-section dataset, in a first stage, the TOC from Phaethon was derived also using the BP cross-sections. During the campaign both instruments were monitoring the TOC continuously during each day, but not in synchronized mode. The Brewer measurements were available every about 4 min while Phaethon provided TOC every 6 min from spectra averaged over 3 min. To compare the two datasets the Phaethon data were matched with the closest Brewer measurements as long as the time difference between the measurements was smaller than 30 min. A scatter plot of this comparison is shown in Figure 5 for data of all days of the campaign. The range of TOC variation during the campaign was very small (~30 DU), as expected from the season and latitude, therefore the uncertainty of the linear regression is quite large (r^2 = 0.87). Phaethon seems to overestimate the TOC on average by ~2 DU.

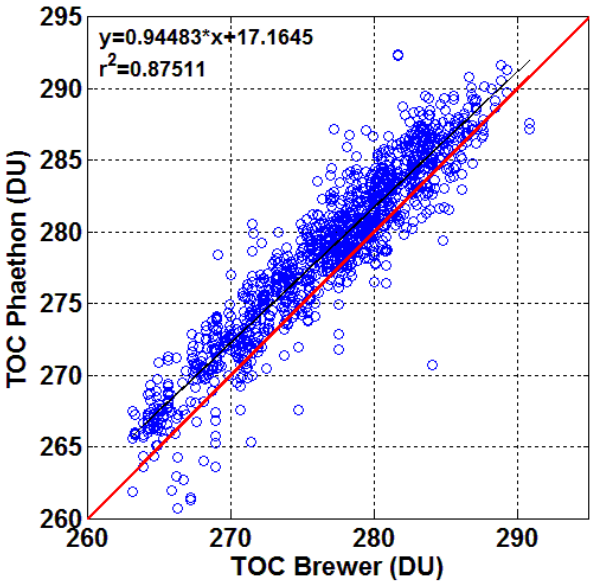

Figure 5. Scatter plot between TOC derived by Brewer and Phaethon. The black line represents the linear regression on the data shown on the top left.

Figure 6 shows a comparison of TOC during the campaign as derived by the Brewer and Phaethon using different ozone absorption cross-section datasets in the DOAS retrieval of Phaethon data. The relevant statistics are summarized in Table 1. The best agreement is found for BP at 228 K, with an average difference of ~0.7%. For the Bremen cross-sections, the one for 223 K leads to an average underestimation of Phaethon TOC by ~2.5%, while the 233 K dataset to overestimation of ~1.6%.

Table 1: Statistics of the comparison of TOC derived by Phaethon and Brewer #183 during the campaign. The DOAS retrieval of Phaethon TOC was based on different ozone cross sections.

O_3 absorption cross-section	Mean difference (%)	Std (% difference)
Bass(228K)	0.69	0.78
Bremen(223K)	-2.47	0.77
Bremen(233K)	1.65	0.79

Conclusions

This study discusses the evaluation of TOC derived from Phaethon system against a reference Brewer spectrophotometer during a 14 day campaign that was held in Izaña, Tenerife, Spain in September 2016. The direct-sun spectral radiance data that were acquired during the campaign have been used to determine the slant column density of the reference spectrum that is used in the DOAS retrieval. Three different Langley regression methods have been tested, using either subjective or objective criteria for the removal of outlier data points. All three methods resulted in very similar estimates of the SCD_{REF}, particularly those based on objective criteria.

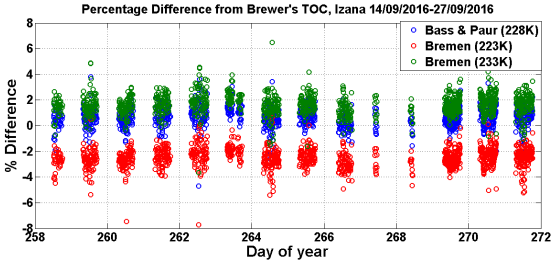

Figure 6. Percentage difference between TOC derived by Brewer based on BP cross-section and Phaethon for different cross-section datasets.

Based on this estimate of SCD_{REF}, the TOC data derived by Phaethon have been compared with the data of Brewer #183 which is one of the reference triad Brewer maintained at Izaña Observatory. When the same dataset of ozone absorption cross-sections, [*Paur and Bass*, 1984], are used in both systems, the agreement is very good with an average overestimation by Phaethon of ~0.7±0.8 %. Use of the Bremen cross-sections at temperatures 223 K and 233 K in the TOC retrieval by Phaethon resulted in underestimation of 2.4 % and overestimation of 1.6%, respectively.

Acknowledgment This work is conducted in the framework of REG(AUTH) of EMRP JRP ATMOZ. The EMRP is jointly funded by the EMRP participating countries within EURAMET and the European Union.

References

Danckaert, T., C. Fayt, M. v. Roozendael, I. d. Smedt, V. Letocart, A. Merlaud, and G. Pinardi (2013), QDOAS Software user manual, 117 pp, BIRA-IASB and S[&]T, http://uv-vis.aeronomie.be/software/QDOAS.

Drosoglou, T., A. Bais, I. Zyrichidou, A. Poupkou, N. Liora, C. Giannaros, MarilizaKoukouli, N. Kouremeti, S. Dimopoulos, D. Balis, and D. Melas (2016), Comparison of ground-based tropospheric NO2 columns with OMI/AURA products in the greater area of Thessaloniki by means of an air quality modeling tool, paper presented at 13th International Conference of Meteorology, Climatology and Atmospheric Physics, Thessaloniki, Greece, 19-21 September 2016.

Gkertsi, F., A. F. Bais, T. Drosoglou, K. Fragkos, I. Fountoulakis, and N. Kouremeti (2016), Total Ozone Data Retrieval from the Phaethon DOAS System, paper presented at 13th International Conference of Meteorology, Climatology and Atmospheric Physics, Springer, Thessaloniki, Greece, 19-21 September 2016.

Kiedron, P. W., and J. J. Michalsky (2016), Non-parametric and least squares Langley plot methods, *Atmos. Meas. Tech.* ***9***, 215-225.

Kouremeti, N., A. F. Bais, D. Balis, and I. Zyrichidou (2013), Phaethon: A System for the Validation of Satellite Derived Atmospheric Columns of Trace Gases, in *Advances in Meteorology, Climatology and Atmospheric Physics*, edited by C. G. Helmis and P. T. Nastos, pp. 1081-1088, Springer Berlin Heidelberg.

Paur, R. J., and A. M. Bass (1984), The ultraviolet cross-sections of ozone: II. results and temperature dependence, *Ozone Symposium, Chalkidiki*, 611-616.

Platt, U., and J. Stutz (2008), *Differential optical absorption spectroscopy. Principles and Applications*, Springer-Verlag, Berlin Heidelberg.

Redondas, A., S. F. León-Luis, V. Carreño, B. Hernández, J. López-Solano, A. Berjón, D. Santana-Díaz, and M. Rodriguez (2016), Stability of the RBCCE triad during the period 2005-2015, in *Quadrennial Ozone Symposium*, edited, Edinburgh, UK.

Theil, H. (1950), A rank-invariant method of linear and polynomial regression analysis, *I, II, III, Nederl. Akad. Wetensch., Proc.* **53**, 386–392, 521–525, 1397–1412.

A Fourier Transform Spectroradiometer for measurements of the relative direct solar spectral irradiance from 305 nm – 380 nm with a resolution of <0.05 nm

I. Kröger, S. Riechelmann, P. Sperfeld, and S. Winter

Physikalisch-Technische Bundesanstalt, Braunschweig, Germany

Introduction

A Bruker Vertex 80 Fourier Transform Spectroradiometer (FTS) was adapted for performing high-resolution relative direct solar spectral irradiance measurements [1]. The adaptations included the development of an entrance optics suitable for direct solar spectral irradiance measurements, a spectral adapted monitor filter radiometer as well as a temperature controlled transport housing of the combined instrument. During the Total Ozone Measurements Intercomparison at Izaña, Tenerife, high-resolution direct spectral irradiance measurements were performed in order to determine a high resolution UV range relative extra-terrestrial spectrum (ETS) using the Langley extrapolation method.

Instrumentation

The suitability of a Fourier Transform Spectroradiometer for *global* solar UV measurements has been shown in Ref. [2]. Here we present the adaptation of a FTS for *direct* solar UV measurements that needed an additional development of a suitable entrance optics. The new entrance optics of the FTS and the FTS itself was previously described in Ref [1]. The entrance optics shown in Fig. 1 consists of a tube with a clear aperture of 50.8 mm. The incoming light is focused by a biconvex lens with focal length f = 200 mm on a plane 50 mm behind the entrance of the quartz glass fiber bundle of diameter of 7 mm. This enables a homogeneous illumination of the fiber bundle as well as an optical gain of a factor of approximately 50 that leads to a significant improvement of the signal to noise ratio (SNR). The field of view (FOV) is limited by the tube extension and an aperture at the end of the tube. It was experimentally determined to be approximately ± 3.5°.

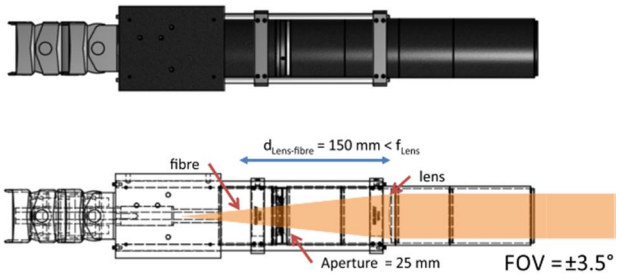

Figure 1. Technical drawing of the entrance optics. [1]

A GaP-diode combined with an UG11 bandpass filter was chosen as broadband detector that is limiting the spectral responsivity of the instrument from 250 nm to 400 nm.

The long-term stability i.e. reproducibility of the FTS measurements is crucial for the applicability of this instrument for Langley extrapolation measurements. The parameters for optimal performance are summarized in Table 1.

Stability tests were performed using a very stable Xenon lamp (Hamamatsu LC8) as well as the halogen lamp integrated in the FTS instrument. Repetitive measurements (30 s duration) of the spectrum were performed over several hours. Unfortunately, the instability of the absolute scale of the FTS was found to be > 5 %. However, the *relative* spectrum, i.e. the spectrum normalized to its integral value as well as the relative shape of the spectrum, was found to be much more stable (< 0.5 %). Since for the Langley extrapolation method measurements at different air masses (AM) during the course of a day are needed, the stability of the absolute scale during the day is crucial. Therefore, a monitor filter radiometer (FR) was designed for correcting this instability.

Table 1. FTS Parameters for the direct solar spectral irradiance measurements.

Resolution:	2 – 4 cm^{-1}
Phase resolution:	4 – 8
Aperture:	1.5 mm
Detector:	RT-GaP (+UG11)
Scanner Velocity:	20 kHz
Gain:	8 x B
High freq. limit:	33500 cm^{-1}
Laser wavenumber:	15802.38 cm^{-1}
High Pass filter:	On
Low Pass filter:	Automatic
Acquisition:	Double sided, Forw. + Backward
Phase correction:	Power Spectrum
Zerofilling factor:	4
Apodization func.:	Blackman-Harris 3-Term

The filter radiometer correction factor f_{FR} can be derived as

$$f_{FR} = \frac{U_{FR}/R_{shunt}}{\int s_{FR}(\lambda)\cdot E_{rel,FTS\ corr}(\lambda)d\lambda}, \quad (1)$$

where U_{FR} is the measured voltage corresponding to photocurrent of the filter radiometer, R_{shunt} is the shunt resistance, $s_{FR}(\lambda)$ is the spectral responsivity of the filter radiometer, and $E_{rel,FTS\ corr}$ is the radiometric corrected normalized relative spectral irradiance measured by the FTS.

By multiplying the FTS measurement counts with the correction factor f_{FR} that has been derived simultaneously, the absolute instability over time is compensated.

The filter radiometer consists of a 2.2 mm x 2.2 mm GaP photodiode combined with a UG11 filter. It is mounted on a Peltier element and into a housing. A Pt100 temperature

sensor is attached to this housing for temperature stabilization. In order to define the field of view of the filter radiometer the detector is incorporated into a tube with round 1.5 mm and 3 mm apertures as well as an additional aperture for stray light reduction.

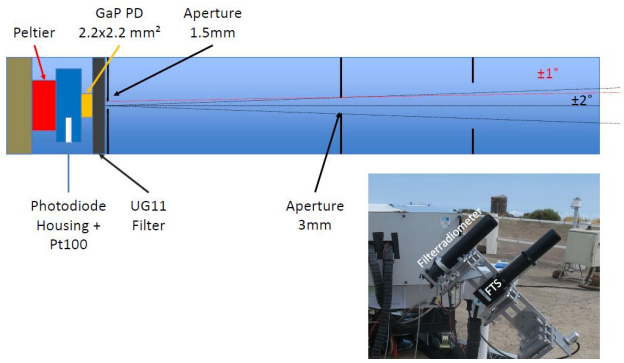

Figure 2. Schematic of the filter radiometer as well as an image of the FTS and filter radiometer entrance optics mounted on a solar tracker.

A schematic is shown in Fig. 2. The corresponding instrumentation consists of a Hameg power supply, a relay switching unit and a Keithley 2001 multimeter for temperature stabilization of the detector. The set point temperature is 30 °C. The photocurrent is determined by using a high precision Burster shunt resistance (1 kOhm) and a Keithley 2182A Nanovoltmeter. All instruments are located within the temperature stabilized transportable housing of the FTS. The temperature of the shunt resistance as well as the Keithley multimeter could be kept constant at ± 3 K over the course of a day. The combined uncertainties related to linearity, accuracy and temperature coefficients of the multimeter and shunt resistance are in the order of < 0.01 % and can therefore be neglected. The temperature of the photodiode and the filter was stabilized to ± 0.2 K.

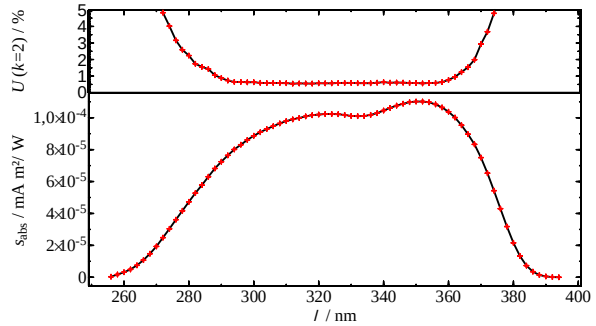

Figure 3. Spectral responsivity of the filter radiometer (bottom) and its expanded measurement uncertainty (top).

The spectral responsivity (see Fig. 3) as well as the spectral temperature coefficient of the filter radiometer was calibrated prior to the measurement campaign using the DSR-facility at PTB.

During operation at Izaña Observatory, typical photocurrents < 3 µA were obtained, so that the photodiode can be considered to operate in its linear working range. The uncertainty related to the temperature coefficient of the filter radiometer was determined to be < 0.2 % (due to the blocking of the spectral range with high temperature coefficient > 380 nm).

Both FTS entrance optics and filter radiometer were mounted on a solar tracker. Correcting the (radiometric and background corrected) FTS spectra by multiplication with the monitor filter radiometer correction factor f_{FR} the uncertainty related to the stability of the FTS spectrum can be reduced to approximately < 0.2 %.

The solar tracking was performed using a sun-sensor with an accuracy of approx. 0.01°. The alignment of the FTS and the filter radiometer entrance optics was carried out by measuring the plateau of the corresponding FOV and consecutively setting the alignment to the center of the plateau using alignment screws. The air masses used for the Langley extrapolation method are derived from the solar tracker, which calculates it by deriving the solar zenith angle from its GPS coordinates and the GPS time.

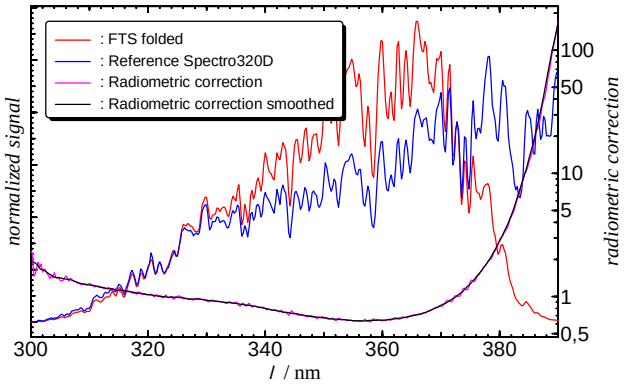

Figure 4. The radiometric correction function is derived from a comparison of a calibrated reference spectroradiometer (blue) and the FTS (red) using natural sunlight at clear sky conditions.

Determination of the radiometric correction function of the FTS

An ordinary radiometric calibration of the FTS using a calibrated standard lamp is not possible since the entrance optics of the FTS contains a lens that collimates the incident irradiance on the entrance of the optical fiber. The divergent beam of the lamp will lead to different locations of the wavelength dependent focal plane compared to the parallel beam of the sun. This results in different wavelength dependent coupling of the radiation into the optical fiber leading to a different relative spectrum.

To overcome this limitation, the radiometric calibration was performed by a direct comparison with a radiometric calibrated reference spectroradiometer using direct natural sunlight at clear sky condition. The reference spectroradiometer was a Spectro320D double-monochromator system having a fiber based entrance optics for direct spectral irradiance. That system is thoroughly characterized and calibrated traceable to the PTB spectral irradiance scale. A series of 15 measurements was performed. The integration time of the FTS was matched to the integration time of the Spectro320D. Both spectra were corrected by subtracting the background signal. Since we are interested in a relative correction function, both spectra were normalized to its integral value. For comparison the high resolution spectra of the FTS were folded with the known slit function of the Spectro320D. The result is shown in Fig. 4. The radiometric correction function of the FTS is the average of the ratio between

reference spectrum and FTS. Finally, the correction function was smoothed in order to remove artefacts from the folding algorithm. Uncertainties related to the radiometric correction originate from the radiometric reference as well as the standard deviation of the 15 subsequent calibrations, i.e. the reproducibility of the calibration. In conclusion, the major uncertainty contributions to the relative direct spectral irradiance scale of the FTS measurement are summarized in Fig. 5.

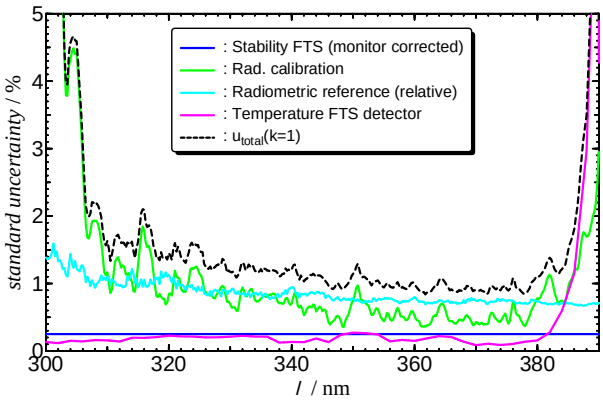

Figure 5. Uncertainty budget for a measurement of the relative direct spectral irradiance scale of the FTS measurement.

Wavelength correction of the FTS

During test measurements, it was observed that there is a systematic wavelength shift to higher wavelengths and an increasing asymmetry of the line shape if the internal FTS aperture size is increased (i.e. for higher throughput and better signal to noise ratio). This observation is exemplary shown in Fig. 6.

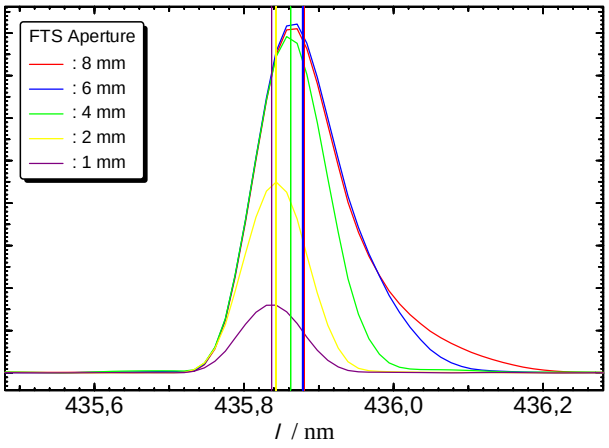

Figure 6. The measured line shape and the center wavelength of a Hg-line changes dependent on the chosen internal FTS aperture.

An estimate of an aperture size related wavelength correction function was determined by measuring several lines of an Hg-discharge lamp dependent on internal aperture size. As shown in Figure this wavelength error is dependent on wavelength and aperture size. It can be minimized going to low aperture sizes to the cost of lower throughput and a reduced signal to noise ratio. However, in the case of direct spectral irradiance measurements with the collecting entrance optics the FTS could be operated with an aperture size of 1.5 mm and sufficient high SNR. According to Fig. 7, the uncertainty related to the wavelength scale of the FTS was estimated to be < 0.01 nm. This also includes other uncertainty contributions (see Ref. [2]).

FTS Measurements at the Total Ozone Measurements Intercomparison at Izaña Observatory

The total ozone measurements intercomparison at Izaña Observatory was carried out from 12th – 30th of September 2016. The FTS instrument was located on a platform close to the observatory (Figure 8).

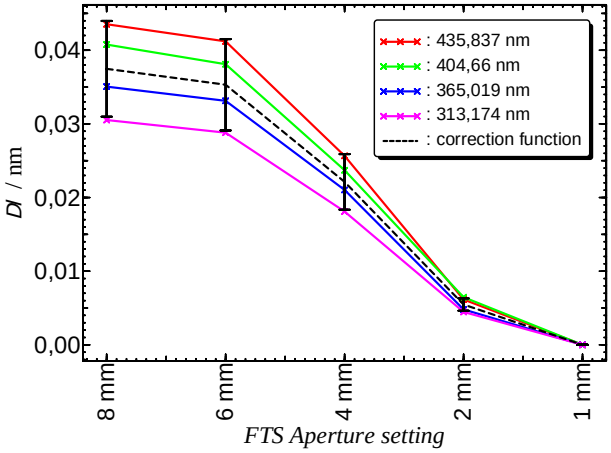

Figure 7. Empirical derived estimated systematic wavelength error of the FTS dependent on the chosen internal aperture.

Measurements were typically performed automated and continuously from sunrise to sunset. Prior sunrise and after sunset measurements of the background signal of both filter radiometer and FTS spectra were taken using a covering cap on the entrance optics tubes. These measurements were used for the background correction of the daily collected data.

Figure 8. Picture of the combined FTS instrument during the total ozone measurements intercomparison at Izaña Observatory.

In the following exemplary data collected on 14th of September will be shown. From the data the solar tracker recorded, the air mass values were correlated to the assigned UTC time stamp (Figure 9).

The filter radiometer measured the photocurrent in steps of 1 s. Exemplary data of a day with good atmospheric conditions is shown in Fig. 10. The dotted line denotes the background measurement with a cap on the filter

radiometer entrance optics. The air mass values are correlated to the filter radiometer measurement via the time stamp and the tracker data. The fluctuations at noon are most likely related to atmospheric conditions.

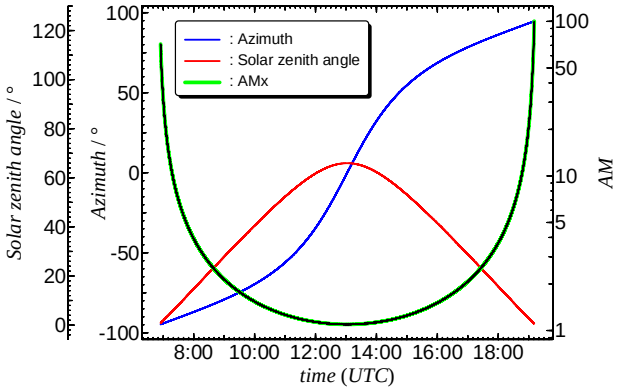

Figure 9. Air mass (AM) calculated from Tracker data and corresponding filter radiometer current.

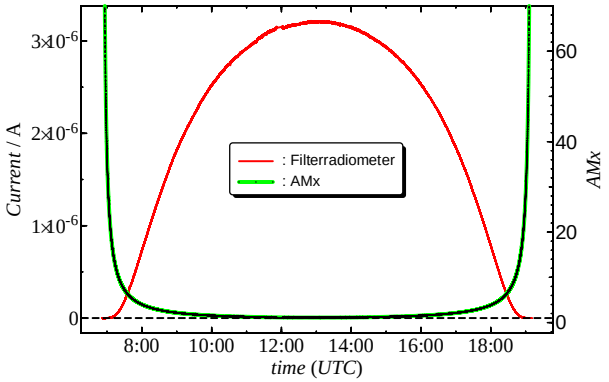

Figure 10. Photocurrent measured with the filter radiometer over the course of a day on 14th of September.

Using the filter radiometer as a monitor and using the corrections previously described, high-resolution relative spectra over air mass can be determined as

$$E_{\mathrm{FTS,rel}} = (counts_{\mathrm{FTS}}(\lambda) - \overline{counts}_{FTS,dark}(\lambda)) \cdot f_{\mathrm{rad,corr}}(\lambda) \cdot f_{\mathrm{FR}}, \quad (2)$$

where $counts_{\mathrm{FTS}}(\lambda)$ is the measured spectrum, $counts_{\mathrm{FTSdark}}(\lambda)$ is the measured averaged background spectrum, $f_{\mathrm{rad,\,corr}}(\lambda)$ is the radiometric correction function, and f_{FR} is the filter radiometer correction

One measurement takes approximately 30 s, which corresponds to an internal averaging of 53 interferograms. A series of air mass-dependent spectra is shown in Figs. 11 and 12.

These spectra are measured with a resolution of 4 cm^{-1} corresponding to a wavelength resolution < 0.05 nm. Figure 11 shows the dynamic range of the FTS spectra over 3 orders of magnitude. Spectra could be recorded even for high air masses. However, the dynamic range is probably not sufficient for the application of the Langley extrapolation method in the spectral range below 305 nm.

The high spectral resolution and the wavelength stability over the course of one day can be seen in Fig. 12, where all FTS spectra from AM1.1 – AM12 in the spectral range from 317 nm – 318.3 nm are shown.

Based upon such a dataset the *relative* extra-terrestrial spectrum can be derived. The absolute high resolution ETS is then derived by the combination of the *relative high resolution* FTS ETS and an *absolute low resolution* ETS derived from a reference spectroradiometer, such as the QUASUME spectroradiometer from PMOD/WRC. This work is described by Gröbner et al. [3].

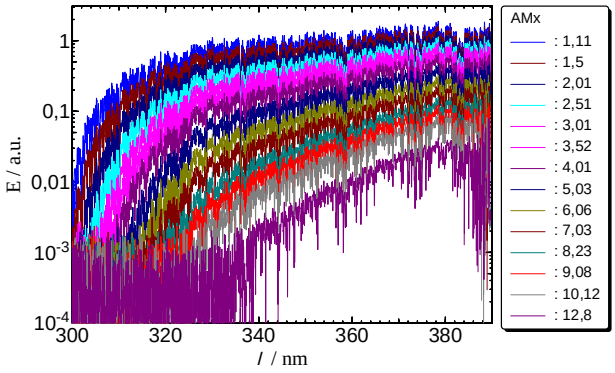

Figure 11. Exemplary corrected FTS spectra for air masses ranging from AM1.1 – AM12 for the 14th of September showing the dynamic range over three orders of magnitude.

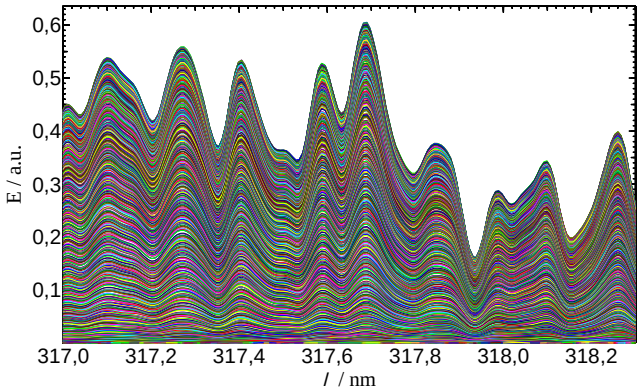

Figure 12. All FTS spectra measured from AM1.1 – AM12 in the spectral range from 317 nm – 318.3 nm showing the high wavelength resolution (< 0.05 nm) and the wavelength stability of the instrument.

Conclusions

A combined FTS instrument consisting of a solar tracker including suitable mounts for different entrance optics, a filter radiometer monitor and the Bruker Vertex 80 FTS itself were characterized and prepared for outdoor measurements of the direct solar irradiance. During the Total Ozone Measurements Intercomparison at Izaña high resolution spectra of the direct solar irradiance were measured from 300 nm – 380 nm with a spectral resolution of < 0.05 nm dependent on the air mass from AM1.1 – AM20. From these datasets, a *relative* high-resolution ETS can be derived.

Acknowledgement The research work leading to this article was partly carried out within the EMRP ENV59 project "ATMOZ". The EMRP is jointly funded by the EMRP participating countries within EURAMET and the European Union.

References

[1] I. Kröger und S. Winter, "Adaptation of a Fourier Transform Spectroradiometer for outdoor measurements of the direct solar spectral irradiance," *UV News* **11**, 31-31 (2016).

[2] P. Meindl, M. Wähmer und C. Monte, "Usability of a Fourier transform spectroradiometer for absolute surface spectral solar UV irradiance measurements," *Optics Express* **22**, 25071-25083 (2014).

[3] J. Gröbner, I. Kröger, L. Egli und H. Gregor, "Determining the solar extraterrestrial irradiance spectrum from the surface," *UV News* **12**, 24-27 (2017).

Determining the solar extraterrestrial irradiance spectrum from the surface

Julian Gröbner[1], Ingo Kröger[2], Luca Egli[1], and Gregor Hülsen[1]

1. Physikalisch-Meteorologisches Observatorium Davos, World Radiation Center, Davos, Switzerland
2. Physikalisch-Technische Bundesanstalt, Braunschweig, Germany

Introduction

Studies aiming at modelling the transfer of the solar radiation through the atmosphere require as main parameter the solar spectrum incident on the top of the atmosphere, for instance to calculate the surface UV radiation using satellite sensors. Similarly, investigations combining solar radiation measurements with radiative transfer calculations to retrieve atmospheric constituents need an accurate representation of the extraterrestrial solar spectrum.

In recent years satellite experiments have measured the solar extraterrestrial spectrum from space to avoid atmospheric absorption and scattering effects, especially at wavelengths shorter than 300 nm where ozone and oxygen in the atmosphere absorb all incident radiation. While pre-launch calibration and characterisation procedures reach very low uncertainties, once in space the possibilities of verifying or recalibrating such an instrument become very challenging. As recent studies have demonstrated (e.g. Schöll et al., 2016), the solar spectra measured from satellite platforms can differ significantly between each other, due in part to instrument degradation issues arising from the harsh space environment and the difficulties in accounting for possible instrument changes between the pre-flight calibration and their operation in space. In a strict metrological sense, such measurements cannot be considered traceable to SI since metrological traceability inherently requires the repeated demonstration of the uninterrupted traceability to primary standards which currently is not available to instruments located in space.

In contrast, while surface-based measurements of the solar irradiance have the disadvantage of needing to account for changing atmospheric conditions, the considerable advantage over space-based instruments is the possibility of recalibrating ground-based instruments and thereby validating and confirming their traceability to SI.

In this study we present ground-based direct spectral solar irradiance measurements obtained with the transportable reference double monochromator spectroradiometer QASUME and a high resolution Fourier Transform Spectrometer (FTS) over the wavelength range 300 nm to 500 nm. A high resolution absolute extraterrestrial solar spectrum is then derived by applying the Langley-plot technique to the measurements of each instrument before combining them to a single solar spectrum.

Instruments and Methods

Measurement location

The measurements were performed at the Izaña Atmospheric Observatory (IZO) located on the island of Tenerife, Canary Island, Spain from 12 to 25 September 2016. IZO is a high mountain station at an elevation of 2373 m.a.s.l above a strong subtropical temperature inversion layer, which acts as a natural barrier for local pollution and low-level clouds. QASUME was installed on the roof of the measurement building at about 20 m above ground, while the FTS was operated on the ground.

QASUME

The transportable reference spectroradiometer QASUME consists of a double monochromator DM150 from Bentham with a focal length of 150 mm and two 2400 lines/mm gratings resulting in a resolution of about 0.86 nm. The whole system resides in a temperature controlled enclosure to allow outdoor operation under constant ambient conditions. The solar radiation is collected with a temperature stabilised diffuser connected via an optical fiber to the entrance slit of the monochromator. A portable lamp system allows the calibration of the whole system while being deployed in the field. A detailed description of the system can be found in Gröbner et al., 2005, and Hülsen et al., 2016. A collimator tube with a field of view of 2.5° is mounted on an optical tracker to which the diffuser head can be fitted, allowing the measurement of direct solar spectral irradiance.

A comprehensive uncertainty budget for global solar spectral irradiance measurements was discussed in Hülsen et al., 2016. Due to the fact that direct solar irradiance measurements are not affected by the directional response of the diffuser nor by the diffuse sky radiation distribution, the resulting expanded uncertainty for direct solar spectral irradiance measurements are reduced from 3.1% for global irradiance measurements to 1.83% in the spectral range 300 nm to 500 nm.

QASUME was calibrated every day using a portable 250 W lamp monitoring system in order to verify its stability and demonstrate its traceability to SI with the quoted uncertainties as described in Hülsen et al., 2016.

FTS

The transportable Fourier Transform Spectroradiometer (FTS) consists of a Bruker Vertex80 Fourier Transform Spectrometer with a customized fibre based entrance optics for direct spectral irradiance measurements, i.e. a collimator tube with a field of view of approximately ± 3.5°. The instrument is installed in a temperature controlled transportable housing. The internal detector is a UG11-filtered GaP-photodiode covering the spectral range from 300 nm to 390 nm. The wavenumber resolution of the FTS was set to 2 cm^{-1} resulting in a wavelength resolution of less than 0.025 nm for this wavelength range. The wavelength scale of the FTS is inherently traceable to SI using a stabilised internal HeNe laser. The wavelength uncertainty is estimated to be equal or less than 0.01 nm.

The entrance optic was mounted on an optical tracker together with a monitor-filterradiometer. The monitor filterradiometer is a temperature controlled UG11 filtered GaP-photodiode mounted within a collimator tube. The

monitor correction turned out to be necessary to correct for the instability of the absolute scale of the FTS spectrum. The monitor correction is a scaling factor derived from the ratio of the measured filterradiometer current and the product of the measured radiometric corrected FTS spectrum and the spectral responsivity of the filterradiometer determined previously at PTB.

The radiometric calibration of the FTS was performed by a comparison with a calibrated spectroradiometer under natural sunlight condition. The expanded uncertainty for measurements of the relative direct solar spectral irradiance was determined to be 2% to 4% in the spectral range 310 nm to 380 nm.

Results

Direct solar irradiance measurements were performed in the period 14 to 24 September 2016. The extraterrestrial solar spectrum was retrieved from the measurements by applying the Langley-Plot method to individual half-days in which there were cloud-free conditions. The Beer-Lambert law can be written as,

$$\log I_\lambda = \log I_\lambda^0 - \tau_\lambda m, \quad (1)$$

where I_λ is the irradiance measurement at wavelength λ, I_λ^0 the solar irradiance at the top of the atmosphere, τ_λ the total optical depth through the atmospheric column and m the airmass. By using measurements of one half-day and applying a linear regression of the data versus airmass m, it is possible to retrieve the intersect, I_λ^0, and the slope, τ_λ, assuming that the atmosphere remained constant during this period. Obviously this criterium is never exactly fulfilled, and therefore measurement sites are chosen to minimize the effect of atmospheric variability on this method. For measurements in the wavelength range 300 nm to 500 nm, the most important atmospheric component affecting the measurements is the atmospheric ozone in the wavelength range shorter than 340 nm, followed by changes in atmospheric aerosols. These conditions are satisfied at IZO, since it is a high altitude station with very low aerosol concentrations, and due to its low latitude in proximity of the equator, also the total column of atmospheric ozone is very constant during this period of the year.

Figure 1 shows the measurements of QASUME on 15 September.

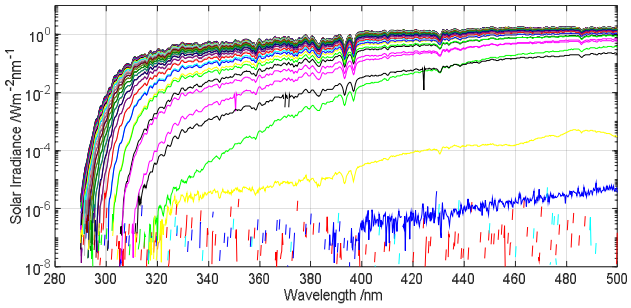

Figure 1. Direct solar spectral irradiance from QASUME on 15 September 2016.

As can be seen in Figure 1, the solar spectrum extends over more than 6 orders of magnitude. In order to retrieve the extraterrestrial solar spectrum over the 300 nm to 500 nm wavelength range, measurements between airmass 1.1 and 3.5 are extrapolated to zero airmass using Equation 1. The resulting solar spectrum at zero airmass for the morning and afternoon measurements of 15 September 2016 (see Figure 1) are shown in Figure 2.

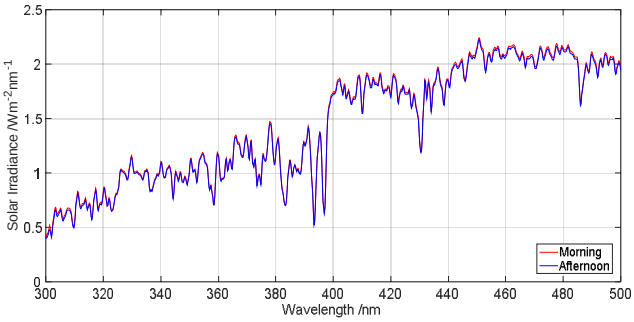

Figure 2. Extraterrestrial solar spectra retrieved from the direct solar spectral irradiance measurements of QASUME shown in Figure 1.

In total 17 half-days are available from QASUME for deriving an extraterrestrial (ET) solar spectrum. The objective criteria for rejecting data were 1) if clouds developed during the measurement period and obscured the solar disk and 2) instrument malfunction. A criterium based on the atmospheric stability (aerosol optical depth absolute value or variability) was not included so as not to introduce a possible bias to the retrieved solar ET spectra.

Figure 3 shows the ratios of all 17 solar ET spectra to their average.

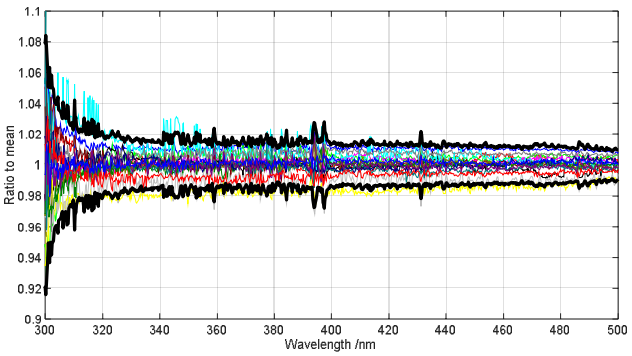

Figure 3. Ratio of the 17 solar ET spectra retrieved from QASUME measurements. The black curves represent the standard deviation of the measurements multiplied by 2.

The variability of the retrieved solar ET spectra shown in Figure 3 as the thick black line was calculated as twice the standard deviation of the measurements. It is mostly due to atmospheric changes in total column ozone and aerosol optical depth on particular half-days. This variability gradually increases from 1.1% at 500 nm to 2.0% at 320 nm, followed by a more rapid increase to 7% at 300 nm. Assuming that the observed variability is independent between each application of the retrieval procedure and therefore occurs randomly, we can calculate the standard error of the resulting average extraterrestrial solar spectrum and combine it with the uncertainty of the measurements mentioned previously. The resulting relative expanded uncertainty U of the average QASUME solar ET spectrum (k = 2, assuming a 95% coverage probability) is less than 2% between 305 nm and 500 nm, and rising to 3% at 300 nm. In summary, the solar ET irradiance spectrum derived from applying the Langley-plot technique to QASUME

measurements has an expanded uncertainty of 3% or less between 300 nm and 500 nm.

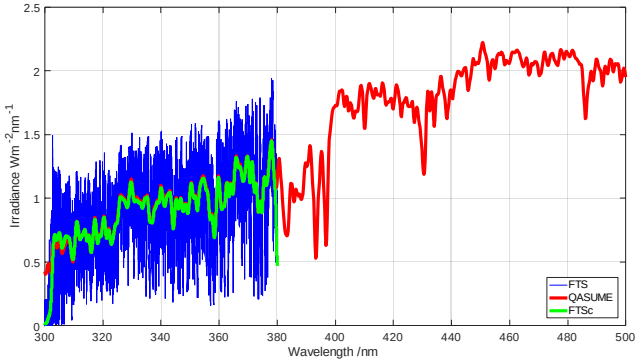

Figure 4. Solar ET spectra derived from QASUME (red) and FTS measurements (blue). The green curve represents the FTS ET spectrum convolved with the QASUME slit function.

The same procedure was applied to the FTS measurements to derive a solar ET spectrum. In the case of the FTS, the measurements from 20 to 22 September with a spectral resolution of 0.025 nm were used to retrieve the average ET spectrum for the FTS. Additional FTS measurements before and after these dates were also available but with different spectral resolutions and not covering the whole day to allow for retrieving an ET spectrum. Figure 4 shows the QASUME derived solar ET spectrum, the high resolution FTS solar spectrum, and the FTS solar spectrum convolved with the slit function of the QASUME spectroradiometer.

As can be seen in the figure, the FTS derived ET spectrum is only valid for wavelengths longer than 305 nm. At shorter wavelengths, the sensitivity of the instrument did not allow measurements at high enough airmass to perform a zero-airmass extrapolation.

The composite QASUMEFTS solar ET spectrum

The following procedure was applied to derive a solar ET spectrum in the range 304.8 nm to 379 nm with the high resolution from the FTS and the low absolute uncertainty of QASUME: The scale of the QASUME ET spectrum (red curve in Figure 4) was transferred to the high resolution FTS spectrum (blue curve in Figure 4) by calculating the ratio between the FTS ET spectrum convolved with the QASUME slit function (green curve in Figure 4) and the QASUME spectrum and applying it to the high resolution FTS ET spectrum. The resulting solar ET spectrum extends from 304.8 nm to 379 nm, has a spectral resolution of 0.025 nm and has an expanded uncertainty of 2% over the whole wavelength range based on the QASUME uncertainty as discussed previously.

In order to extend the high resolution solar ET spectrum over the full wavelength range of the QASUME spectrum, we applied the same procedure described in the previous paragraph using the high resolution solar spectral atlas from Kitt Peak for the wavelength range 300 nm to 304.8 nm and 379 nm to 500 nm to transfer the QASUME irradiance scale to the Kitt Peak high resolution solar spectrum. Furthermore, we used ATLAS-3 for the wavelength range between 280 nm and 300 nm even though no information from QASUME nor the FTS could be applied to this part of the solar spectrum.

The resulting composite solar ET spectrum extends from 280 nm to 500 nm; the expanded uncertainty *U* of 2% or better is valid for the wavelength range 305 nm to 500 nm, while between 280 nm to 300 nm the estimated uncertainty is slightly higher and based on the ATLAS-3 solar spectrum (Thuillier et al., 2004).

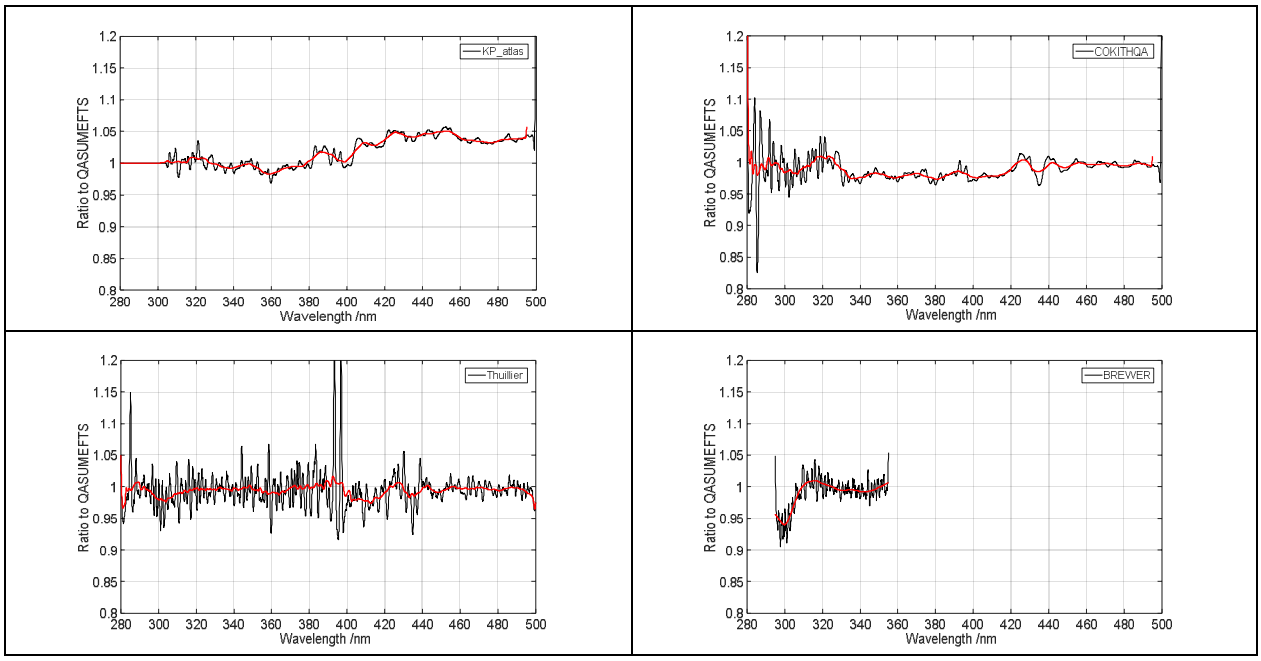

Figure 5. Ratio between extraterrestrial solar spectra and the QASUMEFTS solar spectrum. From top to bottom: Kittpeak combined with Atlas-3 (KP_atlas), Spectrum created in the EMRP SolarUV project (COKITHQA, Egli et al., 2012), Solar spectrum SOLSPEC (Thuillier et al., 2004), and Solar spectrum derived at Maunaloa (Gröbner and Kerr, 2001).

Discussion

We have compared the newly derived extraterrestrial solar spectrum QASUMEFTS with several solar spectra commonly used in the community. The spectra were convolved with a common triangular 1 nm bandpass slit function and shifted to air wavelengths where necessary. Figure 5 shows the ratio between these solar spectra and the QASUMEFTS spectrum. Furthermore, the ratios were also smoothed with a 10 nm running mean to reduce the spectral noise in order to highlight the differences in absolute irradiance between the spectra and the QASUMEFTS spectrum. As can be seen in the figures, the absolute agreement between the spectra is in general better than 5%. High frequency spectral noise is seen in the COKITHQA spectrum at short wavelengths and in the Thuillier spectrum. The latter is due to the medium resolution of this spectrum (about 0.15 nm) and the corresponding limitations in convolving this spectrum with a 1 nm slit function. Furthermore, some wavelength alignment differences might also affect the ratio. The Brewer spectrum was derived from measurements obtained at Maunaloa by the same technique as described here (Gröbner and Kerr, 2001). The agreement is excellent above 310 nm, while at shorter wavelengths an under-estimation of up to 5% at 300 nm is apparent.

Conclusions

The QASUMEFTS solar spectrum is a high resolution solar extraterrestrial spectrum combined from ground-based measurements with a fourier-transform spectrometer and a medium resolution scanning double monochromator spectroradiometer. As described in this manuscript, the spectrum has the high spectral resolution from the measurements of the FTS and the absolute irradiance level from the QASUME measurements. The resulting QASUMEFTS spectrum has therefore an expanded uncertainty of 2% across the wavelength range from 305 nm to 500 nm, lower than any published solar extraterrestrial spectra so far. This spectrum has been validated by comparison to solar spectra widely used in the community and can be used as a benchmark solar spectrum.

Acknowledgments NSO/Kitt Peak FTS data used here were produced by NSF/NOAO. The data is available from ftp://vso.nso.edu/pub/Kurucz_1984_atlas/. This work has been supported by the European Metrology Research Programme (EMRP) within the joint research project EMRP ENV59 "Traceability for atmospheric total column ozone." The EMRP is jointly funded by the EMRP participating countries within EURAMET and the European Union.

References

Egli, L., Gröbner, J., Shapiro, A.,:2012. Development of a New High Resolution Extraterrestrial Spectrum, PMOD/WRCAnnual report 2012, http://www.pmodwrc.ch/annual_report/2012_PMODWRC_Annual_Report.pdf

Gröbner, J., and J. Kerr, Ground-based determination of the spectral ultraviolet extraterrestrial solar irradiance: Providing a link between space-based and ground-based solar UV measurements, *J. Geophys. Res.* **106**, 7211-7217 (2001).

Gröbner, J., J. Schreder, S. Kazadzis, A. F. Bais, M. Blumthaler, P. Görts, R. Tax, T. Koskela, G. Seckmeyer, A. R. Webb, and D. Rembges, Traveling reference spectroradiometer for routine quality assurance of spectral solar ultraviolet irradiance measurements, *Appl. Opt.* **44**, 5321-5331 (2005).

Hülsen, G., J. Gröbner, S. Nevas, P. Sperfeld, L. Egli, G. Porrovecchio, and M. Smid, Traceability of solar UV measurements using the QASUME reference spectroradiometer, *Appl. Opt.* **55**, 7265-7275 (2016).

Schöll, M., De Wit, T.D., Kretzschmar, M. and Haberreiter, M.: 2016, Making of a solar spectral irradiance dataset I: observations, *J. Space Weather Space Clim.* **6**, A14 (2016). Doi: 10.1051/swsc/2016007.

Thuillier, G., Floyd, L., Woods, T.N., Cebula, R., Hilsenrath, E., Hersé, M., Labs, D., In: Pap, J., Fox,P. (eds.) Solar Variability and Its Effect on Climate, *AGU Monogr.* **141**, 171 (2004). doi:10.1029/141GM13.

Operation of a wavelength ruler for the characterization of spectroradiometers for O_3 measurement at the 2016 Izaña field campaign

O. El Gawhary[1], N. van der Leden[1], A. Berjón[2], A. Redondas[2,3], L. Egli[4], I. Kröger[5], P. Sperfeld[5], and J. Gröbner[4]

1. VSL, Dutch Metrology Institute, Delft, the Netherlands.
2. University of La Laguna, Tenerife, Spain
3. AEMET, Agencia Estatal de Meteorologia, Tenerife Spain.
4. Physikalisch-Meteorologisches Observatorium Davos, World Radiation Center, Davos, Switzerland
5. Physikalisch-Technische Bundesanstalt, Braunschweig, Germany

Abstract

In September 2016, within the EMRP project ENV59 ATMOZ: *Traceability for the atmospheric total column ozone*, a three-week measurement campaign has been organized at the Centro de Investigación Atmosférica de Izaña, Tenerife, Spain. The goal of the campaign was to gather different types of instruments, Dobson and Brewer spectroradiometers or new type of scanning of array-based instruments to perform a series of co-located Total Column Ozone (TOC) measurements. Both Meteorology Institutes and National Metrology Institutes (NMIs) have participated in the campaign.

Besides to these measurements, a series of lab and on-field calibration activites have taken place as well. One of these activities concerned the calibration of the wavelength scale of instruments. In this newsletter we report on some of the *in-situ* wavelength scale calibrations performed through a portable wavelength ruler developed by VSL within the said project.

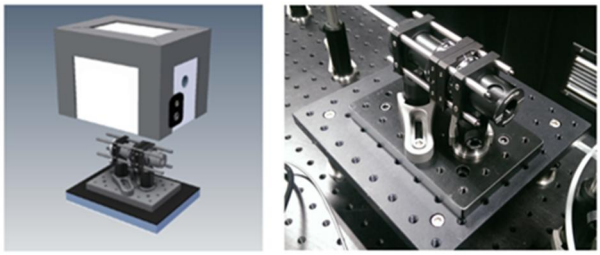

Figure 1. A view of the wavelength ruler in all its main components (left) and a detail on the actual realization for the optical components (right).

INTRODUCTION

Spectroradiometers, measuring spectral radiance or irradiance, require calibration of their wavelength scale. In the UV part of the spectrum there are no many reference lines available and they are not equally distributed in the spectral range of interest. Additionally, they can consist of multiplets or they can be of low intensity. Finally, not all the wavelength standards can be conveniently used for on-site calibrations. VSL has realized a wavelength ruler for wavelength scale calibration in the range 290 – 350 nm. The basic idea behind this instrument can be found in previously available documents and will not be repeated here [1-9]. In the following section we will describe how the system works and how it can be operated to perform on-field wavelength scale calibrations.

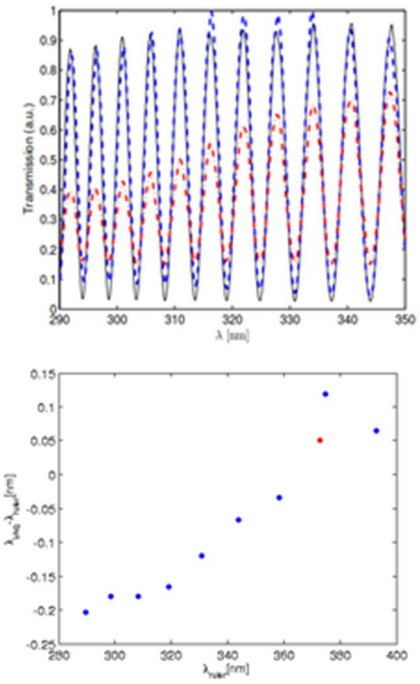

Figure 2. Spectral response of the wavelength ruler as measured by three different systems. Top: Transmission as measured by three different systems. The red curve has been measured by a double-monochromator system available at VSL. The blue and black curves have been measured by two array spectrometers produced by two different manufacturers. Bottom: difference between reference wavelength and wavelength scale of an array spectrometer. The red dot represents the measured wavelength of a reference laser line at 372 nm.

MEASUREMENT PRINCIPLE

The wavelength ruler is essentially a properly designed spectral filter which provides a regular interference-like pattern. If such pattern is stable enough and known, it can be used to determine the accuracy of the wavelength scale of the instrument of interest. A typical measurement consists of, at least, three measurements:

1. a dark measurement, with no input signal offered to the spectroradiometer,
2. a measurement with the light coming from a broad-band source directly measured by the spectroradiometer to be calibrated, and
3. a measurement where the wavelength ruler is inserted between the light source and the spectroradiometer.

By taking the ration between the dark-measurement corrected data from step 3 and step 2, one is essentially left

with the reference spectrum of the wavelength ruler which can then be used to determine the wavelength scale of the instrument of interest. In our case, the light source used to perform the measurements is a Light-Driven Light Source (LDLS) Energetiq EQ-99, arranged in a way to produce a collimated beam of radius of about 20 mm diameter. A long pass filter at 280 nm has also been placed on the beam path, in order to prevent radiation below that wavelength from reaching the instruments.

An overview of the ruler is shown in Fig. 1 while in Fig. 2 we provide a typical measured spectrum.

Figure 3. Wavelength scale calibration, by means of the wavelength ruler, of different instruments. The light source used for the measurements (LDLS-Energetiq 99) is on the breadboard. In the picture, its beam is measured by a Brewer instruments at daylight conditions.

During the measurement campaign of Izaña, different types of instruments have been measured and under different measurement conditions. Fig. 3, Fig. 4, Fig. 5, Fig. 6 give an overview of the different configurations employed to perform the measurements.

Figure 4. Wavelength scale calibration, by means of the wavelength ruler, of different instruments. In this picture it is also shown (right panel) how the measurements can take place into a light-tight box where a fiber-coupled instrument is being measured.

SOME MEASUREMENT RESULTS

In Fig. 7 we show the wavelength scale of the device measured with respect to the scale of the ruler as measured at VSL before the campaign.

There appears to be some common feature among all the measurements (in particular a little bump at 316 nm which is visible in almost all the measurements). That is very likely something that comes from VSL scale. However in that point the deviation bewteen the scale of the FTS instument of PTB and the ruler scale is 0.048 nm which is at the edge of what can actually be achieved with the instrument at *in-situ* measurement conditions.

Figure 5. Wavelength scale of the ruler measured by the Fourier Transform Spectro(radio)meter of PTB.

The other instruments shown in the Fig. 7 are two Bewer spectroradiometers operated by AEMET, an array-based instrument developed by PMOD (Avodor) and an instrument by GigaHertz Optik instrument (operated by PTB during the campaign), denoted by PTB BTS2048-UV-S.

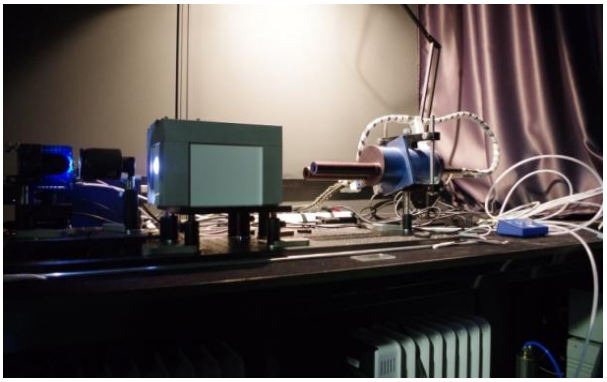

Figure 6. The LDLS and the wavelength ruler used for indoor calibration. The wavelength ruler is the white box interposed between the LDLS source and the device under test.

As it is possible to appreciate from Fig. 7, each instrument covers a particular spectral range, with all ranges overlapping in the spectral region from 290 nm to 355 nm. The positions of the peak wavelengths for each line has been determined by means of a centroid method, where the line shape of each measured line has been used as weighting factor to determine the expectation value of the corresponding central wavelength. For all instruments, only not partially measured lines have been used to determine the peak wavelengths. For some of the instruments, independent methods have also been employed to assess the wavelength scale. This is the case, for instance, for the scale deviation of the PTB BTS2048-UV-S spectroradiometer, which has been independently assessed thorugh Hg-lines, line spread functions with tuneable lasers and calculations with Matshic. The offset

of about -0.1 nm indicated in Fig. 7 is consistent with what found by using the said methods.

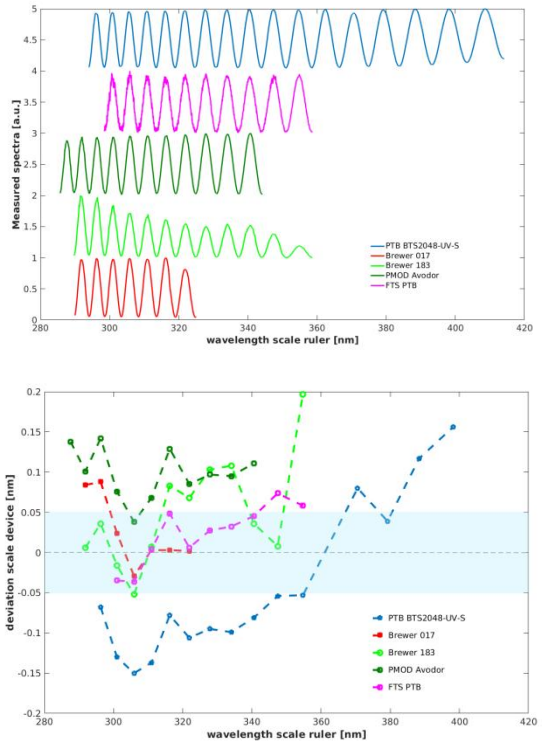

Figure 7. Results of the in-situ wavelength scale calibration of different instruments. The upper panel shows the spectra measured by the different types of instruments each covering its own spectral range. The lower panel shows the derived positions for the lines peaks. The light-blue interval, centred on 0 nm deviation, is just shown to guide the reader's eye and indicates the region within ± 0.05 nm deviation in the wavelength scale.

CONCLUSIONS

In this document we have reported on the on-site calibration of the wavelength scale of different types of spectroradiometers during TOC measurement campaign of Izaña, in September 2016, using a properly designed wavelength ruler, to be operated in the UV part of the spectrum between 280 – 350 nm. Considered the very diverse measurement conditions and the large diversity of the instruments characterized, the system has shown a very good portability and robustness for on-field measurements and surely show promise to further precise and accurate wavelength scale calibration in the UV range.

Acknowledgement This work has been supported by the European Metrology Research Programme (EMRP) within the joint research project EMRP ENV59 "Traceability for atmospheric total column ozone." The EMRP is jointly funded by the EMRP participating countries within EURAMET and the European Union.

References

1. O. El Gawhary et al., *UVNews* **11**, 42-45 (2016).
2. B. Lyot, Comptes Rendus **197**, 1593 (1933).
3. B. Lyot, Ann. Astrophys. **7**, 31 (1944).
4. J. W. Evans, JOSA **39**, 229-242 (1949).
5. A.M. Title, Appl. Opt. **14**, 445 (1975).
6. A.M. Title, Solar Phys. **33**, 521 (1973).
7. A.M. Title, Appl. Opt. **14**, 229 (1975).
8. A.M. Title, Appl. Opt. **15**, 2871 (1976).
9. G. Yang, Z. Zheng, H. Li, and X. Liu, Appl. Opt. **49**, 1280-1287 (2010).

The design and development of a tunable and portable radiation source for field instrument characterization

Geiland Porrovechio[1], Tim Burnitt[2], Petr Linduška[1], Martin Stanek[3] and Marek Šmíd[1]

1. Czech Metrology Institute, Okružní 31, 638 00 Brno, Czech Republic
2. Principal optics, 33 Lunds Farm Road, Woodley, Reading,RG5 4PZ, UK
3. Czech Hydrometeorological Institute, Zámeček 594/24, 500 08 Hradec Králové, Czech Republic

Introduction

The most reliable total column ozone measurements are obtained from UV spectroradiometers, measuring the differential absorption of ozone in direct solar irradiance measurements. Two instruments, the Dobson and Brewer spectrophotometers, are responsible for the most extensive ground-based measurements producing benchmark datasets used to infer the long-term evolution of the ozone layer. The Dobson spectrophotometer network has the most extensive dataset, starting in 1926.

Dobson and Brewer spectrophotometers are the main instruments used to monitor the ozone layer, even though Dobson spectrophotometers are no longer being manufactured. Even though each network-type is in itself consistent, total column ozone retrieved from the two instrument types differ by up to 3 %, which is significantly larger than the consistency of better than ±0.5 % which can be achieved within Brewer or Dobson instruments. Therefore this large discrepancy currently precludes a merging of both datasets and an eventual replacement of one instrument with another type.

There is therefore a need for an improved characterization and calibration of the Dobson and Brewer instruments, particularly by involving the reference instruments of each network. This will have an impact on the whole global observing network by disseminating improved ozone measurements with known uncertainties.

The bandwidths and center wavelengths of the Dobson spectrophotometer are not known for each instrument, but assumed to be equal to the world reference Dobson. Currently tunable monochromatic sources are complex and cumbersome systems that are only found in a few laboratories world-wide. The design and develop a field tunable and portable radiation source for the wavelength range 300 nm to 350 nm will be used to characterize the ozone positions of Dobson instruments in the field with uncertainties of better than 0.05 nm in wavelength using novel accordion gratings applied to the UV spectral region.

Design

The Tunable Portable Source (TuPS) is intended as an instrument to be used for determining the slit function and wavelength scale uncertainty of a Dobson Spectrophotometer. Both the slit function and the wavelength scale accuracy are critical parameters when comparing spectral measurements made by different instruments as the spectrum measured is the convolution of the spectrum being measured and the Dobson instrument slit function that, in general, is wavelength dependent.

The tunable portable source should be able to cover the wavelengths of interest with the necessary high resolution, irradiance level and stability (Table 1). The system is envisaged as a combination of a broadband source and a tuning system; the latter rejects all but a narrow wavelength band, thus rendering the combination as a narrow-band, tunable source and should be able to operate in the range 290 nm – 350 nm.

Table 1. Required Specifications.

Wavelength range	290 – 350 nm
FWHM of selected wavelength	0.1 nm
Wavelength uncertainty	0.05 nm

Moreover it was seen to be advantageous if the system could be constructed from readily available components. Readily available UV-enhanced aluminum mirrors can provide reflectance across the wavelength region of interest of greater than 90% at angles of incidence of up to 45º.

Considerations of Source

The range of portable sources covering the range 290 nm – 350 nm is limited. A good candidate is the Hamamatsu UVCL (UV Cathode emitting Light source). This has a wavelength peak at 305 nm. If the peak of the spectrum is a relative value of 1.0, then the values at the edges of the range (290 nm and 350 nm) is 0.4. Alternatively, an optical fiber coupled high intensity broadband Laser Driven Light Source (LDLS) was used as input radiation source was considered as a backup UV radiation source [3].

It is likely that the source will be fibre-coupled to the spectrometer. The concept of collimating the output of the fibre was considered, however this would result in a very small beam width and consequently very little utilization of the area of the grating and thus reduced finesse in the output spectrum.

Selection of Wavelength

A wavelength-dependent image of the entrance aperture will appear at the image plane of tuning device, manifested, due to the continuity of the source, as a continuous spectrum at the image plane. The width of the wavelength band exiting the system is therefore to be selected by defining the width of the exit aperture. There are two features that should be noted; firstly the spatial extent of a given wavelength interval is proportional to the sine of the diffraction angle and secondly that there will be there will be a spatial variation in wavelength across the exit aperture. If the former appears to be a problem, then the exit aperture width could be a controlled by a variable slit in order to keep the wavelength range constant regardless of diffraction angle. Given the small wavelength extent of the

output, the latter is unlikely to be a problem. Note that at considerable loss to the system output flux, it could be configured such as to create a homogeneous wavelength field (by combining a double grating system in what is known as “subtractive mode”).

As an additional mechanism for fine-tuning the selected exit wavelength, the slit itself could be mounted on a translation stage such that it can be shifted along the image plane

Preliminary Schematic Diagram and Dispersion Considerations

The below (Fig. 1) is intended as an exercise in visualisation in order to aid the conception of the system. This shows the zero order reflection (black) as well as the first order diffracted rays 290 nm, 320 nm and 350 nm (shown respectively in blue, green and red for clarity).

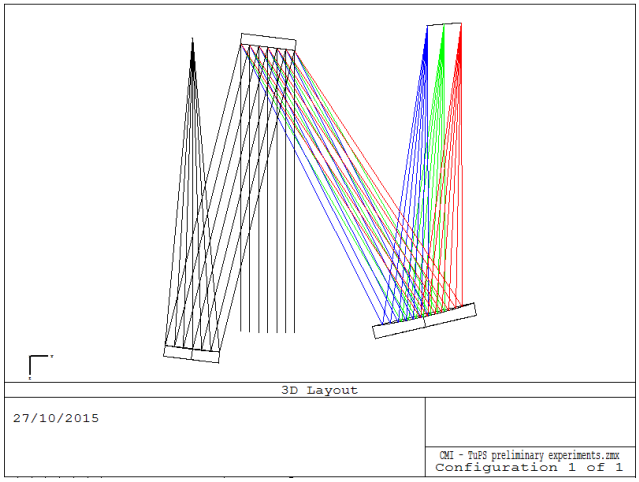

Figure 1. Preliminary Schematic Diagram and Dispersion Considerations.

The above concept makes use of a 1500 l/mm grating. With the current optics this results in a dispersion at the image plane of 3.4 nm/mm. 0.1 nm would therefore require a 30 µm slit. If the grating were replaced with a 2400 l/mm, the increased dispersion would result in

2.14 nm/mm at the image plane, requiring a 46 µm slit. Alternative optics could be used to further increase the dispersion if required at the cost of increased overall size. Currently, this schematic covers around 150 x 150 mm.

Prototype realization

The system is optically similar to a spectrometer but modified to act as a tunable filter for a broadband source, thus producing a tunable source.

The alignment procedure is detailed in a separate document. Essentially, first off-axis paraboloid mirror OAP1 is aligned relative to the input pinhole. The grating angle is then zeroed by retro-reflecting the beam from OAP1 back onto the input pinhole. The grating is then rotated to the zero order position, which defines the optic axis for the subsequent components. A first order line is then used to set up the remaining system. This step is required as if there is small rotation of the grating about the optic axis, it will manifest itself by tilting the optic plane (that is, the plane in which the optic axis lies). This does not adversely affect the optical performance of the system, but it can lead to a difference in the vertical position of the exit focal plane image between the zero and first orders.

The system was initially aligned with a tungsten lamp placed close to the entrance pinhole. This proved to be sufficiently bright for alignment. However, it did not allow for the use of the first order for alignment of components subsequent to the grating. Instead, an Ar+ laser was used as the source. This was coupled to the system by means of a multi-mode fibre placed before the input pinhole. The Ar+ laser could produce laser lines at 337.5 nm and 356.4 nm. There is also a line at around 351 nm, however the exact wavelength is unreliable and therefore it can be used only for checking bandwidth rather than defining the wavelength scale.

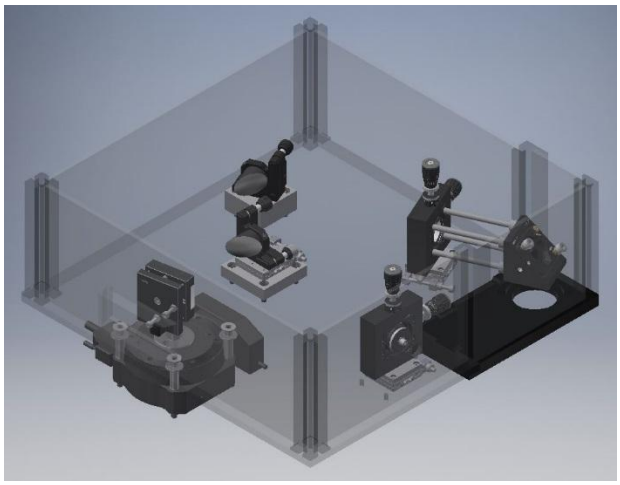

Figure 2. TuPS Prototype model.

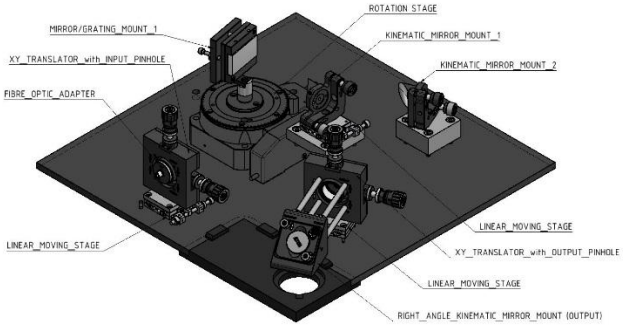

Figure 3. TuPS Prototype description.

The design defined that a pinhole between 60 and 80 µm should produce 0.1 nm resolution. Due to off-the- shelf availability, tests were carried out with 200 µm and 50 µm pinholes. The 200 µm pinhole was selected, and it was anticipated that the greater throughput would help with alignment of the system. The system was initially set up according the original design. That design allowed a reasonable separation between OAP1 and the beam between the grating and second off-axis paraboloid mirror OAP2. This was to allow sufficient space various stages required for OAP1. As it turned out, such a separation was not required. Therefore, two options existed for modifying the system; reducing the angle between OAP1>grating>OAP2, or retaining the angle, but shortening the distance OAP1–grating and grating-OAP2. The former could increase the resolution, whereas the latter would make the system more portable. As the resolution was sufficiently good, the decision was made to produce a more compact system.

A detector was placed behind the exit pinhole in order to measure the output power. Scans, logging the power

at regular angular intervals were run in "positive" (increasing angle) and "negative" (decreasing angle) directions in order to gauge the performance of the rotation stage upon which the grating was mounted. Experimentation suggested that the stage could be moved with a minimum step size of 0.001°. This was beyond the technical specification of the stage, but appeared to work.

Characterization of the TuPS

Wavelength scale calibration

The TuPS wavelength scale calibration, i.e. the determination of the relation between the TuPS grating angle and the selected wavelength at the TuPS output, was performed using the fiber coupled CMI tunable laser facility (OPO). The OPO wavelength accuracy is better than 0.05 nm [1,2]. The XYZ position of the OPO optical fiber relative to the TuPS input 100um pinhole (IP) was optimized to deliver the highest output signal that was measured at the TuPS 100um wide output slit (OS) . The optical radiation at the OPS was measured by a calibrated 10 mm x 10 mm Si photodiode in conjunction with a calibrated transimpedance amplifier with I/V gain set to 1e8. The measurements were performed at wavelengths ranging from 305 nm to 330 nm with 5 nm step. For each wavelength a set of 100 grating angle values were set around the expected angle with an angular step of 0.001 °.

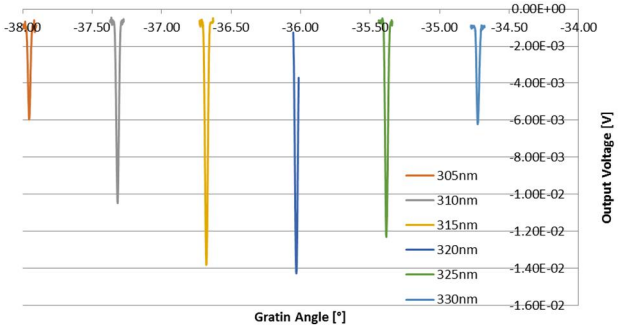

Figure 4. TuPS wavelength calibration with OPO facility.

For each wavelength the angular position of the peak was calculated. The resulting relation between the TuPS grating angle and the TuPS wavelength at the OS was then determined.

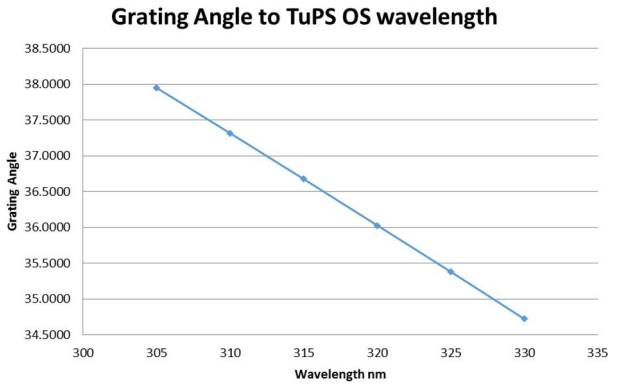

Figure 5. Grating angle to wavelength.

TuPS bandwidth

Using the same data set and the quasi linear relation between grating angle and wavelength is also possible to easily assess the bandwidth performance of the TuPS. The measured Full Width at Half Maximum (FWHM) 0.02° can be transformed in wavelength using a simple linear transformation and has been determined to be equivalent to about 0.150 nm. In the figure below the calculation performed at 310 nm using the OPO as monochromatic source.

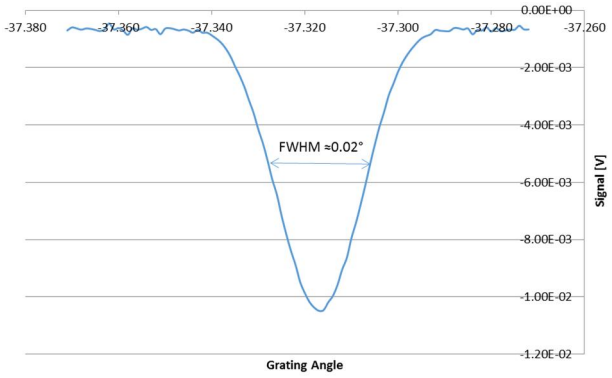

Figure 6. Angular FWHM with OPO laser set at 310 nm.

TuPS output optical power

In order to have enough optical power at the TuPS OS to be detected with a sufficient signal to noise ratio by the Dobson instrument an optical fiber coupled high intensity broadband Laser Driven Light Source (LDLS) was used as input radiation source [3]. Using the same measurement setup used for the TuPS wavelength calibration described above it was also possible to measure the optical power from 300 nm to 350 nm. Considering the beam shape and its relatively low divergence angle the Si photodiode with its area of 10 mm x 10 mm was positioned respect the TuPS OS to reasonably underfill its sensitive area. The measured values are above 20 nW in all range of interest. Based on the data acquired in CMI during the Dobson calibration campaign performed using the CMI monochromator based facility the optical power value of 21 nW is sufficiently intense to be detected by the Dobson with a convenient signal to noise ratio.

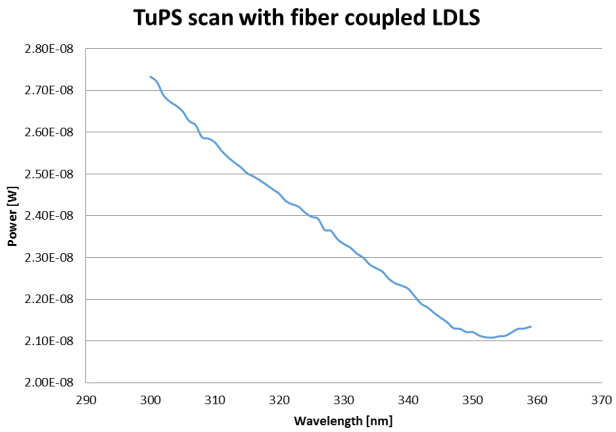

Figure 7. Measured optical power at TuPS OS.

Conclusions

The Tunable Portable Source (TuPS) was developed as an instrument to be used for determining the slit function and center wavelength of a Dobson Spectrophotometer. TuPS was characterized at CMI for both bandwidth and the central wavelength accuracy all over the spectral range of

interest. Wavelength scale calibration was performed using the fiber coupled CMI tunable laser facility – 1kHz ns pulsed OPO resulting the uncertainty < 0,1 nm. The same facility was used to determine the bandwidth of the TuPs emitted quasi-monochromatic radiation. The values smaller then 0,02 nm FWHM were measured over all intended spectral range of interest. First Dobson characterization measurements are currently going on in Czech Hydrometeorological Institut in Hradec Kralove.

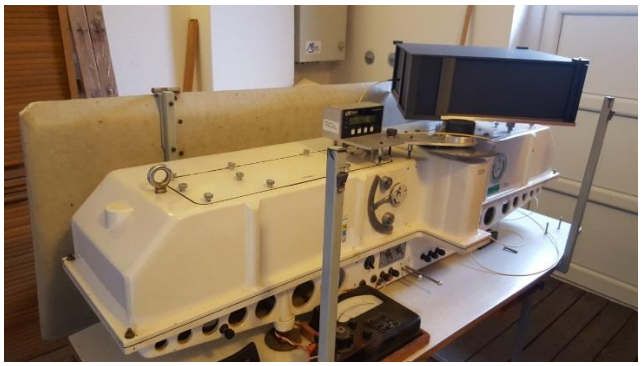

Figure 8. First measurement of Dobson spectrophotometers.

References

1. http://ekspla.com/wp-content/uploads/2011/06/NT242-datasheet.pdf
2. Petr Balling, Pavel Mašika, Petr Křen, and Miroslav Doležal, "Length and refractive index measurement by Fourier transform interferometry and frequency comb spectroscopy," *Meas. Sci. Technol.* **23**, 094001 (2012). DOI 10.1088/0957-0233/23/9/094001
3. http://www.energetiq.com/fiber-coupled-laser-driven-light-source-long-life-compact.php

Regular articles

A long journey resulting in CIE 220:2016 "Characterization and Calibration Method of UV Radiometers"

Anton Gugg-Helminger,

Gigahertz-Optik GmbH, Germany, http://www.gigahertz-optik.de/

Summary

This article gives a short overview of the history of the document CIE 220:2016 Characterization and Calibration Method of UV Radiometers [1] and its most important content. In particular, the subject of spectral mismatch is covered. The technical document CIE 220 prepared by CIE Technical Committee TC 2-47 describes quality indices for UV radiometers, which enable manufacturers and users to characterize instruments on a common basis. To harmonize CIE documents, the quality indices described in this document relate to the quality indices described in Joint ISO/CIE International Standard ISO/CIE 19476:2014(E) (formerly CIE S 023/E:2013).

History and success of the document

The starting point of the CIE 220 was 18 years ago. A working group pursuing the work was established in the First Workshop of the "Thematic Network for Ultraviolet Measurements" in Espoo, March 2 and 3, 1998. The Network was funded by the Standards, Measurements and Testing program of the Commission of the European Communities, as project number SMT4-CT97-7510.

Within the Working Group 1 "Guidance for UV power meter classification for particular applications," chaired by Anton Gugg-Helminger, the document "Characterizing the Performance of Integral Measuring UV-Meters" was prepared. It was published in *UVNews* **6** in November 2000. [2]

This publication was taken over to the CIE within the technical committee TC2-47 with chair Gan Xu in 2001. The new title was "Methods of Characterization and Calibration of Broad Band UV Radiometers."

In 2006 Armin Sperling became the new chair and finished this long process in 2016 "Characterization and Calibration Methods of UV Radiometers."

From the initial idea through to the finished document, it has taken 18 years of work all around the world. The published document provides helpful guidance on the characterization of UV radiometers.

To harmonize CIE documents, the quality indices described in CIE 220 relate to the quality indices described in Joint ISO/CIE International Standard ISO/CIE 19476:2014(E) (formerly CIE S 023/E:2013), and references are made to those where applicable.

Unlike photometers, the subject of ISO/CIE 19476:2014(E), UV radiometers may be designed for various actinic spectra and different spectral ranges. Therefore, instead of only one defined spectral reference source (CIE Source A) used in ISO/CIE 19476:2014(E) three reference spectra as shown in Figs. 1 and 2 are proposed in CIE 220 to support the generic spectral characterization of UV radiometers for various applications.

Spectral mismatch evaluation

Spectral mismatch is a major uncertainty source, maybe the largest one, hence one of the most important characterization parameters of a UV radiometer.

After the first publication in 2000, Gigahertz-Optik GmbH started to measure the relative spectral responsivity of each broad-band UV radiometer that was delivered, and is possibly still the only manufacturer doing so. With this knowledge, every customer is able to calculate the spectral mismatch $a(Z)$ value. The application of this $a(Z)$ value is a key parameter for precise measurements. It allows correction of the measured value, corresponding to the calibration source and not to the actual source measured. In CIE 220, the $a(Z)$ value is called $a^*_{\mathrm{act,R,Z}}$, the spectral mismatch.

The spectral mismatch $a^*_{\mathrm{act,R,Z}}$ is defined as the ratio of the effective responsivity of the meter head with respect to the radiant quantity of the test source $s_{\mathrm{act,Z}}$, to the effective responsivity with respect to the reference source $s_{\mathrm{act,R}}$ as

$$a^*_{\mathrm{act,R,Z}} = \frac{s_{\mathrm{act,Z}}}{s_{\mathrm{act,R}}} = \frac{\int_0^\infty X_{\lambda,\mathrm{Z,rel}}(\lambda)\times s_{\mathrm{rel}}(\lambda)\times \mathrm{d}\lambda}{\int_0^\infty X_{\lambda,\mathrm{Z,rel}}(\lambda)\times A_{\mathrm{act}}(\lambda)\times \mathrm{d}\lambda} \Big/ \frac{\int_0^\infty X_{\lambda,\mathrm{R,rel}}(\lambda)\times s_{\mathrm{rel}}(\lambda)\times \mathrm{d}\lambda}{\int_0^\infty X_{\lambda,\mathrm{R,rel}}(\lambda)\times A_{\mathrm{act}}(\lambda)\times \mathrm{d}\lambda}, \qquad (1)$$

where $X_{\lambda,\mathrm{R,rel}}(\lambda)$, $X_{\lambda,\mathrm{Z,rel}}(\lambda)$ are the relative spectral distributions of the reference-spectrum source R and that of source Z, respectively.

The reciprocal of this spectral mismatch is called the spectral mismatch correction factor

$$F^*_{\mathrm{act,R,Z}} = 1/a^*_{\mathrm{act,R,Z}}. \qquad (2)$$

This factor can be used to correct measurement results as

$$Y_{\mathrm{R}} = Y_{\mathrm{Z}} \times F^*_{\mathrm{act,R,Z}}, \qquad (3)$$

where Y_R is the corrected value with respect to the reference spectrum source R, and Y_Z is the uncorrected reading of the radiometer when measuring source Z.

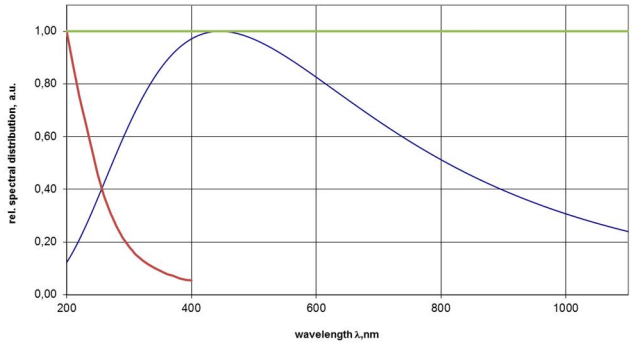

Figure 1. Reference spectra defined in CIE 220 in the range 200 – 1100 nm. The red curve denotes relative spectrum of a D2 lamp, blue curve a black body radiator at T = 6500 K, and the green curve is unity irradiance.

If the quality of a broad-band UV radiometer has to be evaluated without knowing the exact spectral power distribution of the measured source, within the CIE 220 three reference spectra are given. With these three reference spectra, the user can evaluate the quality of a broadband UV radiometer with respect to these reference light sources. Hence, the user is at least able to compare the UV radiometer to other meters even if the spectral distribution of the source being measured is not known.

The reference spectra have been defined for a wide range from 200 nm to 1100 nm, due to the long wavelength response of commonly used silicon detectors.

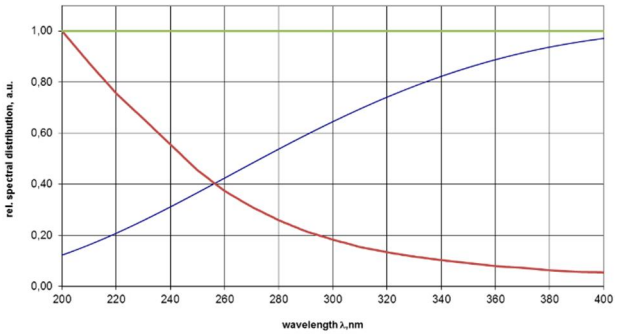

Figure 2. Reference spectra of Fig. 1 in the wavelength range 200 – 400 nm. Colors are as in Fig. 1.

For situations where the three defined spectra are not sufficient for the evaluation of the spectral mismatch of a UV radiometer, ten further sources are given in *UVNews* **6** [2]. These spectra are illustrated in Fig. 3.

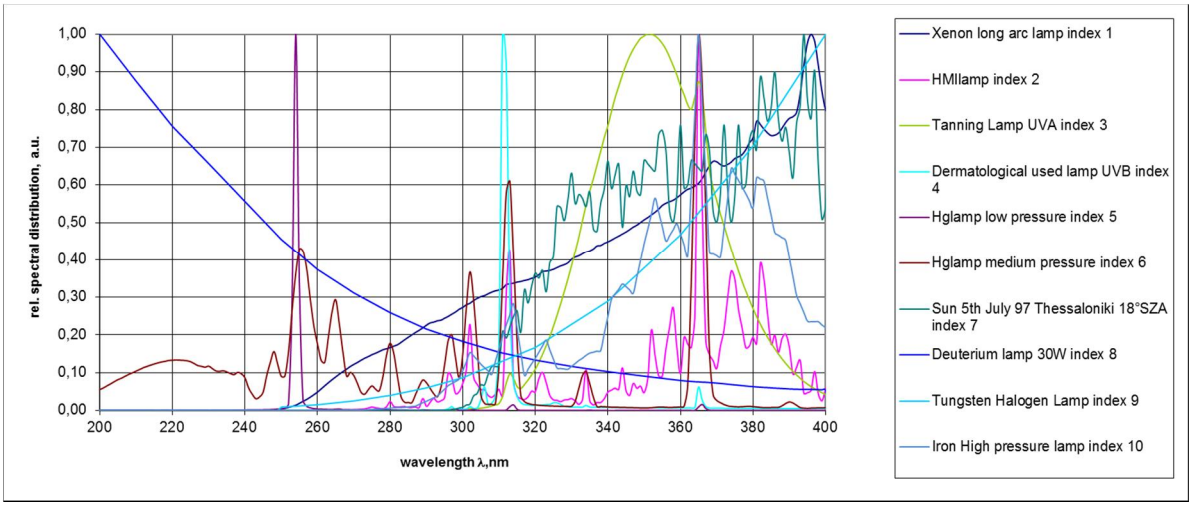

*Figure 3. Ten different spectral distributions of real sources defined in UVNews **6** [2].*

Note: The spectral distributions of Fig. 3 are not specified as reference spectra in CIE 220 or any other official CIE documents. However, as a "golden rule" one can say, the closer the spectral mismatch correction factors are to 1 for different reference spectra, the better the broad-band UV radiometer can measure sources of unknown spectral power distributions.

Example evaluation for a UVA radiometer

In the following, an example of a UVA radiometer is given. The radiometer has been designed for the ICNIRP [3], former ACGIH [4], weighting function as shown in Fig. 4. The UVA radiometer corrections are evaluated with the reference spectra of CIE 200 and *UVNews* **6**.

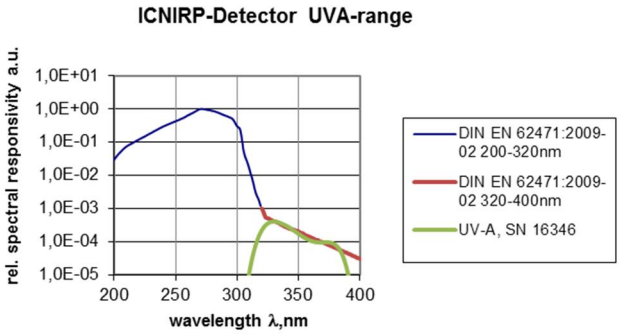

Figure 4. ICNIRP actinic curve in the wavelength range 200 – 400 nm.

The evaluated UVA radiometer matches quite well with the three reference spectra of CIE 220 as seen in Table 1. The spectral mismatch factors $a^*_{\mathrm{act,R,Z}}$ are within 1.5 % even without applying spectral mismatch correction factors.

Table 1. Spectral mismatch factors for a UVA meter used as an ICNIRP-weighted radiometer, with reference spectra of CIE 220.

Reference spectrum	$a^*_{act,R,Z}$
BB 6500K	0,992
D2	0,985
EE	0,992

Table 2 lists spectral mismatch factors of the same detector, evaluated for the ten sources defined in *UVNews* **6**. These results show a wider range of spectral mismatch correction values and thus by not applying them a larger residual error.

*Table 2. Spectral mismatch factors for a UVA meter used as an ICNIRP-weighted radiometer, with reference spectra of UVNews **6**.*

Reference spectrum	$a^*_{act,R,Z}$
Xenon long arc lamp, index 1	1,011
HMI lamp, index 2	0,993
Tanning Lamp UVA, index 3	0,999
Dermatological used lamp UVB, index 4	1,062
Hg lamp low pressure, index 5	1,377
Hg lamp medium pressure, index 6	1,360
Sun 5th July 97 Thessaloniki 18°SZA (or use AM1.5), index 7	1,184
Deuterium lamp 30W, index 8	0,996
Tungsten Halogen Lamp, index 9	0,986
Iron High pressure lamp, index 10	1,088

Depending on the application, this detector might be sufficient for at least seven or eight of the sources. However, for at least two sources the mismatch factor is large, and a correction is highly recommended.

By analyzing the data in more detail, we can see that the Hg-lamp shows no or very little emittance in the spectral range 320 – 400 nm for which the detector is designed. This explains the large deviation with this lamp.

Evaluation of the spectral mismatch factor is a good way to test the detector performance for an intended application. However, this can only be done if the values of the relative spectral distributions of the measured source, the calibration lamp, and the detector are available. Hence to reduce the additional measurement error introduced by the spectral mismatch error of the UV broad band radiometer, this data is needed from the manufacturer.

Short- and long-wavelength range response characteristic of UV radiometers

In photometry, the long and short wavelength response is easier to check than in the UV region. This is due to the smooth photometric $V(\lambda)$ curve and the smooth standard illuminant A. Therefore, optical glass filters are recommended for the evaluation. In the UV region, however, the reference spectra and light sources are more complicated.

In this chapter the short and long wavelength response of a UV radiometer and its impact on measurements is explained with the help of an example. If we measure the long pass filter response with a 2 mm thick WG320 Schott optical glass filter (Fig. 5), which should be suitable to check the long wave response for this detector device (50% transmission value will be at 320 nm), we should get a usable result. We get a result value of 2% for the long wavelength responsivity.

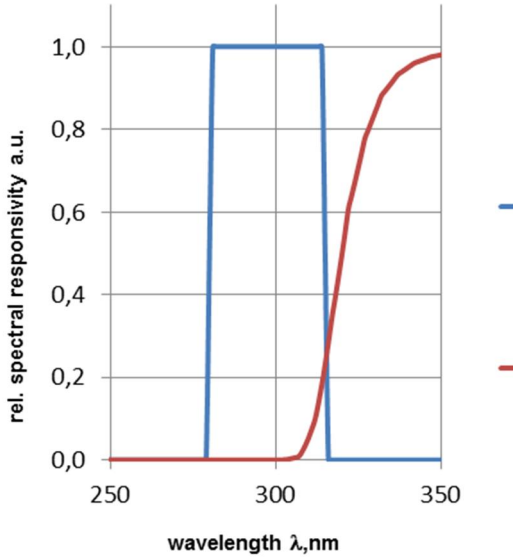

Figure 5. UVB-radiometer actinic curve (blue line) and the transmittance of long pass filter WG320 (red curve).

In practice, according to the WG320 filter's data sheet specification, the 50% value could vary from 314 nm to 326 nm (Fig. 6). When measuring with these two filters, we get result values between 0.2% and 9%. It is quite clear that these values do not express the performance of the UV detector, but originate from the wide spectral tolerance of the long pass wavelength filter. Therefore this evaluation is not suitable in the UV range. The same principle applies to the short wavelength response.

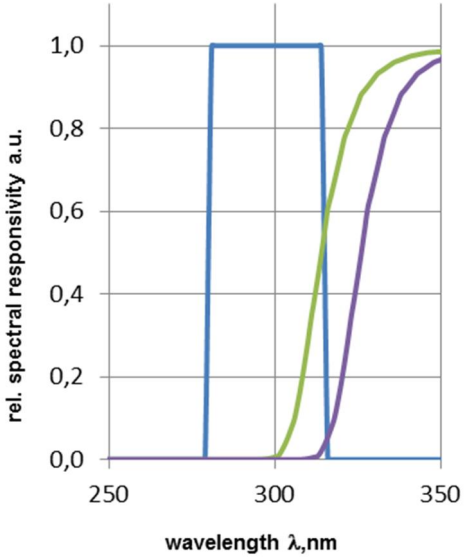

Figure 6. UVB-radiometer actinic curve (blue line), and possible long pass filter curves of WG320: 50% at 314 nm (green line) and 50% at 326 nm (purple line).

Due to the tolerance problems, the short-wavelength range response index $f_{sh,act}$ and the long-wavelength range response index $f_{lo,act}$ have to be calculated directly from the measured relative spectral responsivity of the UV radiometer being characterized instead of the filter method. CIE 220 does not recommend the filter method for evaluating the out of band response. Also the fluorescence of the filter has to be taken into account.

The characteristics of the respective out-of-band response of the radiometer, i.e. the short-wavelength range response index, $f_{sh,act}$, and the long-wavelength range response index, $f_{lo,act}$, are determined as the ratio between the relative upper and lower out-of-band responsivity to the relative in-band responsivity of the UV radiometer with respect to the action spectrum of interest,

$$f_{sh,act} = \frac{\int_{\lambda_{sh,A_{act}}}^{\lambda_{sh,Sensor}} s_{rel}(\lambda)\times d\lambda}{\int_{\lambda_{lo,A_{act}}}^{\lambda_{sh,A_{act}}} s_{rel}(\lambda)\times d\lambda} \qquad (4)$$

and

$$f_{lo,act} = \frac{\int_{\lambda_{sh,A_{act}}}^{\lambda_{lo,Sensor}} s_{rel}(\lambda)\times d\lambda}{\int_{\lambda_{lo,A_{act}}}^{\lambda_{sh,A_{act}}} s_{rel}(\lambda)\times d\lambda} \quad , \qquad (5)$$

where $\lambda_{sh,Sensor}$ is the wavelength where the responsivity of the detector used in the UV radiometer becomes negligible (i.e. below the expected uncertainty of the measurements) on the short wavelength side. This wavelength may be set to 200 nm; $\lambda_{lo,Sensor}$ is the wavelength where the responsivity of the detector used in the UV radiometer becomes negligible (i.e. below the expected uncertainty of the measurements) on the long wavelength side; $\lambda_{sh,Aact}$ is the short wavelength edge of the actinic function for which the UV radiometer is designed; $\lambda_{lo,Aact}$ is the long wavelength edge of the actinic function for which the UV radiometer is designed; and $s_{rel}(\lambda)$ is the relative spectral responsivity of the UV radiometer.

The out-of-band indices $f_{sh,act}$ and $f_{lo,act}$ are defined independently from the used calibration and application sources. The actual out-of-band signal of a UV radiometer will depend on the signal of the used sources in the out-of-band range of the spectrum. Therefore, $f_{sh,act}$ and $f_{lo,act}$ serve only as general information about the detector and cannot be used to correct measurements.

CIE 220 recommendation for UV radiometer datasheets

CIE 220 is the first document which states a list of quality indices for UV radiometers which should be included in the datasheets of such instruments.

Compared to photometry (ISO/CIE 19476:2104(E)) there are only individual f_x-values defined and no f_{tot}. This is practical since for many UV applications not every f_x-value is needed. However manufacturers should state all of the f_x-values to give the user the chance to evaluate the f_x-values needed for their application.

For reference instruments (highest quality instruments) the manufacturer should ideally provide the following data for each individually measured and characterized instrument:

- the target action spectrum;
- the reference-spectrum sources used for calculations of effective responsivities;
- the type of calibration source used to calibrate the effective responsivity under specific conditions;
- the spectral response;
- the wavelength corresponding to peak spectral responsivity;
- the usable dose or irradiance range, as appropriate;
- the target angular response (cosine, 2π etc.);
- the allowed operating temperature interval and associated temperature coefficient;
- the calibration temperature during calibration of the reference instrument;
- the allowed humidity during operation;
- the tabulated values of the spectral responsivity including assigned uncertainties;
- the tabulated values of the angular response;
- the quality indices including estimated uncertainties;
- the reference plane of calibration.

With the help of this information, the users will be able to perform reliable measurements and to calculate uncertainty budgets for their measurement.

Uncertainty evaluation

The final measurement uncertainty associated with a UV radiometer depends on the calibration and measurement itself. Hence, an uncertainty budget of the measurement and the calibration are needed. The uncertainty budget for the calibration needs to be provided by the manufacturer.

For instance, within the calibration certificate, spectral mismatch correction factors with their assigned uncertainties should be provided for typical sources for which the UV radiometer might be used or even for user specific sources.

Major sources of uncertainty during calibration are:

- Calibration uncertainty of the standard lamp for spectral radiant quantity;
- Measurement uncertainty of the spectral distribution of the calibration source;
- Calibration uncertainty of standard detector used for measurement of spectral responsivity;
- Calibration uncertainty of the working standard meter;
- Drift of the standard lamp used due to aging;
- Aging of working standard meter due to changes of the filter transmittance, detector's spectral responsivity and its electronic circuit ;
- Non-linearity and range change of the standard meter;
- Measurement uncertainty of electrical quantities (e.g. current measurement from photodiode) in the standard meter if they are measured separately using a current or volt meter;
- Calibration uncertainty of amplifiers ;
- Drift of amplifier;

- Stability of the radiant quantity from the UV source;
- Straylight falling on the detector in the calibration;
- Positioning uncertainties of both test and standard meter heads;
- Alignment of the meter heads relative to the beam;
- Spatial non-uniformity of detectors' responsivities;
- Spatial non-uniformity of irradiating beam;
- Temperature change of the meter head due to heating by the radiation of calibration source;
- Uncertainty caused by the low display resolution of some industrial UV radiometers;
- Uncertainty of time interval measurement for dosage (time integrated) calibration; and
- Random uncertainties (type A) during calibration.

The uncertainty evaluation should be made by qualified professionals according to the methods, standards and conditions recommended.

Conclusions

After 18 years of work, the technical report CIE 220 has finally been published, which provides a helpful guidance for UV radiometers. By correct application of the stated methods within the document, users are able to reduce the measurement uncertainty of UV radiometers. However, precise and detailed information about the meter has to be provided by the manufacturers.

Finally, with this information and the stated methods in CIE 220, different detectors, UV radiometers, broad-band UV radiometers and other UV instruments can be compared.

References

1. CIE 220:2016, *Characterization and Calibration Method of UV Radiometers* (CIE, Vienna, Austria, 2006) 52 p.
2. Working Group 1: Guidance for UV power meter classification for particular applications, "Characterizing the Performance of Integral Measuring UV-Meters," *UVNews* **6**, Part A: Final report of WG1, 26 p. (2000).
3. ICNIRP (International Commission on Non-Ionizing Radiation Protection) Sliney DH, Cesarini JP, De Gruijl FR, Diffey B, Hietanen M, Mainster M, Okuno T, Soderberg PG, Stuck B, eds., "Guidelines on limits of exposure to ultraviolet radiation of wavelengths between 180 nm and 400 nm (incoherent optical radiation)" *Health Phys*. **87**, 171–186 (2004).
4. ACGIH (American Conference of Governmental Industrial Hygienists), 1992-1993 Threshold Limit Values for Chemical Substances and Physical Agents and Biological Exposure Indices, ISBN: 0-936712-99-6.

Effective stray light suppression with the BTS2048-UV series array spectroradiometer

Ralf Zuber

Gigahertz-Optik GmbH, Germany, http://www.gigahertz-optik.de/

Introduction

Stray light can be a major problem for measurements with array spectroradiometers, especially in the UV region since the detection limit of the measurement device can be significantly reduced. Thus the application of array spectroradiometers in the UV is often limited, and double monochromator-based systems with long measurement times must be chosen. In this article, some methods of stray light suppression are briefly shown. In addition the unique design of the BTS2048-UV series meter to overcome the limitation of stray light in array spectroradiometers in the UV is introduced.

Stray light discussed here, also known as "false" light, is signal that is detected during a spectrometer measurement additional to the measurement signal dedicated for the selected wavelength ranges. These signals cannot be separated and thus the stray light considerably distorts the measurement result. The amount of stray light in a measurement strongly depends on the light source and the spectrometer itself. Inside a spectrometer unit, stray light can originate from:

- Scattering at the optical diffraction grating (grooved gratings),
- Interfering of the 0th order of the optical diffraction grating,
- Appearance of higher orders of the optical diffraction grating,
- inter-reflections between mirrors, detector, grating, entrance slit, housing,
- diffuse reflection of optically imperfect surfaces.

Ways to suppress stray light inside an array spectroradiometer

There are different ways to reduce stray light inside an array spectroradiometer. In the following, some of the methods are described.

Optical design

The basis for satisfying stray light reduction is a well and neatly developed spectrometer unit. Optical simulations are often used to optimize modern spectroradiometers since the complexity of optical beam paths can hardly be overlooked. Through various simulations (e.g. by ZEMAX), the spectroradiometers can be optimized to meet the high demands. For instance, the image sharpness must be optimized, the 0th order blocked, and higher orders removed diligently from the beam path towards the detector.

Besides the design, the choice of the optical components is also crucial. For instance the quality of the mirror coating is decisive for the proportion of diffusely reflected radiation and thus the resulting amount of stray light. The quality of the optical grating is also essential for the amount of resulting stray light.

Mathematical correction (stray light matrix)

With the help of tunable lasers (OPO optical parametric oscillator), spectrometers can be analyzed and characterized at any wavelength. Thus, so called line spread functions (LSF) can be determined, which together form a signal distribution function (SDF) characterization matrix of the spectrometer. This means that the data collected from the LSF measurements can be used to spectrally characterize the device and its stray light properties.

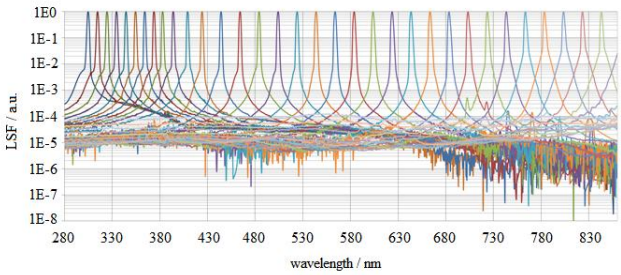

Figure 1. LSF of a spectroradiometer measured using an OPO.

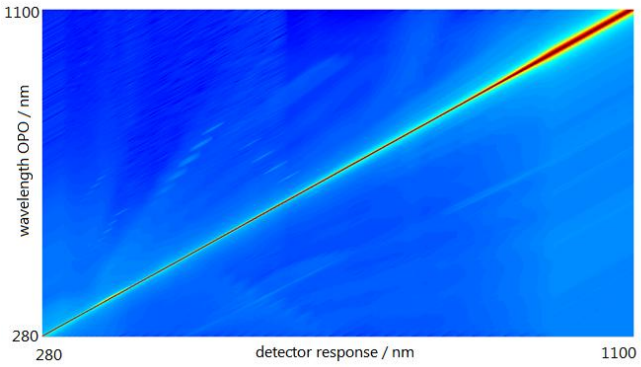

Figure 2. Visualization of a SDF correction matrix.

With these data sets and the measurement data from a current measurement, mathematical correction methods according to (Zong *et al.*, 2006) or (Nevas *et al.*, 2012) can be used for different applications. Practical experiences show that the level of stray light can be reduced by about 1 or 2 orders of magnitude (depending on the measurement device and the quality of the characterization). In Fig. 3, an example of a white LED measurement is shown.

However, this method has a limitation – for optimal stray light suppression the LSFs must be measured for the entire sensitive spectral range of the detector. For silicon, this ranges from 200 nm to 1100 nm. In UV devices which have a usable spectral range from e.g. 200 nm to 400 nm only a minor part of the stray light can be corrected. Stray light that is originating from the spectral range above 400 nm is called out of range (OoR) and cannot be corrected with this method! Hence for these devices with a limited spectral range, a more appropriate method is needed.

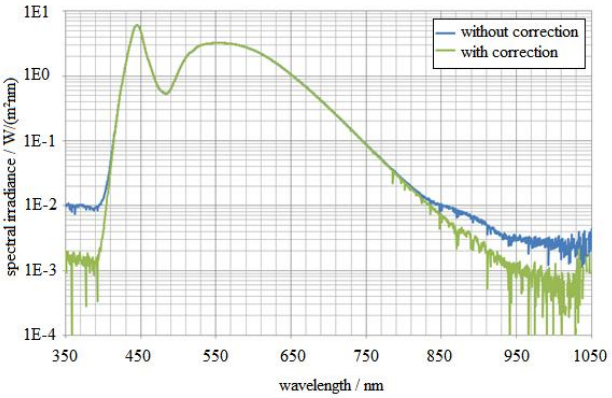

Figure 3. Mathematical stray light correction applied to a white LED measurement (green is corrected, blue is not).

Optical filtering

A well-known method of stray light correction in the UV range is based on long-pass filters such as Schott GG435. The GG435 is used to perform an additional measurement during calibration where the amount of OoR stray light is directly determined. This signal can then be subtracted from the raw data and thus applied to the resulting calibration data. This method enables calibrations with reduced stray light influences but the subsequent measurement of other light sources may still have a different stray light influence.

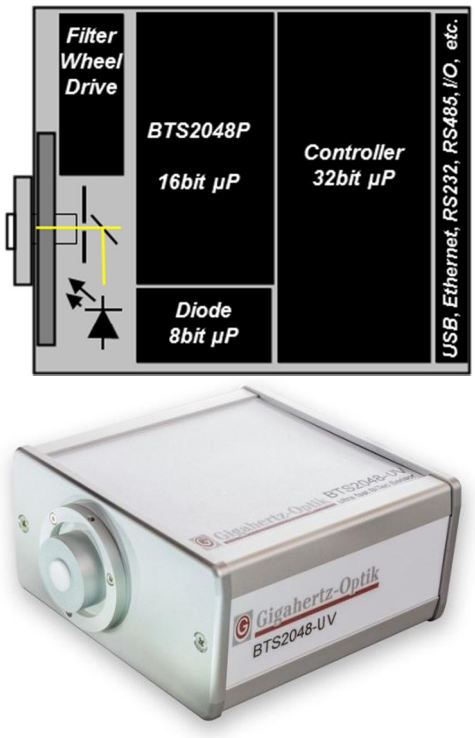

Figure 4. BTS2048-UV-S with an integrated filter wheel, 16 bit ADC for the back-thinned CCD, 8 bit SiC diode and a 32bit electronic control unit.

An innovative way to optimize stray light suppression, particularly in the critical UV range, is combining a spectroradiometer with several optical longpass filters and bandpass filters within the device. Bandpass filters basically allow the approximation of a single array spectroradiometer to a double monochromator since the bandpass filter is significantly reducing the radiation entering the spectroradiometer and thus the potential for stray light generation. With the use of long pass filters the above described method can be applied during calibration and at each measurement.

The BTS2048-UV series spectroradiometers

The combined optical filter method has been integrated into the BTS2048 series. Technically an integrated miniaturized quick filter wheel, with 4 or 8 filter positions for different optical filters, and fully automated firmware/software has been developed to achieve a compact (size is about 103 mm x 107 mm x 52 mm) and versatile spectroradiometer with satisfying stray light suppression capabilities (Figure 4).

Depending on the amount of different optical filters installed, extensive measurement routines can be realized. For instance the measurement routine can be optimized for fast measurement time or it can be adapted to specific light sources like the sun. Therefore several sub-measurements with different filters can be performed and combined to produce an accurate measurement with the preferred performance for the application.

Solar measurements

For solar UV measurements conventional UV/VIS devices do not possess sufficient stray light suppression capabilities. In particular, high-quality spectroradiometers that are optimized for the UV range are needed for UV index, erythema, blue light hazard and ozone measurements among others. As mentioned, standard devices quickly reveal their limits in terms of stray light suppression (see Egli *et al.*, 2016). In addition, the devices must be temperature-stabilized and weather-proof since long measurement sequences are often required. The BTS2048-UV-S-WP combines all of these capabilities in one device. A comparison of a solar measurement of the BTS2048-UV-S-WP with the results of a double monochromator measurement illustrates the high dynamics of the stray light corrected array spectroradiometer (Fig. 5).

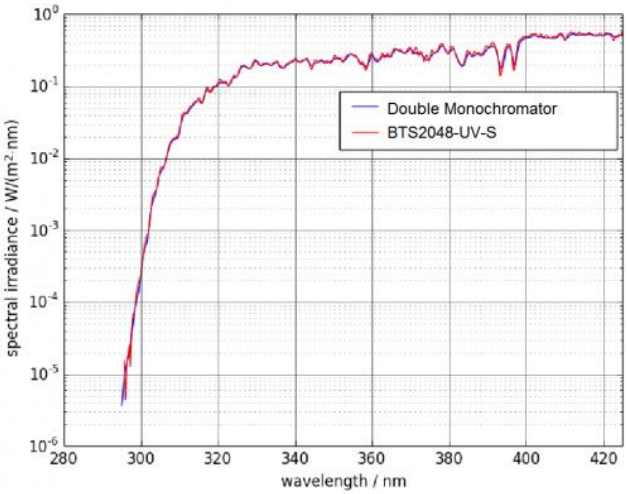

Figure 5. Comparison of the BTS2048-UV-S with double monochromator measurement. The optical bandwidth of the BTS2048-UV-S-WP is 0.8nm, and of the double monochromator is 1 nm.

This measurement shows that the stray light suppression is almost as good as that of the double monochromator which is the widely accepted measurement device of solar

measurements. Another advantage of the array spectroradiometer is its high measurement rate. While a double monochromator needs several minutes to receive one solar UV spectrum, the measurement time of the BTS2048-UV-S is in the range of a few seconds. This allows measuring continuously the solar spectrum to trace changes and fluctuation.

During a total Ozone measurement intercomparison at Izaña, Tenerife, in 2016 (http://rbcce.aemet.es/2015/11/24/atmoz-intercomparison-campaign-at-izana-tenerife-september-2016/) the performance (stray light suppression quality, absolute radiometric precision and wavelength precision) of the BTS2048-UV-S-WP was proved by calculating the total ozone column from direct solar measurements carried out with the optimized array spectroradiometer system.

Photobiological safety measurements

The BTS2048-UV series can perform stray light corrected and absolute radiometric calibrated spectral measurements down to 200 nm which makes it suitable for photobiological safety measurements in the UV spectral range. Even fast processes like welding can be precisely measured time resolved and spectroradiometricaly. This is an example application which cannot be addressed with slow scanning double monochromators. Even integral measuring filter-diode based detectors cannot reach this performance as they do not obtain any spectral data. The compact and lightweight size of the BTS2048-UV series enables direct measurements in many different situations and working places.

UV LED measurements

For LED measurements spectroradiometers that are optimized for the visible spectral range are often used. Thus, their stray light suppression in the UV range is usually insufficient which results in large measurement uncertainties. However, the results of such measurements and the required stray light suppression depend on the intended application and the available boundary conditions. In a dark room or integrating sphere where just the UV LED is present the stray light influence might be less significant. However if there is ambient light present a sufficient stray light suppression is essential. This should especially be considered when measuring white LED with a non-negligible UV content. It is therefore recommended to use at least one of the stray light correction methods available for UV/VIS spectroradiometers. If applicable, a spectroradiometer that was specifically developed for the UV range should be used.

High power UV measurements

In some applications such as UV curing or UV water disinfection, light sources with very high power spectral irradiances are used. Conventional spectroradiometers are very sensitive so that the high-power radiation has to be reduced significantly using attenuation methods. On the other hand, typical calibration sources have comparably low spectral power. This results in the demand of a high dynamic range and linearity of the instrument besides the good stray light reduction. The BTS2048-UV series spectroradiometer meets these requirements with its wide range of measurement integration times from a few microseconds up to several seconds. The stray light or bandpass measurements are performed with the same integration times as the main measurement and ensure the full implementation of effective stray light suppression at every radiant power level.

Conclusions

With the BTS2048-UV series a powerful stray light suppression method is now integrated in an array spectroradiometer which enables high quality measurements in the UV region to be performed. A comparison with a double monochromator showed that even challenging solar measurements can be precisely performed. This opens new applications since fast time resolved spectral measurements are now possible. In addition the new spectroradiometer is very compact which simplifies system integration and transport.

References

Egli L, Gröbner J, Hülsen G, Bachmann L, Blumthaler M, Dubard J, Khazova M, Kift R, Hoogendijk K, Serrano A, Smedley A, and Vilaplana J M, "Quality assessment of solar UV irradiance measured with array spectroradiometers," *Atmos. Meas. Tech.* **9**, 1553–67 (2016).

Nevas S, Wübbeler G, Sperling A, Elster C, and Teuber A, "Simultaneous correction of bandpass and stray-light effects in array spectroradiometer data," *Metrologia* **49**, S43 (2012).

Zong Y, Brown S W, Johnson B C, Lykke K R, and Ohno Y, "Simple spectral stray light correction method for array spectroradiometers," *Appl. Opt.* **45**, 1111–9 (2006).

CIE 127:2007, *Measurement of LEDS* (CIE, Vienna, Austria, 2007) 38 p.

CIE 198:2011, *Determination of Measurement Uncertainties in Photometry* (CIE, Vienna, Austria, 2011) 30 p.

CIE 214:2014, *Effect of Instrumental Bandpass Function and Measurement Interval on Spectral Quantities* (CIE, Vienna, Austria, 2011) 84 p.

BTS2048-UV, https://www.gigahertz-optik.de/en-us/product/BTS2048-UV

BTS2048-UV-S, https://www.gigahertz-optik.de/en-us/product/BTS2048-UV-S

BTS2048-UV-S-WP, https://www.gigahertz-optik.de/en-us/product/BTS2048-UV-S-WP

Risk assessment of artificial UV radiation sources

Ljiljana Udovicic, Marco Janßen, and Winfried Janßen

Federal Institute for Occupational Safety and Health (BAuA), Dortmund, Germany

1. Introduction

Optical radiation can cause damage to the human eye and skin. For example, acute overexposure to ultraviolet (UV) radiation can lead to photokeratitis and photoconjunctivitis (inflammation of the cornea and conjunctiva, respectively) or cataract (clouding of the eye's lens). In Europe, the Directive 2006/25/EC [1] must be taken into account when assessing the safety of employees at workplaces with artificial radiation sources. This Directive aims to improve the health and safety of employees by establishing exposure limit values to protect eyes and skin against coherent (laser) and non-coherent optical radiation. The employer is obliged to carry out a risk assessment regarding artificial optical radiation. The methodology applied in the assessment, measurements and/or calculations follows the corresponding European standards. In case the exposure limit values are exceeded, the employer shall take immediate action to reduce exposure below the exposure limit values.

Where available, manufacturer's data may be used to assist the risk assessment and the implementation of the protective measures. In case of non-coherent optical radiation sources, the risk group classification according to the harmonized Lamp Safety Standard EN 62471 "Photobiological safety of lamps and lamp systems" (in Germany DIN EN 62471 [2]) can support the risk assessment.

This paper presents the assessment of photobiological eye safety in the UV spectral range following the requirements of the Standard EN 62471 and using the example of two light emitting diode (LED) sources of UV radiation: a lamp UV Inspector 711 (Helling) and a single UV LED 365 (Seoul Semiconductor).

Table 1. Exposure limit values for non-coherent optical radiation in UV spectral range laid down in Directive 2006/25/EC.

Hazard	Wavelength	Exposure limit value	Comment
Actinic UV	180 nm - 400 nm	H_S = 30 J·m^{-2}	daily value, 8 h
UVA	315 nm - 400 nm	H_{UVA} = 10 000 J·m^{-2}	daily value, 8 h

Table 2. Risk groups of Standard EN 62471.

Risk Group	Risk	Basis
Exempt	no risk	No photobiological hazard
Group 1	low risk	The risk is limited by normal behavioural limitations.
Group 2	moderate risk	The risk is limited by the aversion response to bright light sources. However, such aversion responses do not occur universally.
Group 3	high risk	The source may pose a risk even for momentary exposure.

Table 3. Emission limit values for the actinic UV- and the UVA-hazard as well as the maximum exposure duration for the respective risk group according to Standard EN 62471.

Hazard		Exempt Group	Risk Group 1	Risk Group 2
Actinic UV	Effective irradiance E_S	0.001 W·m^{-2}	0.003 W·m^{-2}	0.03 W·m^{-2}
	Exposure duration	30 000 (8 h)	10 000 s	1000 s
UVA	Irradiance E_{UVA}	10 W·m^{-2}	33 W·m^{-2}	100 W·m^{-2}
	Exposure duration	1000 s (16 min)	300 s	100 s

In the UV spectral range (100 – 400 nm), the eye-related hazards are the actinic UV- and the UVA-hazard. Exposure limit values of Directive 2006/25/EC aimed to protect against those two hazards are listed in Table 1. In order to protect the cornea and the conjunctiva, a maximum effective radiant exposure* H_S is limited to 30 J·m^{-2} within an 8 hour working day. To protect the lens, a maximum radiant exposure H_{UVA} is set to 10 000 J·m^{-2} within an 8 hour working day.

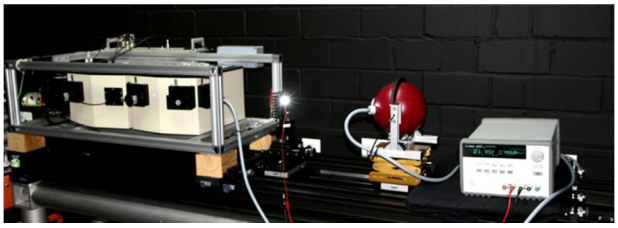

Figure 1. Experimental setup for irradiance measurements, consisting of (left to right) a double monochromator, an LED (here visible), an integrating sphere and a power supply.

2. Lamp Safety Standard EN 62471

According to the Lamp Safety Standard EN 62471 sources of non-coherent optical radiation are classified into one of four risk groups subject to their potential photobiological hazard (Table 2). A risk group provides information on exposure duration for which an exposed person remains below the emission limit value of the respective group. There is no risk (Exempt Group), if one can be exposed to the optical radiation of a lamp without restriction, a high risk (Risk Group 3), if the emission limit value is already exceeded in a short time. The emission limit values of the risk groups have been derived from the exposure limit values laid down in the Directive 2006/25/EC. They are listed in Table 3 together with the permissible duration for exposure to UV radiation.

The Standard EN 62471 describes the measurement methods and conditions for the assessment of photobiological hazards. In order to determine the risk group of a source emitting UV radiation, its spectral irradiance $E(\lambda)$ has to be measured at a specified distance. The standard defines two different measuring distances, depending on the intended use of the source: the distance in which the illuminance equals 500 lx for general lighting service lamps and the distance of 20 cm for non-general lighting sources. Most lamps emitting a relevant amount of UV radiation are non-general lighting sources.

As an input optics, the standard recommends an integrating sphere. A 7 mm aperture is recommended for sources that do not produce a spatially uniform irradiance. For the assessment of photobiological hazards based on irradiation measurements, the field of view of the detector should be limited to 1.4 rad (80°), but only if the optical source is larger than this recommended field of view.

3. Experimental procedure

The spectral irradiance $E(\lambda)$ was measured with a double monochromator (DTM 300, Bentham Instruments). Figure 1 shows the experimental setup for irradiance measurements. The wavelength accuracy of the double monochromator was checked by means of an Hg (Ar) lamp (L.O.T.-Oriel). An integrating sphere with a diameter of 150 mm (UPK-150, Gigahertz Optik) and a 7 mm aperture was used as input optics. The optical input signal was coupled into the double monochromator via an optical waveguide. A cooled photomultiplier (DH-30 TE, Bentham Instruments) was used as a detector. The measurements were carried out at a distance of 20 cm. Since both sources were smaller than the recommended field of view of the detector, the field of view was not limited.

The double monochromator was calibrated by means of a 1000 W halogen calibration lamp (LDV 1000 H, Omtec), traceable to the calibration standard of the National Metrology Institute of Germany (PTB). The calibration was performed with a bandwidth of 4 nm in steps of 1 nm. The spectral irradiance was recorded with a PC and evaluated with corresponding software (BenWin+ from Bentham Instruments).

To evaluate the actinic UV-hazard, the spectral irradiance $E(\lambda)$ was weighted by the function $S(\lambda)$ (for details see [3]) and integrated over the corresponding wavelength range:

$$(E_S)_{exp} = \int_{180\,nm}^{400\,nm} E(\lambda) \times S(\lambda) \times d\lambda \qquad (1)$$

To assess the UVA-hazard, the spectral irradiance $E(\lambda)$ - not spectrally weighted - was integrated over the corresponding wavelength range as:

$$(E_{UVA})_{exp} = \int_{315\,nm}^{400\,nm} E(\lambda) \times d\lambda \qquad (2)$$

The experimental values thus determined were compared with the emission limit values of the risk groups.

4. Results

4.1 LED-Lamp UV-Inspector 711

The mobile source UV-Inspector 711 (Helling, Fig. 2), used for non-destructive material testing or the detection of fraud banknotes and credit cards, is operated with 16.8 V.

Figure 2. LED-Lamp UV-Inspector 711 (Helling).

* Radiant exposure H is the radiant energy received by a surface per unit area, or equivalently the irradiance E of a surface integrated over time of irradiation: $H = E \times t$

The lamp contains three UV LEDs with the peak emission wavelength of 365 nm. According to the manufacturer, the irradiance at a distance of 40 cm amounts 30 W·m^{-2}. The manufacturer classifies the source in Risk Group 2.

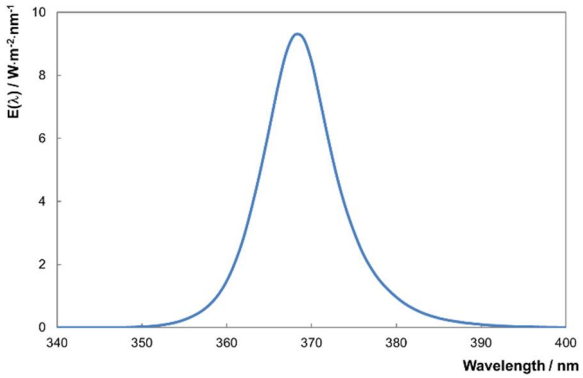

Figure 3. Spectral irradiance E(l) of the UV-Inspector 711 (Helling).

Figure 3 shows the spectral irradiance of the UV-Inspector 711. Table 4 summarizes the results of the risk assessment. Since the measured value of the effective irradiance $(E_S)_{exp}$ exceeds the emission limit values of the Exempt Group and the Risk Group 1, this source is classified with regard to the actinic UV-hazard in Risk Group 2. Similarly, the measured value of the irradiance $(E_{UVA})_{exp}$ exceeds the emission limit values of the Exempt Group and the Risk Group 1. Therefore, with regard to the UVA-hazard, the UV-Inspector 711 can also be assigned to the Risk Group 2.

4.2 UV LED 365

The single UV LED 365 (Seoul Semiconductor, Fig. 4) was operated with a current of 0.03 A according to the specifications of the technical data sheet. Figure 5 shows the spectral irradiance of the UV LED 365.

The measured values of the effective irradiance $(E_S)_{exp}$ and the irradiance $(E_{UVA})_{exp}$ of the UV LED 365 are shown in Table 5. None of the emission limit values were exceeded and the UV LED 365 was classified into the Exempt Group both with regard to actinic UV- and UVA-hazard.

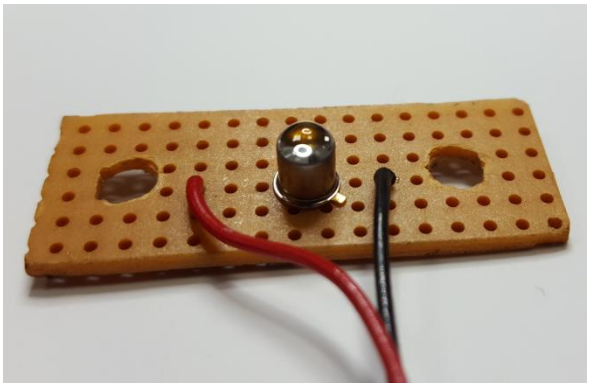

Figure 4. UV LED 365 (Seoul Semiconductor).

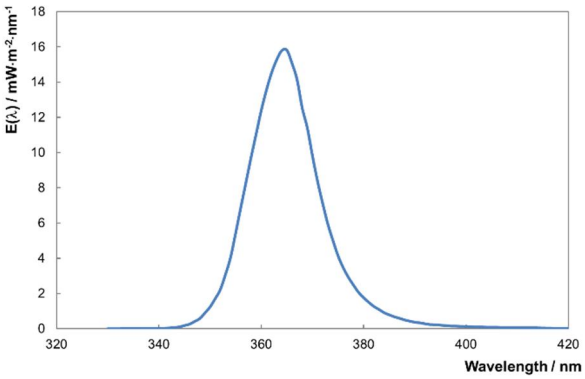

Figure 5. Spectral irradiance E(l) of UV LED 365.

Table 4. Measured values of the effective irradiance $(E_S)_{exp}$ for the actinic UV-hazard and the irradiance $(E_{UVA})_{exp}$ for the UVA-hazard of the UV-Inspector 711 (Helling) together with the corresponding emission limit values of Standard EN 62471.

Hazard		Exempt Group	Risk Group 1	Risk Group 2
Actinic UV	Measured value $(E_S)_{exp}$	0.010 W·m^{-2}		
	Emission limit value E_S	0.001 W·m^{-2}	0.003 W·m^{-2}	0.030 W·m^{-2}
UVA	Measured value $(E_{UVA})_{exp}$	98 W·m^{-2}		
	Emission limit value E_{UVA}	10 W·m^{-2}	33 W·m^{-2}	100 W·m^{-2}

Table 5. Measured values of the effective irradiance $(E_S)_{exp}$ for the actinic UV-hazard and the irradiance $(E_{UVA})_{exp}$ for the UVA-hazard of the UV LED 365 (Seoul Semiconductor) together with the corresponding emission limit values of the Standard EN 62471.

Hazard		Exempt Group	Risk Group 1	Risk Group 2
Actinic UV	Measured value $(E_S)_{exp}$	0.00007 $W \cdot m^{-2}$		
	Emission limit value E_S	0.001 $W \cdot m^{-2}$	0.003 $W \cdot m^{-2}$	0.030 $W \cdot m^{-2}$
UVA	Measured value $(E_{UVA})_{exp}$	0.7 $W \cdot m^{-2}$		
	Emission limit value E_{UVA}	10 $W \cdot m^{-2}$	33 $W \cdot m^{-2}$	100 $W \cdot m^{-2}$

5. Discussion

The aim of this article was to describe the evaluation of eye-related photobiological safety of UV radiation sources according to the requirements of the Standard EN 62471. Two UV radiation sources were evaluated: a lamp UV-Inspector 711 (Helling) and a single UV LED 365 (Seoul Semiconductor). The UV Inspector 711 is assigned to Risk Group 2, in line with the manufacturer's information sheet. The UV LED 365 is assigned to the Exempt Group. As already mentioned, a source assigned to an Exempt Group, should be safe.

In case of the UV LED 365, however, a risk assessment according to the Directive 2006/25/EC would lead to a different conclusion. While the Exempt Group of the Standard EN 62471 regarding the UVA-hazard is based on maximal exposure duration of 1000 s, the exposure limit value of the Directive 2006/25/EC is based on a working day of 30 000 s. This leads to the exposure limit value of 0.33 $W \cdot m^{-2}$ instead of 10 $W \cdot m^{-2}$. The measured value of 0.7 $W \cdot m^{-2}$ is thus above the exposure limit value.

Concerning photochemical retinal hazard, the weighting function $B(\lambda)$ has relatively low values in the region between 300 nm and 400 nm. In case of those two sources the photochemical retinal hazard was not significant.

Acknowledgment The authors would like to thank Dennis Nowack for technical support in carrying out the measurements.

References

1. Directive 2006/25/EC of the European Parliament and of the Council of 5 April 2006 on the minimum health and safety requirements regarding the exposure of workers to risks arising from physical agents (artificial optical radiation) (19th individual Directive within the meaning of Article 16(1) of Directive 89/391/EEC), (OJ L 114, 27.4.2006, p. 38) http://eur-lex.europa.eu/legal-content/EN/TXT/PDF/?uri=CELEX:02006L0025-20140101&from=EN
2. DIN EN 62471 (VDE 0837-471):2009: *Photobiologische Sicherheit von Lampen und Lampensystemen* (IEC 62471:2006, modifiziert); Deutsche Fassung EN 62471:2008
3. L. Udovičić, F. Mainusch, M. Janßen, D. Nowack, and G. Ott, *Photobiologische Sicherheit von Licht emittierenden Dioden (LED)* (Bundesanstalt für Arbeitsschutz und Arbeitsmedizin, Dortmund, Germany, 2013) 195 p. ISBN: 978-3-88261-726-9, http://www.baua.de/de/Publikationen/Fachbeitraege/F2115.html;jsessionid=513AD4CBA02AB95EBF6A209BCEBFC13D.s2t2

News

New High Vacuum Spectrometer

Erik Schoeffel

McPherson, Chelmsford MA, USA, http://www.mcphersoninc.com/

The new McPherson Model 207V is an important part of deep-UV and VUV imaging and analytical spectroscopy systems. It works over a broad spectral range, from the deep UV, through the Visible into the long-wave Infrared. Its clean construction is ideal for contaminant free purge and vacuum applications.

Ultraviolet light is used for many things. When we expose our skin to UVB, it stimulates production of vitamin D, which our bodies need. The ability of UV to inactivate bacteria and viruses lets us use it to sterilize air, surfaces and water. Some substances absorb UV light and fluoresce. Ink in highlighter pens contains a fluorescent dye. Currency and secure documents use fluorescence too. UV light can react with the chemicals of a mineral specimen or diamond. Some minerals and gemstones will phosphoresce or fluoresce under shortwave UV light and not under long wave. UV from astronomical objects tells us about the temperature and chemical composition of these remote objects. When the Earth's atmosphere absorbs the UV, we make the measurements from space. The Hubble's Faint Object Spectrograph (FOS) and the Goddard High Resolution Spectrograph (GHRS) collect and analyze UV light. We can now also make measurements in high-vacuum in the lab, with the McPherson Model 207V.

The Model 207V is a 670mm focal length optically fast f/4.7 monochromator with a vacuum tight housing. Stigmatic performance with off axis parabolic optics is available for the 207V too. With stainless steel housing capable of 10E-6 torr vacuum, this instrument works unfettered over a very wide wavelength range. Depending on the grating(s) installed it can go from 110 nanometers to 15 microns! The vacuum construction is useful for both deep ultraviolet and VUV work and also for the Infrared. Vacuum removes atmospheric constituents (gas or vapor) that absorb light wavelengths of interest in both spectral regions.

Features include Snap-In™ diffraction gratings optimized for spectral resolution and/or for wavelength range coverage. The 50-millimeter wide focal plane is great for work with camera systems. Precise and durable slits are provided for coupling free-space or fiber optic signals.

Do you need deep ultraviolet and infrared imaging? Analytical spectroscopy? The Model 207V works with no interference from atmospheric or ambient gases. It is useful for applications in astrophysics, material and life sciences. Consult McPherson and we will help make sure the spectrometer is ready for implementation in your specific application.

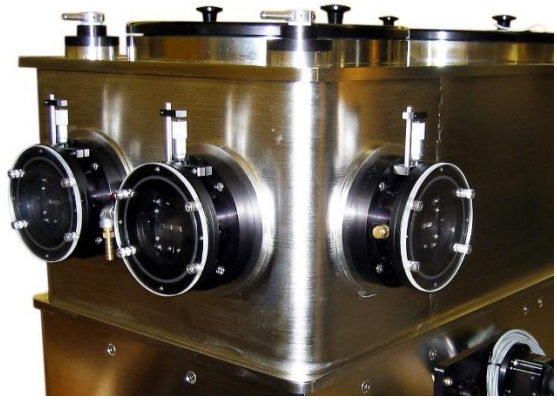

Figure 1. McPherson Model 207V Vacuum Spectrometer.

McPherson designs and manufactures scanning monochromators, flat field imaging spectrographs, vacuum monochromators, and measurement systems for reflectance, transmittance, and absorbance testing. It provides accessories, including light sources, detectors, readout systems, data acquisition software, fiber optics, sample chambers, and light collection assemblies (telescopes and collimators). Its monochromators, spectrographs, and spectroscopy systems used for industrial OEM and research applications. The company's unique components and systems are used in research applications ranging from lasers and lithography, solar, and energy to analytical and biomedical instrumentation. McPherson is a privately held corporation, founded in 1953 and based in Chelmsford, Massachusetts. For more information, visit http://mcphersoninc.com

We look forward to partnering with you on your next optical project. Thank you for your continued patronage.

New Deep-UV Polarization

Erik Schoeffel

McPherson, Chelmsford MA, USA, http://www.mcphersoninc.com/

McPherson (Chelmsford MA USA) is pleased to announce a new vacuum ultraviolet spectral test system VUV-STS. The new system measures reflectance as a function of angle of incidence. It measures optical performance "at wavelength" and can help determine optical constants. It uses special techniques for measuring non-polarized light and works in the 30 to 160 nanometer wavelength region. Transmission can be measured too, although it is not appropriate for many materials at these wavelengths. Options exist to extend operation up to 300 nm.

This new twist from McPherson helps users test materials, multilayers and coatings "at wavelength" in applications like attosecond spectroscopy and HHG, optical design for space applications, wavelength calibration, and thin-film / coating technique design.

Light coming from a monochromator has partial and often variable polarized content. Deep UV and vacuum UV wavelengths present challenges whenever there is polarization. Most laboratory polarizer's rely on crystalline wavelength transmission. Air spaced Rochon prism polarizer's built from magnesium fluoride work to wavelength short as 140 nanometers. The VUV-STS solution is to measure samples in two perpendicular planes of incidence. Then average them to negate influence of specific polarization on reflectance $(I_p-I_s)/(I_p+I_s)$. Measuring in two planes allows us to check the opposite values for each. It finally presents the reflectance for non-polarized incident radiation. This technique can be used for any reflective, diffractive or transmitting sample.

The VUV-STS is a one meter grazing incidence monochromator efficiently coupled to a windowless hollow cathode light source. The sample chamber is mechanically stiff and mounted in widely spaced and well supported bearings. Samples can rotate in two incident planes while under vacuum. Not cycling vacuum improves the quality of measurements. Other features include low noise high gain scintillated photomultiplier detector and easy to use rotation setting and data acquisition software. The McPherson software is for instrument control and does not do film analysis or other post processing – just machine control and data acquisition.

Need a high efficiency Lyman Alpha or 40eV multilayer coating? The McPherson VUV-STS will help you develop or test the parts you are receiving. Call today and we will help make sure the spectrometer is ready for implementation in your specific application.

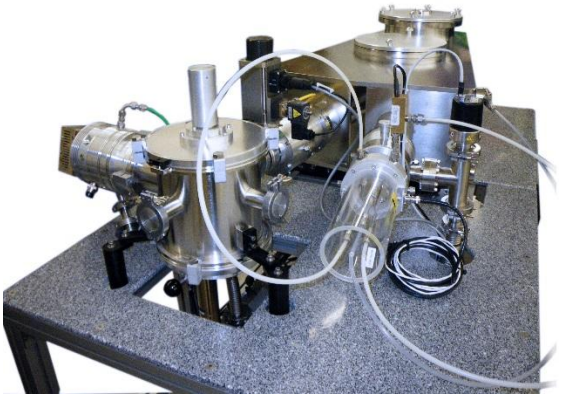

Figure 1. Vacuum ultraviolet spectral test system VUV-STS.

McPherson designs and manufactures scanning monochromators, flat field imaging spectrographs, vacuum monochromators, and measurement systems for reflectance, transmittance, and absorbance testing. It provides accessories, including light sources, detectors, readout systems, data acquisition software, fiber optics, sample chambers, and light collection assemblies (telescopes and collimators). Its monochromators, spectrographs, and spectroscopy systems used for industrial OEM and research applications. The company's unique components and systems are used in research applications ranging from lasers and lithography, solar, and energy to analytical and biomedical instrumentation. McPherson is a privately held corporation, founded in 1953 and based in Chelmsford, Massachusetts. For more information, visit http://mcphersoninc.com

We look forward to partnering with you on your next optical project. Thank you for your continued patronage.

NEWRAD 2017

Tatsuya Zama,

Chairman, NEWRAD 2017 Local Organizing Committee (LOC), NMIJ, AIST Japan

The 13th International Conference on New Developments and Applications in Optical Radiometry (NEWRAD 2017) will be convened at the Miraikan Hall, the National Museum of Emerging Science and Innovation in Odaiba, Tokyo during 13 - 16 June, 2017.

The NEWRAD Conference covers all aspects of optical radiation measurements and a wide range of topics will be presented during our four-day program. In addition to intensive scientific sessions, refreshing social program and excursion to the laboratories in Tsukuba Science City are organized, which are sure to be of interest to all the participants.

Odaiba is the scenic waterfront area lying on an artificial island in Tokyo Bay, which is one of the must-visit tourist destinations in Tokyo. It attracts wide range of generations by its diverse features such as a science museum, hot-spring, huge indoor amusement park, international exhibition center, plenty of shopping malls and restaurants, sport facilities, beautiful seaside parks, spectacular night view etc. So during your stay in Odaiba, you can find a lot of opportunities for sightseeing there. It also has good access from the central Tokyo as well as the Tokyo international airport (Haneda). At the National Museum of Emerging Science (Miraikan), the downstairs of the conference venue, visitors can enjoy interactive exhibitions on advanced science such as the earth environment, space, geography, life science, robots and information technology with hands-on exhibitions and performances by science communicators.

NEWRAD Scientific Committee

- Julian Gröbner (Chairman), Physikalisch-Meteorologisches Observatorium Davos, Switzerland
- Tatsuya Zama (Chairman of LOC), National Metrology Institute of Japan (NMIJ, AIST), Japan
- Antoine Bittar, Solar Tower Systems, Germany
- ames Butler, NASA/Goddard Space Flight Center, USA
- Nigel Fox, National Physical Laboratory, UK
- Erkki Ikonen, Aalto University and Centre for Metrology and Accreditation (MIKES), Finland
- Yoshi Ohno, National Institute of Standards and Technology, USA
- Seung-Nam Park, Korea Research Institute of Standards and Science, Korea
- Maria Luisa Rastello, Istituto Nazionale di Ricerca Metrologica, Italy
- Gerhard Ulm, Physikalisch-Technische Bundesanstalt, Germany

NEWRAD 2017 Secretariat

(For registration, accommodation and payments)

JTB KANTO Corp.

Ibaraki-Minami Corporate Sales Office

TEL: +81-29-860-2872

FAX: +81-29-854-1664

E-mail: mice-tsukuba@kanto.jtb.jp

For general inquiries on NEWRAD 2017

Please contact the local organizing committee:
mailto:newrad2017@newrad2017.jp
http://www.newrad2017.jp/

HELSINKI UNIVERSITY OF TECHNOLOGY